Department of Civil and Environmental Engineering
University of California at Davis
Davis, California 95616

Final Report No. CA10-0928

# Shortening Closure Pour Waiting Time for Bridge Construction

**H.J. Hung**

and

**Y.H. Chai**

June 2011

Final Report submitted to the California Department of Transportation (Caltrans) under Contract No. 59A0567

STATE OF CALIFORNIA DEPARTMENT OF TRANSPORTATION

# TECHNICAL REPORT DOCUMENTATION PAGE

TR0003 (REV. 10/98)

| | | |
|---|---|---|
| 1. REPORT NUMBER<br>CA10-0928 | 2. GOVERNMENT ASSOCIATION NUMBER | 3. RECIPIENT'S CATALOG NUMBER |
| 4. TITLE AND SUBTITLE<br>Shortening Closure Pour Waiting Time for Bridge Construction | | 5. REPORT DATE<br>June 15, 2011<br>6. PERFORMING ORGANIZATION CODE |
| 7. AUTHOR(S)<br>H.J. Hung and Y.H. Chai | | 8. PERFORMING ORGANIZATION REPORT NO. |
| 9. PERFORMING ORGANIZATION NAME AND ADDRESS<br>Department of Civil Engineering<br>University of California, Davis<br>Davis, California 95616 | | 10. WORK UNIT NUMBER<br>11. CONTRACT OR GRANT NUMBER<br>DRI Research Task No. 0928<br>Contract No. 59A0567 |
| 12. SPONSORING AGENCY AND ADDRESS<br>California Department of Transportation<br>Engineering Service Center<br>1801 30th Street, MS 9-2/5i<br>Sacramento, California 95816<br><br>California Department of Transportation<br>Division of Research and Innovation, MS - 83<br>1227 O Street<br>Sacramento, California 95814 | | 13. TYPE OF REPORT AND PERIOD COVERED<br>Final Report<br>4/1/2007 – 10/31/2009<br>14. SPONSORING AGENCY CODE<br>913 |

15. SUPPLEMENTAL NOTES

Prepared in cooperation with the State of California Department of Transportation.

16. ABSTRACT

Current practice in California requires up to 60 days waiting period for closure pour after the release of falsework for both staged construction and widening of existing bridges. The relatively long waiting time is intended to reduce the stress build-up and mitigate the damage in the bridge deck due to the potential differential displacement between the newly constructed deck and previously poured deck. The current waiting period does not take into account the displacement capacity of the closure slab, which varies depending on the dimensions and reinforcement details, as well as the time-dependent differential displacement that will be imposed on the closure slab. In this study, closure pour waiting time is evaluated in three steps. In step 1, a predictive model based on a creep compliance function is used to predict the time-dependent differential displacement across the closure slab in staged construction and widening. The predictive model is shown to correlate well with field measured deflections for two box-girder bridges. In step 2, four full-size closure slabs were tested to determine the displacement capacity of typical California closure slabs. Closure slab of current California details exhibits rather brittle shear failure if the displacement capacity is exceeded. In step 3, a procedure based on the predictive model of differential displacements and laboratory-determined displacement capacity is proposed to determine the waiting time for closure pour. Although a comprehensive parameter study has not been carried out, numerical examples in this study nonetheless indicate that the current waiting period is conservative, especially in staged construction.

| | | |
|---|---|---|
| 17. KEY WORDS<br>closure slab; creep; time-dependent deflection; closure waiting time, box-girder bridges | 18. DISTRIBUTION STATEMENT<br>No restrictions. This document is available to the public through the National Technical Information Service, Springfield, VA 22161 | |
| 19. SECURITY CLASSIFICATION (of this report)<br>Unclassified | 20. NUMBER OF PAGES<br>93 pages | 21. PRICE |

Reproduction of completed page authorized

## DISCLAIMER STATEMENT

This document is disseminated in the interest of information exchange. The contents of this report reflect the views of the authors who are responsible for the facts and accuracy of the data presented herein. The contents do not necessarily reflect the official views or policies of the State of California or the Federal Highway Administration. This publication does not constitute a standard, specification or regulation. This report does not constitute an endorsement by the Department of any product described herein.

For individuals with sensory disabilities, this document is available in Braille, large print, audiocassette, or compact disk. To obtain a copy of this document in one of these alternate formats, please contact: the Division of Research and Innovation, MS-83, California Department of Transportation, P.O. Box 942873, Sacramento, CA 94273-0001.

**ACKNOWLEDGMENT**

The research described in this report was funded by the California Department of Transportation under Agreement No. 59A0567. Special thanks are due to Peter Lee, John Drury, and Darin Kishiyama of Caltrans for their valuable assistance and comments during the design and testing of laboratory specimens as well as the identification of bridges for field deformation measurements. Appreciation is extended to Jonathan Chi and Ehab Wahed of Caltrans for their generosity in time during installation of data acquisition for field monitoring. The authors are also greatly indebted to the technicians of the Civil & Environmental Engineering Department at UC Davis, namely Bill Sluis and Daret Kehlet. We would also like to thank Marcos Torres and Mayra Jimenez, undergraduate assistants funded under UC Davis's California Alliance for Minority Participation, for their assistance during laboratory testing.

# Contents


**1 Introduction** **7**

1.1 Background . . . . . 7

1.2 Current Closure Slab Details . . . . . 9

1.3 Scope of Work . . . . . 11

**2 Field Measurement of Time-Dependent Deformations** **15**

2.1 Introduction . . . . . 15

2.2 Bridge Description and Instrumentation . . . . . 16

2.2.1 The Santa Rosa Creek Bridge . . . . . 16

2.2.2 The San Joaquin River Bridge . . . . . 16

2.2.3 Field Instrumentation . . . . . 18

2.3 Field Results - Deflection and Shortening . . . . . 21

2.3.1 The Santa Rosa Creek Bridge . . . . . 21

2.3.2 The San Joaquin River Bridge . . . . . 26

2.4 Comparison with Caltrans Deflection Curve . . . . . 28

**3 Closure Slab Tests** **31**

3.1 Overview . . . . . 31

3.2 Specimen Details . . . . . 31

3.3 Material Properties and Specimen Construction . . . . . 33

3.4 Test Setup . . . . . 38

3.5 Test Results . . . . . 39

3.5.1 Load-Differential Displacement Response . . . . . 39

3.5.2 Bending Moment and Shear Force Distributions . . . . . 44
3.5.3 Reinforcement Strain Distributions . . . . . 46

**4 Procedure for Determining the Waiting Time for Closure Pour 65**

4.1 Introduction . . . . . 65
4.2 Creep Compliance Function . . . . . 65
4.2.1 Basic Definitions . . . . . 65
4.2.2 Creep Compliance - Short Form of B3 Model . . . . . 67
4.3 Bridge Deflection upon Falsework Release . . . . . 70
4.4 Design Procedure for Closure Pour Waiting Time . . . . . 76
4.4.1 Example 1 - Simply-Supported Bridge . . . . . 80
4.4.2 Example 2 - Three-Span Continuous Bridge . . . . . 84

**5 Conclusions 89**

# List of Tables


1.1 A database of closure slab details for California bridges . . . . . 13

1.1 A database of closure slab details for California bridges (cont.) . . . . . 14

3.1 Matrix for closure slab specimen tests . . . . . 33

3.2 Concrete mix design . . . . . 36

3.3 Concrete compressive strengths at 28 days . . . . . 36

3.4 Bending moments and shear force at critical sections of specimen CP36_8 . . 47

3.5 Bending moments and shear force at critical sections of specimen CP24_8 . . 47

3.6 Bending moments and shear force at critical sections of specimen CP18_8 . . 48

3.7 Bending moments and shear force at critical sections of specimen CP24_12 . 48

4.1 Assumed instantaneous deflections of the three-span continuous bridge . . . 85

# List of Figures


1.1 Bridge widening or staged-construction . . . . . 8

1.2 Closure pour details for bridges with large overhangs . . . . . 10

1.3 Closure pour details for bridges with no overhangs . . . . . 10

2.1 Staged construction of the Santa Rosa Creek Bridge . . . . . 17

2.2 Elevation and cross-sectional views of the Santa Rosa Creek Bridge . . . . . 18

2.3 Closure pour details for the Santa Rosa Creek Bridge . . . . . 19

2.4 San Joaquin River Bridge . . . . . 19

2.5 Elevation and cross-sectional views of the San Joaquin River Bridge . . . . . 20

2.6 Closure pour details for the San Joaquin River Bridge . . . . . 21

2.7 Distribution of linear potentiometers . . . . . 22

2.8 Setup for field measurements of span deflection and shortening . . . . . 23

2.9 Deflected shapes of the Santa Rosa Creek Bridge . . . . . 24

2.10 Mid-span time-dependent deflection of the Santa Rosa Creek Bridge . . . . 25

2.11 Longitudinal shortening of the Santa Rosa Creek Bridge . . . . . 25

2.12 Deflected shapes of span 5 of the San Joaquin River Bridge . . . . . 27

2.13 Mid-span deflection of span 5 versus time at San Joaquin River Bridge . . . 27

2.14 Longitudinal shortening of span 5 of the San Joaquin River Bridge . . . . . 28

2.15 Normalized mid-span deflection . . . . . 30

3.1 Test region for the closure slab . . . . . 32

3.2 Specimen CP36_8 reinforcement details . . . . . 34

3.3 Specimen CP24_8 reinforcement details . . . . . 34

3.4 Specimen CP18_8 reinforcement details . . . . . 35
3.5 Specimen CP24_12 reinforcement details . . . . . 35
3.6 Instrumentation and specimen construction . . . . . 37
3.7 Closure slab test setup . . . . . 39
3.8 Final test setup . . . . . 40
3.9 Force-differential displacement curves of closure slab specimens . . . . . 41
3.10 Final failure of test specimens . . . . . 42
3.10 Final failure of test specimens (cont.) . . . . . 44
3.11 Bending moment and shear force distributions in the closure slab . . . . . 46
3.12 Specimen CP36_8 reinforcement strain . . . . . 51
3.12 Specimen CP36_8 reinforcement strain (cont.) . . . . . 52
3.12 Specimen CP36_8 reinforcement strain (cont.) . . . . . 53
3.13 Specimen CP24_8 reinforcement strains . . . . . 55
3.13 Specimen CP24_8 reinforcement strains (cont.) . . . . . 56
3.13 Specimen CP24_8 reinforcement strains (cont.) . . . . . 57
3.14 Specimen CP18_8 reinforcement strains . . . . . 59
3.14 Specimen CP18_8 reinforcement strains (cont.) . . . . . 60
3.14 Specimen CP18_8 reinforcement strains (cont.) . . . . . 61
3.15 Specimen CP24_12 reinforcement strains . . . . . 62
3.15 Specimen CP24_12 reinforcement strains (cont.) . . . . . 63
3.15 CP24_12 reinforcement strains (cont.) . . . . . 64

4.1 Creep of concrete under a sustained compressive stress . . . . . 66
4.2 Influence of falsework release on creep compliance . . . . . 71
4.3 B3 creep compliance functions at different loading ages . . . . . 71
4.4 Correspondence between span deflection and creep compliance function . . . 75
4.5 Comparison of measured mid-span deflections with the short form of the B3 model . . . . . 77
4.6 Differential deflection with different closure slab width . . . . . 78

4.7 Definition of time parameters - $t_c$ and $t_\infty$ . . . . . 80
4.8 Example 2 - three-span continuous bridge . . . . . 85

# Chapter 1

# Introduction

## 1.1 Background

Two types of construction are commonly used to increase the number of traffic lanes on congested bridges in California. In the first type, the so-called "bridge-widening", one or two new bridges are constructed adjacent to an existing bridge, followed by casting of a closure slab to connect the new bridge to the existing bridge. In the second type, the so-called "staged-construction", two new bridges are constructed in sequence or stages. A new bridge, called the stage I bridge, is built adjacent to the existing bridge to carry the traffic on the existing bridge during re-routing. After the stage I bridge has been completed, stage II construction begins by the demolition of the existing bridge, followed by the construction of a second new bridge at the existing bridge location. The two new bridges are eventually connected by a closure slab to form a smooth continuous deck surface for bridge traffic. Figure 1.1 shows the construction of a closure slab that is applicable to bridge-widening or staged-construction.

Current bridge construction practice in California specifies a fairly long waiting period, requiring up to 60 days from the day of falsework release before the closure slab can be cast. The long waiting period before casting the closure pour is intended to minimize the stress build-up in the closure slab due to the long term differential displacement between the new bridge and the existing bridge, or between the stage I and stage II bridges. Two alternatives are currently prescribed for the waiting period before casting the closure pour,

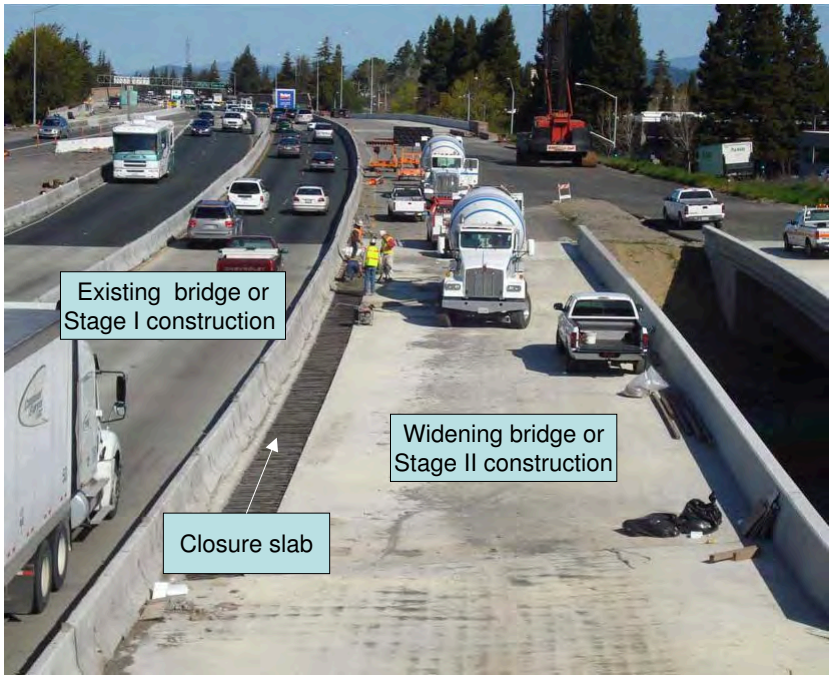


Figure 1.1: Bridge widening or staged-construction

depending on the time of falsework release. The two alternatives are summarized as follows [1]:

- **Alternative 1:** *Falsework shall be released as soon as permitted by the specifications. Closure pour shall not be placed sooner than 60 days after the falsework been released.*
- **Alternative 2:** *Falsework shall not be released less than 28 days after the last concrete deck has been placed. Closure pour shall not be placed sooner than 14 days after the falsework has been released.*

Coupled with the current specifications [2] that falsework shall not be released less than 10 days after the last concrete pour, the actual waiting period for closure pour is 70 days (from last concrete pour) for Alternative 1. On the other hand, Alternative 2 offers a shorter waiting period, reducing the waiting period to 42 days, but the falsework is required to remain in-place for a minimum of 28 days. Implications of longer waiting periods are increased construction cost and undue safety hazards during construction. If Alternative 2 is opted for closure pour, the traffic under the bridge becomes impeded for a longer period

as the falsework is required to remain in place for a longer time. Furthermore, temporary K-rails are placed at the edge of the bridge deck next to the closure, impeding the flow of traffic or reducing the number of traffic lanes in some cases. The longer the K-rails remains in-place, the higher the potential for traffic accidents. Careful considerations of the waiting period for closure pour are thus important for widening of bridges.

## 1.2 Current Closure Slab Details

Standard details have been developed for closure slabs of common bridges in California, including cast-in-place box-girder bridges, precast prestressed I-girder bridges, and steel girder bridges. These details have been developed with an objective of minimizing the potential damage in the closure slab upon time-dependent differential displacement between new and existing bridges. Recommended details for closure, as extracted from the Memo-to-Designers 9-3 [1], are as follows:

- Structures with large overhangs should be attached by removing the concrete from the overhang. There should be sufficient width to develop adequate bond length when lapping the original transverse deck reinforcing to that of widening. Closure pour details for box-girder bridges with a large overhang slab is shown in Figure 1.2.

- Structures with small overhangs, where removal of the overhang would not give sufficient bond length, should be either doweled to the widening or have transverse reinforcing exposed and extended by welding or mechanical lap splice.

- Structures with no overhangs should be attached by doweling the existing structure to the widening. Double row patterns for the dowels perform better than a single row. Benching into the existing exterior girder as a means of support has proven to be unsatisfactory. Closure pour details for box-girder bridges with no overhang is shown in Figure 1.3.

Conceptually, the closure pour and its associated details and waiting period, should be determined with recognition of their relations to the magnitude of the differential dis-

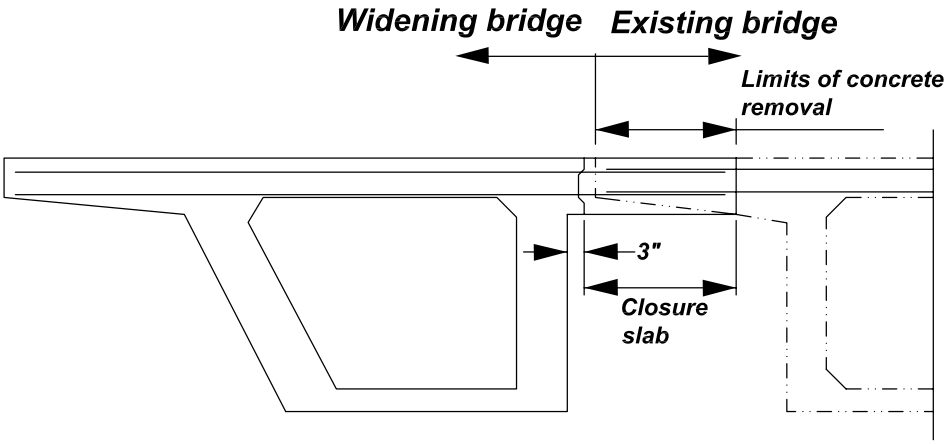


Figure 1.2: Closure pour details for bridges with large overhangs

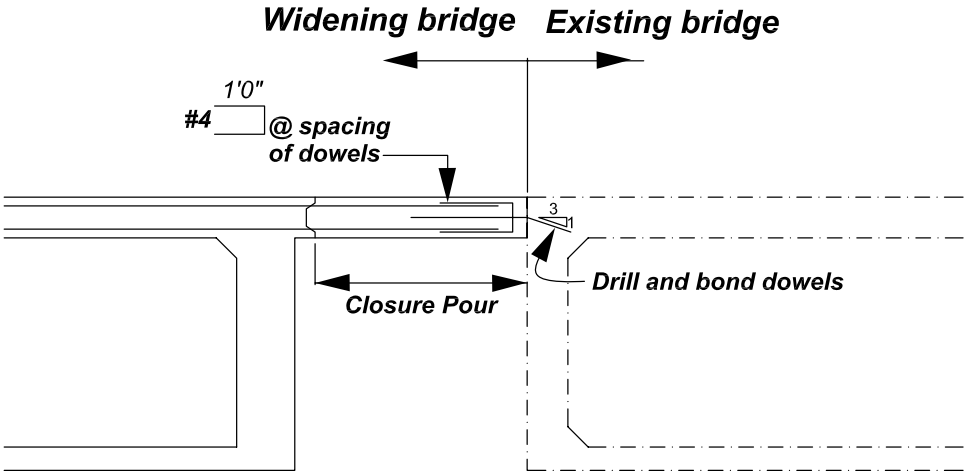


Figure 1.3: Closure pour details for bridges with no overhangs

placement between the existing bridge and widening bridge, or between stage I and stage II bridges. Despite the above recommendations, closure slabs vary considerably in terms of their width and thickness. Table 1.1 shows a summary of the closure pour details for 32 bridges in California. Although the table represents only a small subset of the closure slabs in California, it nonetheless provide a sense on their typical dimensions and reinforcement details. It can be seen that a typical length of the closure slab varies from 2' to 3'4", while its thickness varies from 6.7" to 12". The most common length is 3' while the most common thickness is 12". It is worth noting that a minimum length of 1'6" is recommended for the closure slab in the Memo-to-Designers 9-3 [1]. The minimum length is specified to ensure sufficient flexibility in the closure slab to accommodate the time-dependent differential displacement between two adjacent bridges of different ages. The database in Table 1.1 also provides the basis upon which closure slab specimens are constructed and tested in the laboratory, as reported later in Chapter 3.

## 1.3 Scope of Work

This project investigates the initial phase of time-dependent deflection in bridges during widening or staged construction. In particular, effects of reducing the closure pour waiting time are examined for cast-in-place concrete box-girder bridges. Deflections were measured for two box-girder bridges before and after falsework release for a period up to 12 months. Measured deflections are compared with current Caltrans time-dependent deflection curve, and with a normalized time-dependent deflection, established on the basis of creep-compliance function. Field measured deflections are supplemented by laboratory tests of full-size closure slab specimens, in order to establish a level of tolerable displacements for closure pour design. A procedure for establishing the required waiting time before closure pour is proposed as part of this study. This report is organized into the following chapters.

- Chapter 1 - Introduction
- Chapter 2 - Field measurement of time-dependent deformations

- Chapter 3 - Closure slab tests
- Chapter 4 - Procedure for determining the waiting time for closure pour
- Chapter 5 - Conclusions

| Bridge | Closure Slab | | Long. Reinforcement | | Transverse Reinforcement | | | |
|---|---|---|---|---|---|---|---|---|
| | Width | Thickness | Top (total nos.) | Bottom (total nos.) | Top | Mid. | Bottom | Dowels |
| ALLUVIAL AVENUE UC | 3'2" | 12" | 3 #4 cover 2" | 2 #4, 4 #4 two layers, cover 1" | #5@5" c/c | | #5@5"c/c | |
| CAMINO REAL UNDERRCROSSING | 3' | 12" | 4 #5 cover 2" | 4 #5 cover 1.6" | #5@5"c/c | | #5@3"c/c | |
| CAPBELL STREET UNDERCROSSING | 3' | 12" | 4 #5 cover 2" | 4 #5 cover 1" | #5@5"c/c | | #5@3"c/c | |
| CHURCH STREET UC | 2'6" | 12" | 5 #10 cover 2" | 5 #5 cover 1" | #5@6"c/c | #5@6"c/c | #5@6"c/c | |
| CITRUC AVENUE UC | 2'6" | 12" | 5 #10 cover 2" | 5 #5 cover 1" | #5@6"c/c | #5@6"c/c | #5@5.5" c/c | |
| CYPRESS AVENUE UC | 2'6" | 12" | 5 #10 cover 2" | 5 #5 cover 2" | #5@6"c/c | #5@6"c/c | #5@6"c/c | |
| ETIWANDA AVE UNDERCROSSING | 3' | 12" | 4 #5 cover 2" | 4 #5 cover 1.6" | #6@6.5"c/c | #5@6.5"c/c | #4@6"c/c | |
| EAST SANTA MARIA O.H AND UC | 2'6" | 12" | 4 #5 cover 2" | 4 #5 cover 1" | #5@5.5"c/c | #5@5.5"c/c | | #7 @12" staggered |
| FLORAL AVENUE UC | 3'4" | 8" | 4 #5 cover 2" | 2 #4, 4 #6 two layers, cover 1" | #5@5"c/c | | #5@5"c/c | |
| FRIANT ROAD UC | 2'8" | 12" | 3 #4 cover 2" | 2 #4, 4 #5 two layers, cover 1" | #5@5"c/c | | #5@5"c/c | |
| FORD STREET UC | 3' | 12" | 4 #10 cover 2" | 4 #5 cover 1" | #5@5.5"c/c | #5@5.5"c/c | #5@5.5"c/c | |
| HIGHLAND AVENUE UC | 3'4" | 6.8" | 4 #5 cover 2" | 2 #4, 4 #6 two layers, cover 1" | #4@6.5"c/c | | #5@6.5"c/c | |
| HIGHLAND AVENUE UC (RETROFIT) | 3' | 12" | 4 #10 cover 2" | 4 #5 cover 1" | #5@ 5.5"c/c | #5@5.5"c/c | #5@5"c/c | |
| I-10/RET 38SEP | 2'6" | 12" | 5 #9 cover 2" | 5 #5 cover 1" | #5@5.5"c/c | #5@5.5"c/c | #5@5.5"c/c | |
| MAIN STREET SEPARATION | 2' | 10" | 3 #5 cover 2" | 3 #5 cover 1" | #5@5.5"c/c | #5@5.5"c/c | | #5@9" staggered |
| McCALL AVENUE UC | 3'1" | 7.1" | 4 #4 cover 1" | 4 #4 cover 1" | #5@5.5"c/c | | #5@5.5"c/c | |
| MIRA LOMA OVERHEAD | 3' | 12" | 4 #5 cover 2" | 4 #5 cover 1" | #6@6.5"c/c | #6@6.5"c/c | #5@6"c/c | |
| PALM AVENUE UC | 3' | 12" | 4 #10 cover 2" | 4 #5 cover 2" | #6@5.5"c/c | #6@5.5"c/c | #5@5"c/c | |
| PYRITE STREE UNDERCROSSING | 3' | 12" | 4 #5 cover 2" | 4 #5 cover 2" | #6 @6.5"c/c | #6@6.5"c/c | #5@6"c/c | |
| REDLANDS BLVE OFF-RAMP UC | 3' | 12" | 4 #10 cover 2" | 4 #5 cover 1" | #6@5.5"c/c | #6@5.5"c/c | #5@5"c/c | |
| RELANDS OVERHEAD | 2'6" | 12" | 5 #9 cover 2" | 5 #5 cover 2" | #6 @5.5"c/c | #6 @5.5"c/c | #5@5.5"c/c | |
| ROSE AVENUE | 3'1" | 7.1" | 4 #4 cover 2" | 4 #4 cover 1" | #6@5.5"c/c | | #5@5.5"c/c | |
| ROUTE 5/120 OVERHEAD | 2'6" | 12" | 5 #6 cover 2" | 5 #5 cover 2" | #5@5.5"c/c | #5@5.5"c/c | | #6@6" staggered |

Table 1.1: A database of closure slab details for California bridges

| Bridge | Closure Slab | | Long. Reinforcement | | Transverse Reinforcement | | | |
|---|---|---|---|---|---|---|---|---|
| | Width | Thickness | Top (total nos.) | Bottom (total nos.) | Top | Mid. | Bottom | Dowels |
| SAN JOAQUIN RIVER BRIDGE | 2'11" | 12" | 5 #6 cover 2" | 5 #6 cover 2" | #5@6"c/c | #5@6"c/c | | #6@6" staggered |
| SANTA ROSA CREEK BRIDGE | 2'9" | 10" | 4 #4 cover 2" | 3 #5,4 #5 two layers, cover 1" | #6@5.5"c/c | | #6@5.5"c/c | |
| SECOND STREE UC | 3'4" | 6.7" | 4 #5 cover 2" | 2 #4,4 #6 two layers, cover 1" | #5@6.5"c/c | | #5@6.5"c/c | |
| SFOBB SAN FRANCISCO APPROACH | 3'4" | 10" | 5 #5 cover 2" | 5 #5 cover 1.5" | #6@6"c/c | | #6@6"c/c | |
| SIXTH STREET UC | 2'6" | 12" | 5 #5 cover 2" | 5 #10 cover 1" | #5@5.5"c/c | #5@5.5"c/c | #5@5.5"c/c | |
| SOUTH MADERA OC | 3' | 12" | 4 #5 cover 2" | 4 #5 cover 2" | #5@6.5"c/c | #5@6.5"c/c | #5@6.5"c/c | |
| SOUTH SANTA MARIA UNDERCROSSING | 2' | 12" | 3 #6 cover 2" | 3 #6 cover 2" | #5@6"c/c | #5@6.5"c/c | | #5@6" staggered |
| UNIVERSITY STREET UC | 2'6" | 12" | 5 #9 cover 2" | 5 #5 cover 2" | #5@5.5"c/c | #5@5.5"c/c | #5@5.5"c/c | |
| WINEVILLE ROAD UNDERCROSSING | 3' | 12" | 5 #5 cover 2" | 4 #5 cover 1.5" | #5@6.5"c/c | #5@6.5"c/c | #5@6"c/c | |

Table 1.1: A database of closure slab details for California bridges (cont.)

# Chapter 2

# Field Measurement of Time-Dependent Deformations

## 2.1 Introduction

Time-dependent span deflections were measured during the initial phase of construction for two cast-in-place multi-cell box-girder bridges as a part of this study. The deflections were measured only in the new bridge, on the assumption that, for the existing bridge, the major portion of the time-dependent deformation had occurred at the time of instrumentation, and that the incremental deflection of the existing bridge was small compared to that of the new bridge in the instrumented period, which was about 12 months. The measured span deflection in the new bridge was thus taken to correspond to the differential deflection between the new bridge and the existing bridge. In addition to vertical span deflection, axial shortening of the bridge, which may be significant in the case of post-tensioned box-girder bridges, was also measured. Measurements of vertical span deflection and axial shortening were facilitated by a tensioned-wire installed inside the box-girder in a cell adjacent to the closure pour. The two instrumented bridges, namely the Santa Rosa Creek Bridge and the San Joaquin River Bridge, are described next in this chapter.

## 2.2 Bridge Description and Instrumentation

### 2.2.1 The Santa Rosa Creek Bridge

The Santa Rosa Creek Bridge, located on Highway 101 in Santa Rosa, California, was selected as the first bridge for field instrumentation. The structure, with an eventual total of 8 lanes, was constructed in stages, as shown by the photograph in Figure 2.1. Stage II bridges were aligned on both sides of the stage I bridge, with the two stages constructed approximately 12 months apart. The instrumented bridge corresponded to the stage II bridge serving north bound traffic on Highway 101, i.e. the right bridge in Figure 2.1. The bridge is simply-supported with a span length of 170 ft, as shown in Figure 2.2(a), and has a depth of 7'6" as shown in Figure 2.2(b). The stage I bridge was constructed of four cells while stage II bridges were constructed of two cells, as shown in Figure 2.2(b). Stage I and stage II bridges were connected by a closure slab with width of 2'9" and thickness of 10". Details of the closure slab are shown in Figure 2.3. Reinforcing bars in the longitudinal direction were 4#4 bars for top reinforcement and 7#5 bars for bottom reinforcement with 2" clear cover for the transverse reinforcement. In the transverse direction, #6 reinforcing bars at spacing of 5.5" were used for both top and bottom reinforcement. Couplers, marketed under the tradename 'Quick Wedge Coupler', were used to connect the bottom transverse bars in the closure.

The instrumented section of the Santa Rosa Creek Bridge was post-tensioned 12 days after the last deck concrete pour, with falsework release initiated on the same day after post-tensioning, essentially opting for Alternative 1 described in Section 1.1. It should be noted that the falsework on the instrumented bridge was released in stages with full release accomplished in two days. The closure slab was cast about six months after stage II falsework release - non-intended long waiting period as the instrumented bridge was not on the critical path for overall re-routing of traffic on Highway 101.

### 2.2.2 The San Joaquin River Bridge

The San Joaquin River Bridge, located on Interstate 5 near the city of Lathrop, California, was selected as the second bridge for field measurement. The photograph in Figure 2.4

Figure 2.1: Staged construction of the Santa Rosa Creek Bridge

shows the widening of the bridge during construction, where a new one-lane bridge is added to the freeway serving the north bound traffic. The new bridge is a five-span, conventional reinforced concrete box-girder bridge, with length of 131', 147', 181', 151' and 133' for span 1 to 5, respectively. Structurally, the bridge is divided into two frames, as shown in Figure 2.5(a), with an in-span hinge provided at a distance of 30' from the centerline of pier 3 on span 3. The new bridge is a two-cell cast-in-place box girder with an overall depth of 8' and has a width of 14'4", as shown in Figure 2.5(b). The width of the closure slab is 2'10" and the thickness is 12". In the longitudinal direction, reinforcing bars were provided by 5 # 6 bars for both top and bottom reinforcement, and in the transverse direction, #5 reinforcing bars were provided at 6" spacing for both top and bottom reinforcement. A 2" concrete clear cover was provided for the top transverse and bottom longitudinal reinforcement. Note that, due to the rather short overhang of the existing deck, #6 dowels, staggered at 6" on centers, were used to connect the closure slab to the existing bridge, as shown by the closure slab details in Figure 2.6. Falsework release for the new bridge followed Alternative 2 of "Memo-to-Designers 9-3", with release sequence of span 1 first, followed by span 5, span 4, span

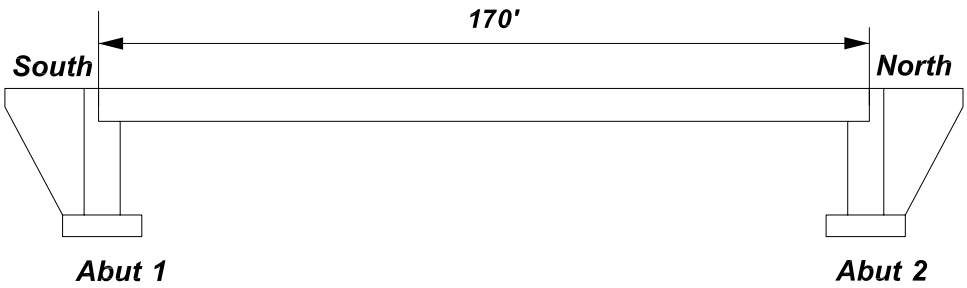


(a) Elevation view

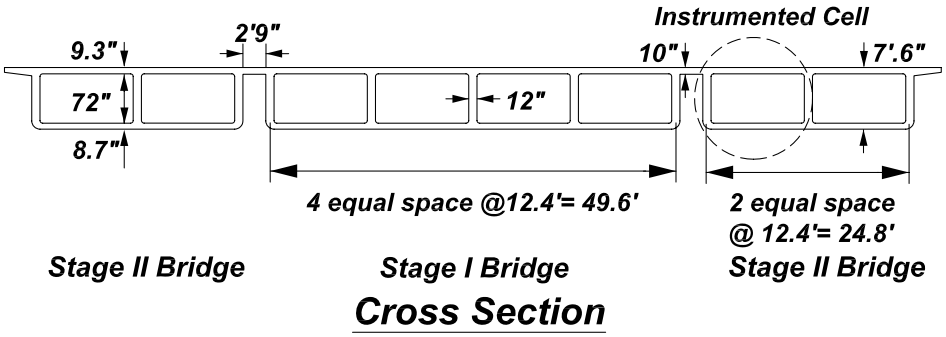


(b) Cross section view

Figure 2.2: Elevation and cross-sectional views of the Santa Rosa Creek Bridge

2 and span 3. It should be noted that, for a continuous bridge, the sequence of falsework release may affect the span deflection, as discussed later in this chapter.

### 2.2.3 Field Instrumentation

As previously noted, the simple span of the Santa Rosa Creek Bridge on stage II northbound structure and span 5 of the widening structure on the San Joaquin River Bridge were instrumented. Span 5 of the San Joaquin River Bridge was selected for instrumentation instead of span 3 (the longest span) due to access difficulty in span 3. Instrumentation setup, which is applicable to both bridges, is shown in Figure 2.8. As noted before, deformations were only measured in the new bridge on the assumption that the time-dependent incremental deflection of the existing bridge will be small compared to that of the newly constructed bridge. Sensors and data-acquisition system were installed inside the box-girder primarily for

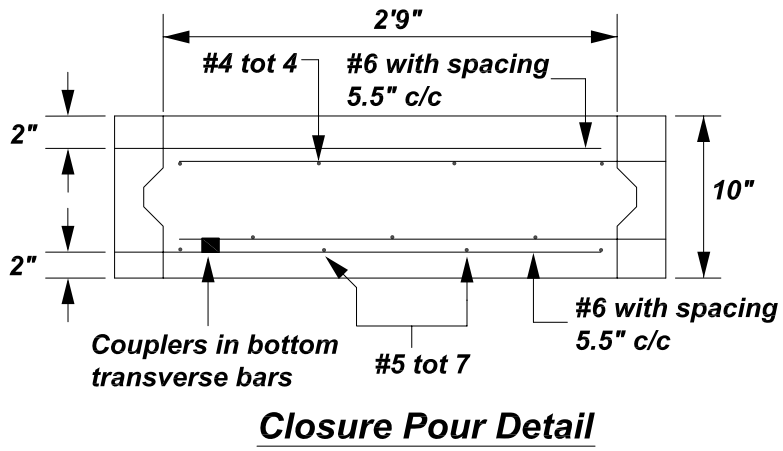


Figure 2.3: Closure pour details for the Santa Rosa Creek Bridge

Figure 2.4: San Joaquin River Bridge

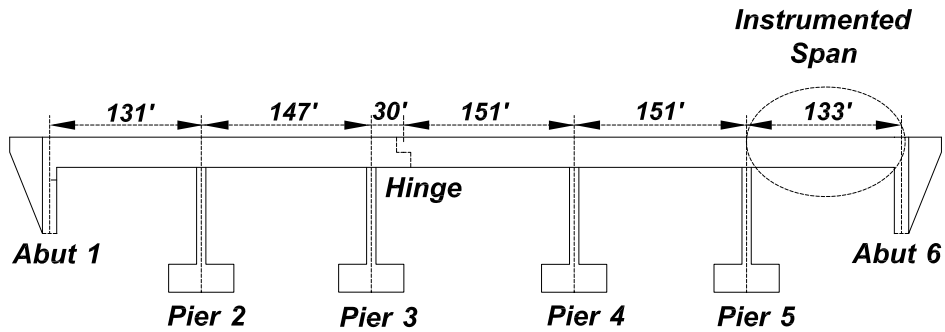


**Elevation**

(a) Elevation

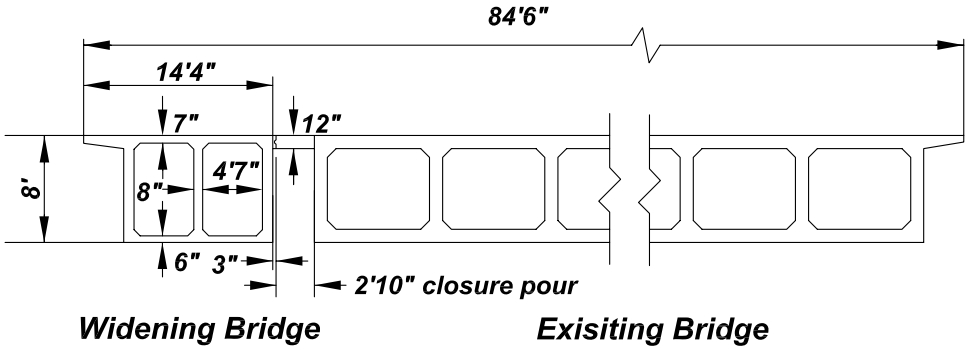


**Cross Section View**

(b) Cross-section

Figure 2.5: Elevation and cross-sectional views of the San Joaquin River Bridge

protection from weather, and security against unauthorized access and potential vandalism.

Seven linear potentiometers, equally spaced at $1/8^{th}$ span, were used to measure the span vertical deflection, and one linear potentiometer was used to measure the bridge longitudinal shortening. The distribution of displacement transducers is shown in Figure 2.7(a) and (b) for the Santa Rosa Creek Bridge and the San Joaquin River Bridge, respectively. Figures 2.8(a)-(e) show the instrumentation setup, including the access hole to the inside of the box-girder and the data acquisition system. For vertical deflection, the linear potentiometers were mounted on steel brackets, which were in turn bolted to the underside of the bridge deck. The tip of the linear potentiometer was attached to a steel wire, wrapped over a pulley and tensioned by a 600 lb weight at one end and anchored to the diaphragm wall at the other end, as shown in Figures 2.8(d) and (e). Assuming no relative vertical

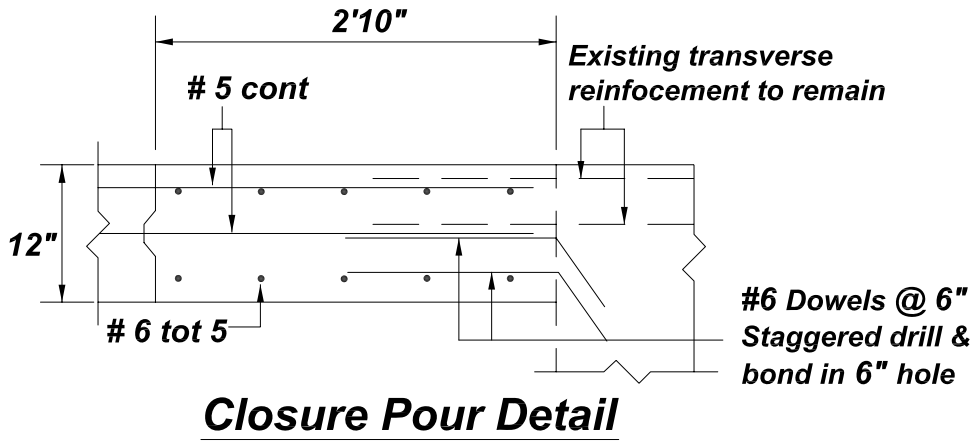


Figure 2.6: Closure pour details for the San Joaquin River Bridge

movement between the two diaphragm walls, the tensioned wire essentially served as a reference line, where displacement induced by span deflection was sensed by the set of linear potentiometers. For longitudinal shortening, the linear potentiometer was mounted on the bracket of the pulley system, as shown in Figure 2.8(e), with the tip of the linear potentiometer targeting 600 lb weight of steel plates. Longitudinal shortening between diaphragm walls resulted in the lowering of the weight, the displacement of which was readily measured by the linear potentiometer. Figure 2.8(f) shows the data acquisition system, provided by National Instrument CRIO 95, for automatic logging of vertical span deflection and longitudinal shortening. The data acquisition system was mounted on the web of the box-girder near the access hole for both bridges.

## 2.3 Field Results - Deflection and Shortening

### 2.3.1 The Santa Rosa Creek Bridge

Figure 2.9 shows the measured vertical deflection of the Santa Rosa Creek Bridge from 1 day to 345 days after full falsework release, where a negative value on the y-axis corresponds to a downward deflection. It can be seen that the vertical deflection due to the combined effects of dead load and prestressing is nearly symmetrical about its mid-span, which is somewhat expected in a simply-supported bridge. The instantaneous mid-span deflection after the full release of falsework was 1.52”. Subsequent time-dependent deformation of the bridge shows

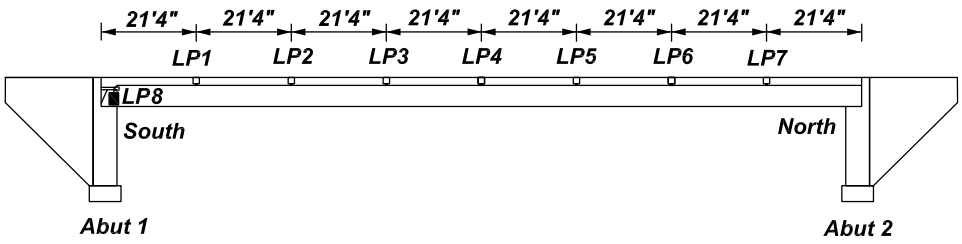


(a) Santa Rosa Creek Bridge

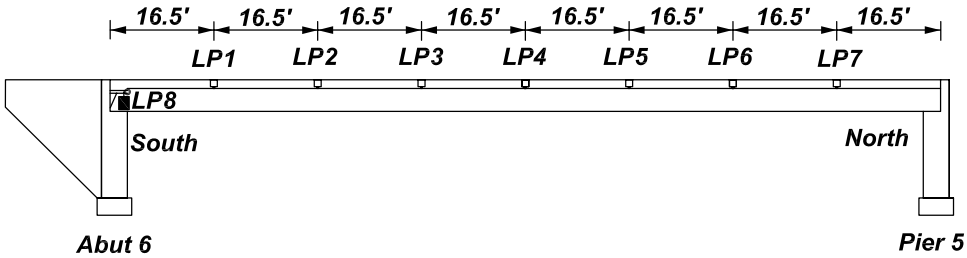


(b) San Joaquin River Bridge

Figure 2.7: Distribution of linear potentiometers

a general shape similar to the instantaneous deflected shape upon falsework release, with the largest deflection occurring at mid-span. This observation supports the notion that the time-dependent deflection may be estimated by multiplying the instantaneous deflection by a time deflection factor.

Figure 2.10 shows the plot of the mid-span deflection of the Santa Rosa Creek Bridge versus time starting from full falsework release up to about one year of monitoring. It can be seen from the figure that the mid-span deflection increased more rapidly during the initial stage, say up to 60 days, compared to the mid-span deflection at later stages. Figure 2.10 shows that the span deflection data was 'stuck' at a constant value of 2.16" from day 70 to day 160. Prior to the data being 'stuck', there was a relatively large increase in the measured mid-span deflection of about 0.11", indicating that the false reading might be due to a slip in the tensioned wire as the wire was wrapped over the pulley in a groove. The deflection data became 'unstuck' after 171 days, the day of the closure, as the new (stage II) bridge began to pick up vibration from the traffic on the existing (stage I) bridge. The data also shows a larger variation in deflection after closure compared to the deflection before closure, since

(a) Access hole

(b) Linear potentiometers

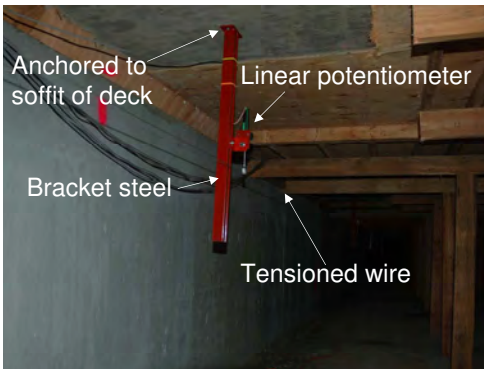


(c) Mounting bracket for linear potentiometers

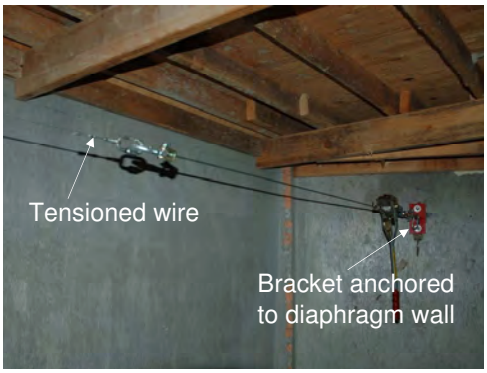


(d) Tensioned wire anchored to diaphragm wall

(e) Pulley system

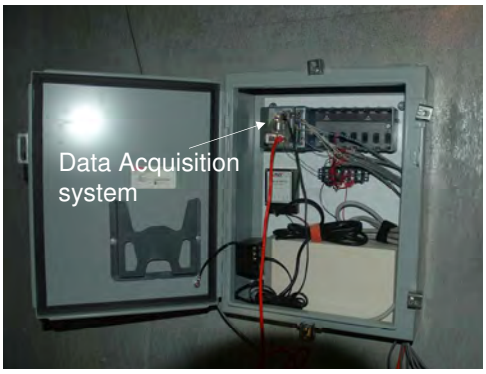


(f) Data acquisition system

Figure 2.8: Setup for field measurements of span deflection and shortening

the new bridge was opened to traffic soon after the closure pour was cast. The presence of live load on the stage II bridge caused an increase in the measured mid-span time-dependent deflection, as evident in the post-closure deflection data.

Figure 2.11 shows the longitudinal shortening of the Santa Rosa Creek Bridge over the same monitoring period of nearly one year. It should however be noted that the x-axis in the figure corresponds to the time after prestressing, which is not the same as the time after fully released falsework, as the operation of falsework release, initiated after prestressing, took about two days to complete. It can be seen from the figure that an 'instantaneous' shortening of about 1" was recorded after prestressing. The shortening of the bridge essentially followed the trend of the vertical deflection, with a large initial but diminishing shortening as time progressed. Overall the bridge shortened by 2.94" over the monitoring period of 347 days. It is worth noting that 2/3 of the shortening was developed in the initial 40 days after prestressing. Note that there was no loss of data in the longitudinal shortening data, unlike the vertical deflection data, since a slip in the tensioned wire in the pulley would not affect the sensing of the longitudinal shortening by the linear potentiometer.

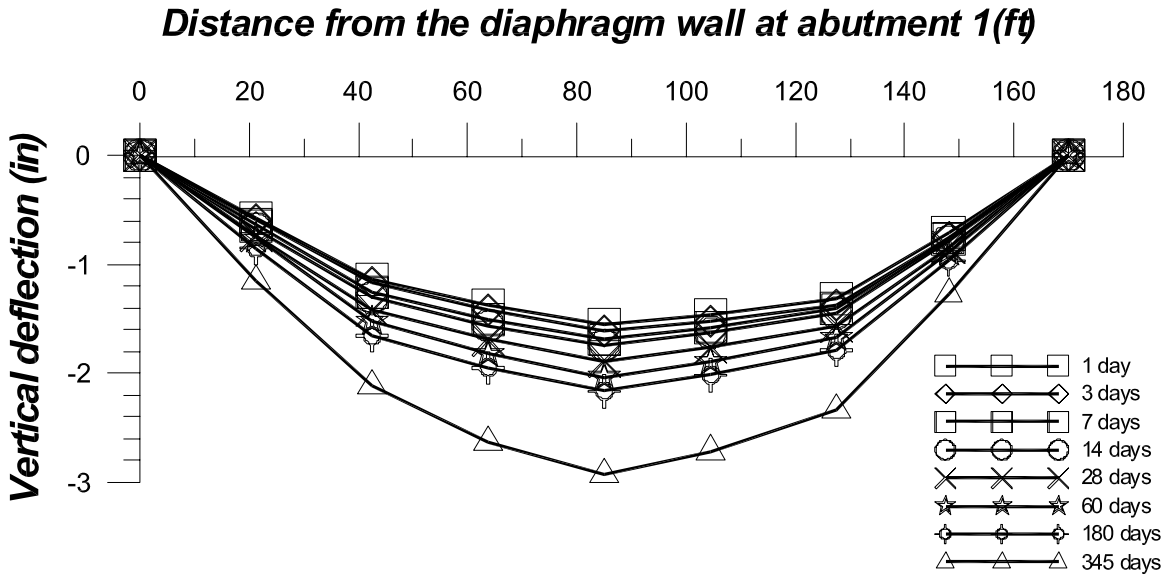


Figure 2.9: Deflected shapes of the Santa Rosa Creek Bridge

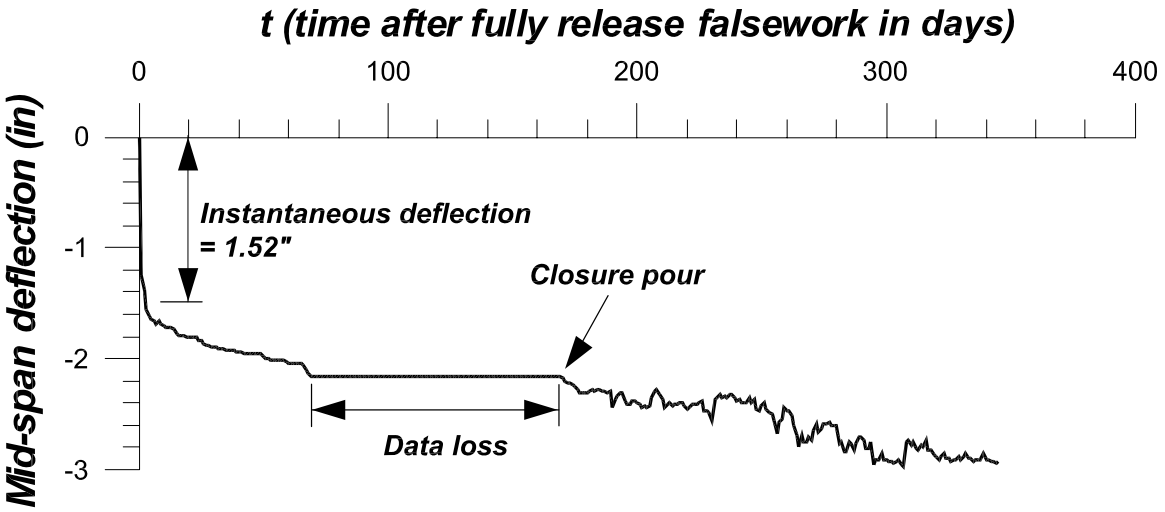


Figure 2.10: Mid-span time-dependent deflection of the Santa Rosa Creek Bridge

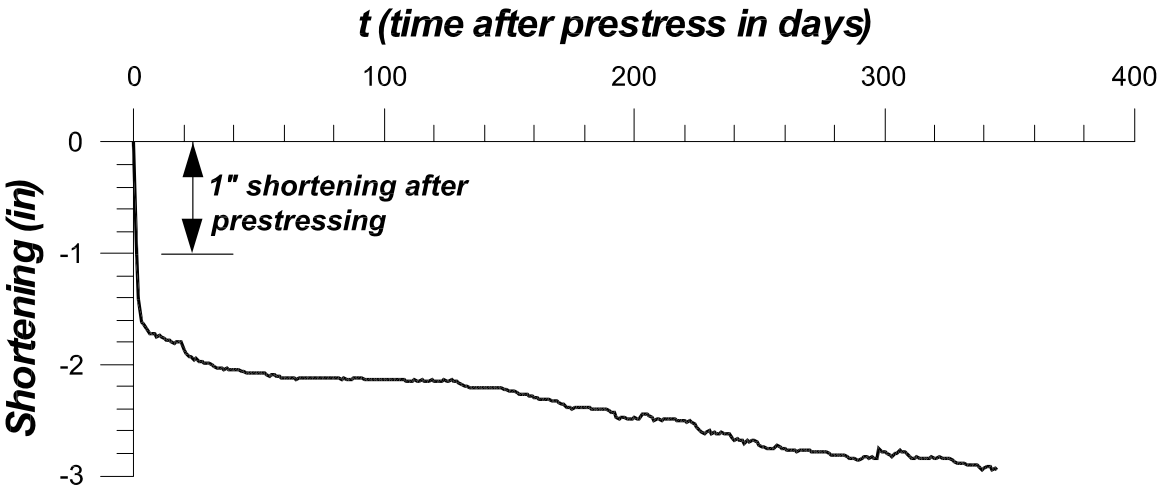


Figure 2.11: Longitudinal shortening of the Santa Rosa Creek Bridge

### 2.3.2 The San Joaquin River Bridge

Span 5, between pier 5 and abutment 6 of the San Joaquin River Bridge, and of length 133', was selected for time-dependent deformation measurement. The deflected shape of the span is shown in Figure 2.12 for a period of about 345 days from the falsework release of span 5. The x-axis corresponds to the distance from the diaphragm wall of abutment 6. It can be seen from Figure 2.12 that, unlike the Santa Rosa Creek Bridge, the deflected shape of span 5 was not symmetrical about its mid-span. A reversal in curvature was noted near pier 5 since the span was made continuous over the pier. Mid-span deflections of 0.56", 0.72" and 1.4" were measured at 1 day, 28 days, and 345 days after release of span 5 falsework.

For the San Joaquin River Bridge, the sequence of falsework release started with span 1, followed by spans 5, 2, 4 and 3. Since the structure was essentially continuous except for an in-span hinge in span 3, falsework release in span 5 as well as in adjacent spans, particularly span 4, affected slightly the measured deflection in span 5. Figure 2.13 shows a plot of the mid-span deflection of span 5 over time, where an instantaneous deflection of 0.56" was measured after full falsework release of span 5. Subsequent falsework release in span 2, being the second furthest span from span 5, did not cause any discernible deflection at mid-span of span 5. However, upon falsework release of adjacent span 4, which was 4 days after falsework release of span 5, a small uplift deflection of 0.01" was recorded at mid-span of span 5. Although the exact date of falsework release for span 3 was not known, its influence on the mid-span deflection of span 5 was not expected to be significant. It is worth noting that the normalization of span 5 deflection by its maximum deflection at different times provided a deflected shape that is nearly invariant with time.

Figure 2.14 shows the time-dependent longitudinal shortening of span 5 of the San Joaquin River Bridge. As the instrumented section of the San Joaquin River Bridge was constructed of conventional reinforced concrete box-girder, longitudinal shortening was significantly smaller compared to that of the prestressed Santa Rosa Creek Bridge. It can be seen from the figure that an initial shortening of about 0.3" occurred in the first 2 to 3 days after falsework release. In addition to shrinkage, the shortening was associated with the com-

pression of the box-girder under its self-weight since the tensioned wire system was installed in the compression region near the top deck of the box-girder. The plot in Figure 2.14 also shows that the longitudinal shortening follows a trend similar to the vertical deflection, with a noticeable influence from falsework release of adjacent span 4. A longitudinal shortening of 0.71" was measured at 345 days after falsework release of span 5.

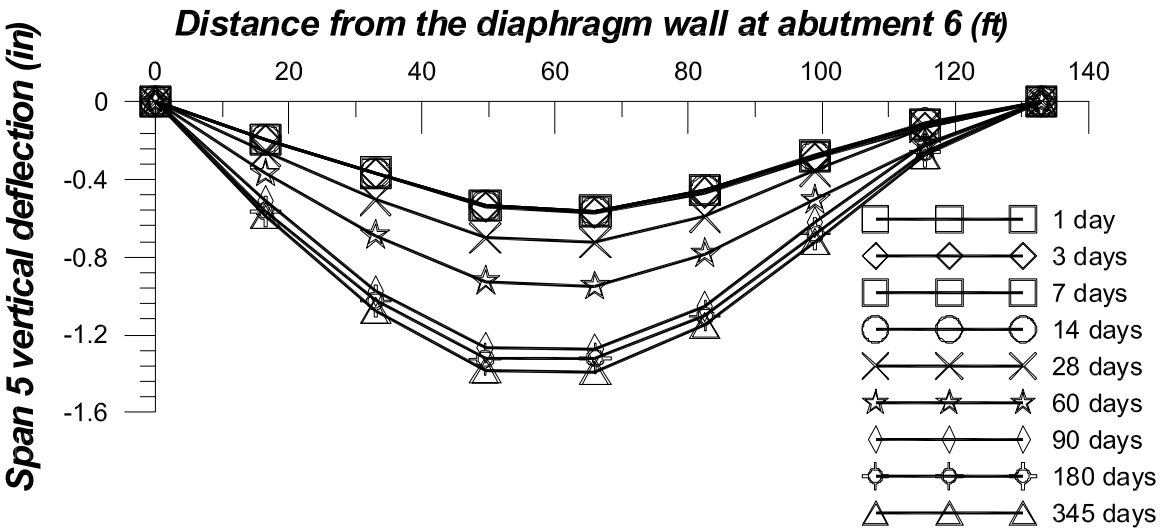


Figure 2.12: Deflected shapes of span 5 of the San Joaquin River Bridge

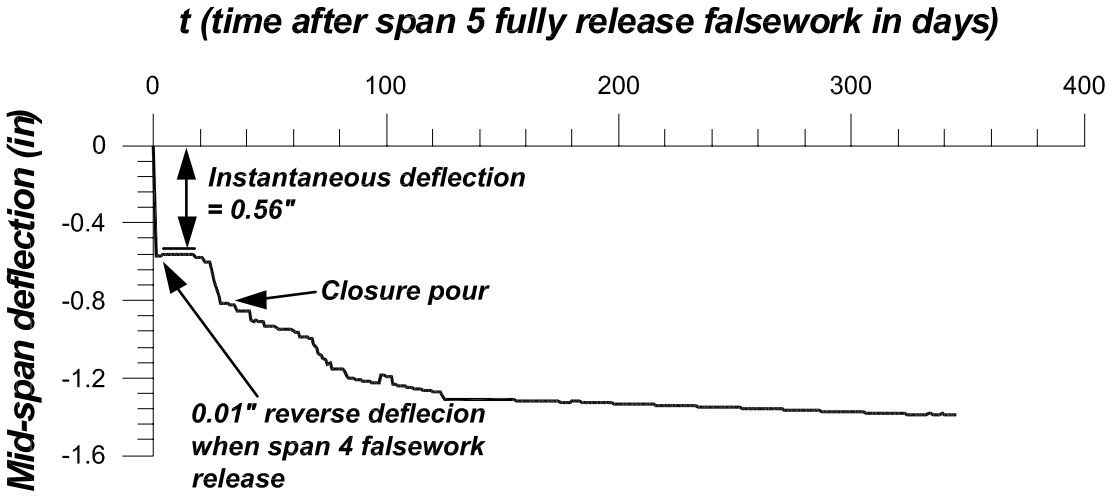


Figure 2.13: Mid-span deflection of span 5 versus time at San Joaquin River Bridge

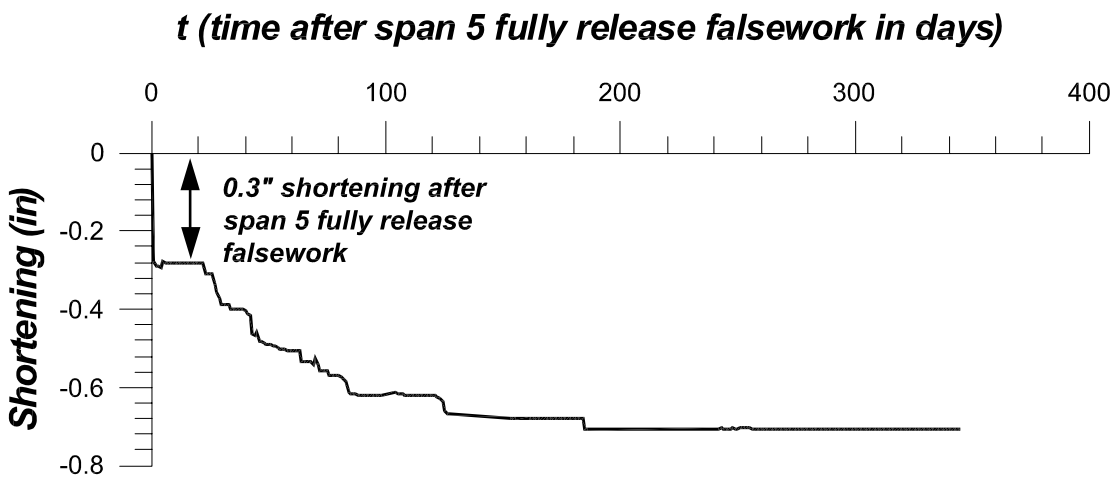


Figure 2.14: Longitudinal shortening of span 5 of the San Joaquin River Bridge

## 2.4 Comparison with Caltrans Deflection Curve

The two bridges selected for instrumentation were characterized by different bridge types and falsework release strategy, resulting in significantly different span deflections and longitudinal shortening. The Santa Rosa Creek Bridge was a simply supported, post-tensioned prestressed concrete bridge, with the contractor opting for Alternative 1 for falsework release [1], which provided a shorter waiting time for falsework release but required a longer waiting period for closure pour. In contrast, the San Joaquin River Bridge was a five-span conventional reinforced concrete bridge where the contractor opted Alternative 2 [1], which required a longer waiting time for falsework release but permitted a shorter waiting period for closure pour. Most notably, the Santa Rosa Creek Bridge registered an almost 3" mid-span deflection one year after falsework release while the San Joaquin River Bridge registered only about 1.4" mid-span deflection in the continuous end-span in almost the same period.

For comparison purposes, the measured mid-span deflections of the two bridges were normalized by their corresponding "instantaneous elastic" deflection following the full falsework release. Note that the "instantaneous elastic" deflection used for normalization is approximate in concept as it is affected by the duration of the falsework release since a complete release may require from a few hours to several days with potential creep and

shrinkage occurring in the release period. Figure 2.15 shows the normalized mid-span deflection of the two bridges, along with their comparisons with the theoretical deflection curve used by Caltrans. Although not directly applicable, as the normalized deflection curve in Memo-to-Designers 11-34 [3] was intended for prediction of the upward deflection of unloaded short cantilever in prestressed concrete box-girder bridges, the theoretical deflection curve is nonetheless plotted in the figure for comparison. It can be seen from the figure that the normalized deflections for the two bridges were quite different, even though both bridges were constructed of typical normal-weight concrete with 28-day design compressive strength in the range of 5000 psi. While many different factors were recognized to be at play, the different normalized deflection curves were likely due to the different ages of the concrete at the time of full falsework release. The falsework for the Santa Rose Creek Bridge was released at age of 12 days and took two days to accomplish a complete release, leading to a large measured 'elastic' deflection after full release falsework. This is in contrast to the San Joaquin River Bridge where the falsework of span 5 was released at age of 33 days and took less than one day to accomplish the complete release. Subsequent division of the measured deflection by the larger measured 'elastic' deflection resulted in the lower normalized time-dependent curve in Figure 2.15. It can also be seen from Figure 2.15 that the theoretical deflection curve by Caltrans [3] provided a fairly good estimate, albeit a slight over-estimation, of the normalized time-dependent vertical deflection of the San Joaquin River Bridge. In contrast, the current Caltrans deflection curve significantly over-estimated the deflection of the Santa Rosa Creek Bridge. The comparison highlighted the importance of incorporating the age of concrete at the time of full falsework release into the deflection prediction curve, and a single curve as implemented in Memo-to-designers 11-34 [3] is inadequate.

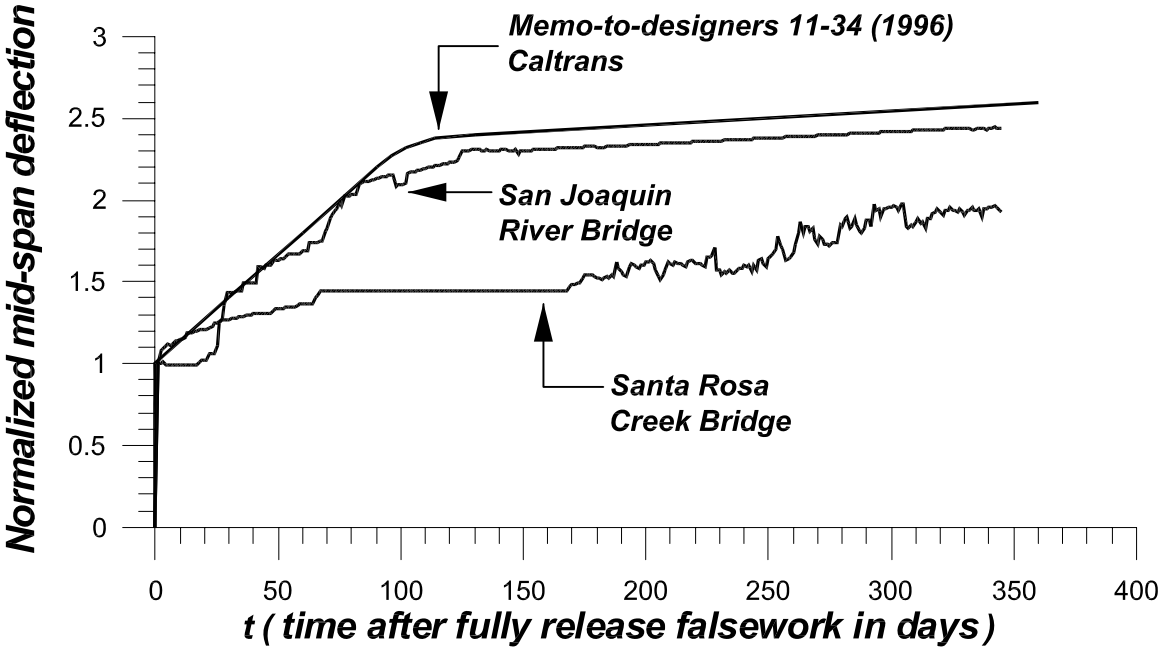


Figure 2.15: Normalized mid-span deflection

# Chapter 3

# Closure Slab Tests

## 3.1 Overview

Laboratory tests were conducted to investigate the behavior of closure slabs when exposed to differential displacement between existing and widening bridges. Main parameters in the test program included the closure slab width and thickness, reinforcement details as well as couplers for the reinforcement. Figure 3.1 shows the test region in typical widening of box-girder bridges. A differential displacement was imposed monotonically across the closure slab to simulate the stress build-up as a result of time-dependent differential deformation. Specimens were constructed full-size in an inverted U-shape, with the slab cast against the overhang of the web from the existing and widening bridges on both sides. Of interests from these tests were reinforcement strains at different levels of differential displacement, and their corresponding crack pattern, as well as the tolerable differential displacement before slab failure.

## 3.2 Specimen Details

Dimensions of closure slab specimens and their reinforcement are shown in Figures 3.2-3.5. The survey of closure slabs in 32 widening or staged construction, summarized earlier in Table 1.1, indicated that the closure slab length generally varies from 24" to 36" and an 8" thickness is common in California. The survey data, as well as the minimum length currently set by Caltrans at 18", provided guidance on the selection of the test specimen dimensions.

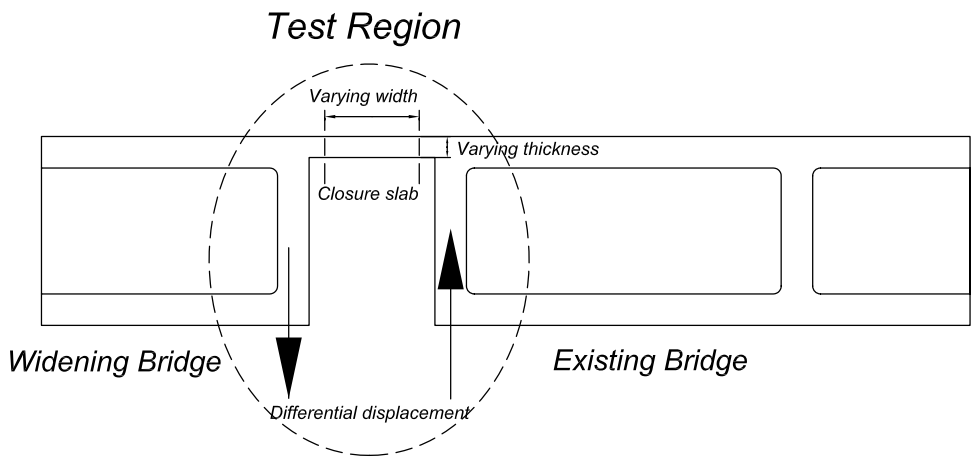


Figure 3.1: Test region for the closure slab

More specifically, three closure slab widths, namely 18", 24" and 36", were used in the test specimens. The closure slab width was defined here as the distance from the construction joint on one side of the slab to the construction joint to the other side, which meant the actual span of the specimen, which included 6" overhang from the web on both sides, was longer than the closure slab length. Three of the specimens had an 8" thickness, while one specimen had a 12" thickness. The decision on using a thickness of 8" for three slabs was made after consultation with Caltrans. The inclusion of a 12" thick slab in the test matrix allowed a comparison of the tolerable displacement limit for two different slab thicknesses, which would indirectly impact the waiting time for closure pour.

Table 3.1 summarizes the matrix for the laboratory tests, where the dimension of the slab specimen in the direction transverse to the bridge axis is referred to as the width, and the dimension in the direction of the bridge axis is referred as the length. Specimens were designated as CP36_8, CP24_8, CP18_8 and CP24_12, where the first numeral corresponded to the width of the closure slab in inches while the second numeral corresponded to the thickness of the slab in inches. For example, specimen CP36_8 represented a closure slab width of 36" and 8" thickness. The length of the specimen was maintained constant at 36" for all four specimens.

Reinforcement for the closure slabs were the same for all four specimens, as shown in Figures 3.2-3.5. Specifically, top and bottom reinforcement consisting of #6@6"c/c were

| Specimens | Width | Thickness | Length |
|---|---|---|---|
| CP36_8 | 36” | 8” | 36” |
| CP24_8 | 24” | 8” | 36” |
| CP18_8 | 18” | 8” | 36” |
| CP24_12 | 24” | 12” | 36” |

Table 3.1: Matrix for closure slab specimen tests

provided in the direction transverse to the bridge axis, while top reinforcement consisting of 4#3 and bottom reinforcement consisting of 4#4 were provided in the direction of the bridge axis. It should be noted that the bars in the direction transverse to the bridge axis were placed 6” from the edge for top bars, and 3” from the edge for bottom bars, in order to stagger the top and bottom reinforcement. Consequently, a total of 5#6 bars were provided in the top region and a total of 6#6 bars were provided in the bottom region of the specimen, resulting in 20% larger area in the bottom reinforcement. Lap-splices were provided in the top and bottom reinforcement in the transverse direction with overlapping bars terminating 2” short of the construction joint on either sides, giving a splice length equaled to the closure slab length minus 4”. In the case of specimen CP18_8 where the closure slab width was only 18”, proprietary couplers (Quick Wedge Couplers), were used to connect the top and bottom reinforcement. The two vertical webs, being not the test region of the specimen, were heavily reinforced to avoid any local failure. Web reinforcement were provided by #9 bars at 4” on-centers on the four faces of the web and by #3 closed-ties at 3” spacing. Heights of the widening and existing webs were 44” and 42” for all four specimens, as can be seen in Figures 3.2-3.5.

## 3.3 Material Properties and Specimen Construction

Normal-weight concrete with maximum aggregate size of 3/4” was used for all four specimens. Table 3.2 summarizes the mix design for the concrete, where a 28-day compressive strength of $f'_c = 5500$ psi was specified. The actual 28-day compressive strengths, summarized in Table 3.3, were 2% to 11 % higher than the target strength. A slump of 4” to 6” was

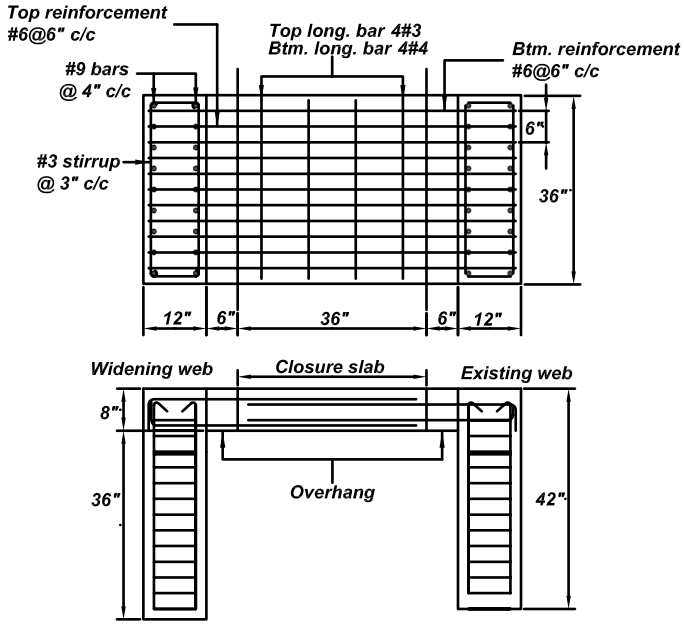


Figure 3.2: Specimen CP36_8 reinforcement details

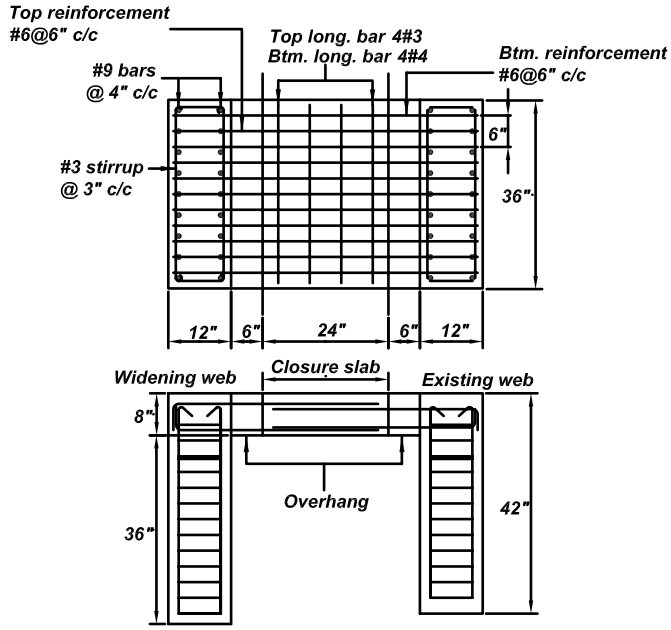


Figure 3.3: Specimen CP24_8 reinforcement details

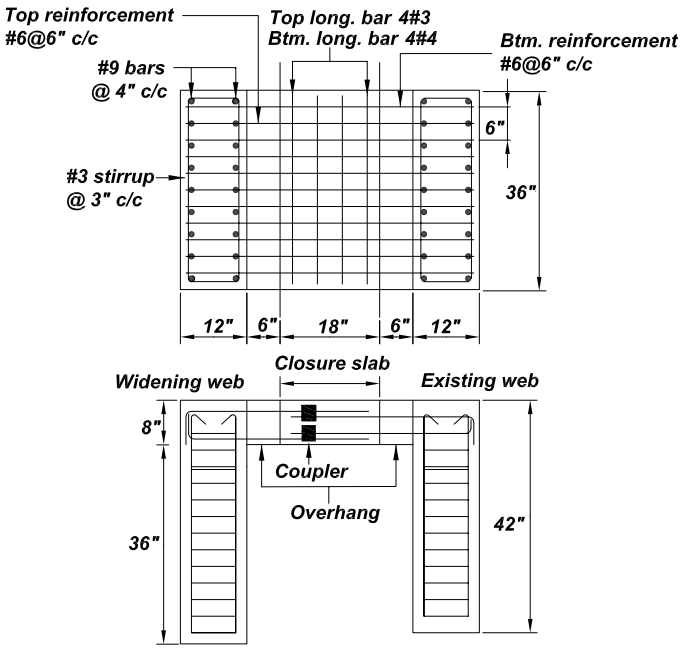


Figure 3.4: Specimen CP18_8 reinforcement details

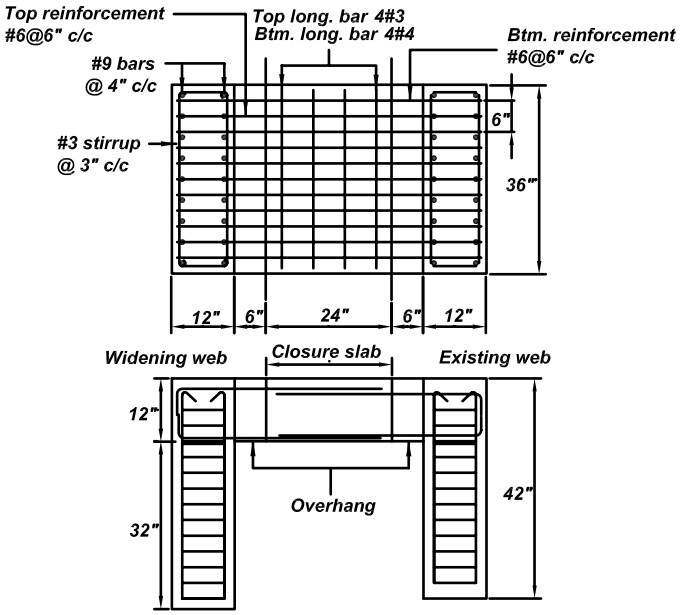


Figure 3.5: Specimen CP24_12 reinforcement details

| Constituents | Weight (lb/yd$^3$) |
|---|---|
| Cement (Type II) | 708 |
| Water | 340 |
| Coarse aggregate (3/4" max size) | 1620 |
| Fine aggregate (sand) | 1292 |

Table 3.2: Concrete mix design

| Specimens | Target compressive strength (ksi) | Actual compressive strength [1] (ksi) | % difference from target strength |
|---|---|---|---|
| CP36_8 | 5.5 | 5.6 | +2 |
| CP24_8 | 5.5 | 5.8 | +5 |
| CP18_8 | 5.5 | 5.9 | +7 |
| CP24_12 | 5.5 | 6.1 | +11 |

[1] based on average of two 6"×12" cylinders

Table 3.3: Concrete compressive strengths at 28 days

specified before concrete placement, and water was slowly added to achieve the target slump. All reinforcement were Grade 60 steel, with a yield strength of 64 ksi for #6 bars, based on the average of 4 tests. No tensile tests were carried for #4 and #3 bars, as these bars were secondary with their orientation in the non-loaded direction.

Test specimens were constructed in two stages, with stage I involving the casting of the two webs and the 6" overhang, followed by stage II which involved the casting of the closure slab against the overhang. Photographs in Figures 3.6(a)-(f) show the installation of strain gages on reinforcing bars, stage I construction of the webs and 6" deck overhang, rough finish in the cold joint at the overhang, formwork for closure slab in the upright casting position, lap-splicing of the main reinforcement in the closure slab, and smooth finish of the top surface of the closure slab. Closure slabs were cast 28 days after the webs and overhangs, and the specimens were tested at 112, 125, 129, and 143 days after the casting of the closure slab for CP36_8, CP24_8, CP18_8 and CP24_12, respectively.

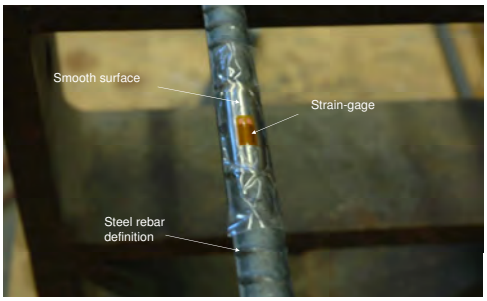


(a) Strain gage installation

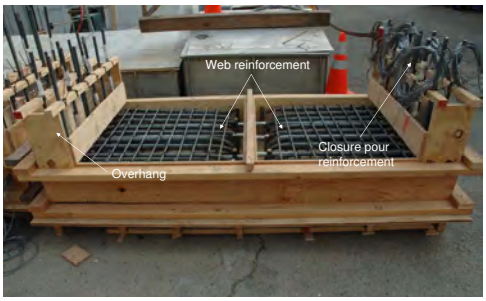


(b) Stage I construction - webs and 6” deck overhang

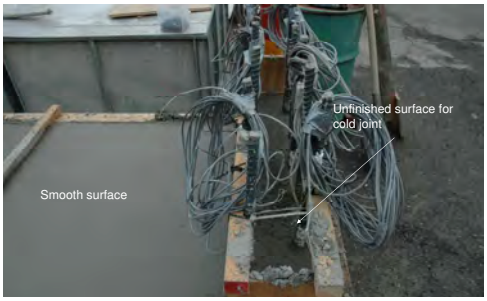


(c) Rough surface finish at cold joint of overhang

(d) Stage II construction - formwork for closure slab

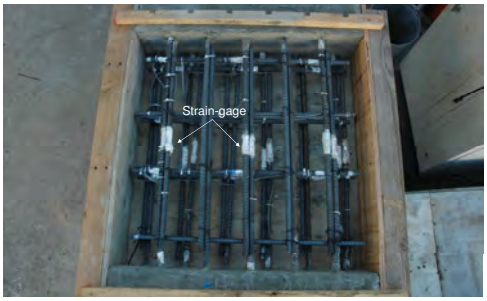


(e) Lap-splicing of main reinforcement in closure slab

(f) Smooth finish for top surface of closure slab

Figure 3.6: Instrumentation and specimen construction

## 3.4 Test Setup

An important consideration in the test setup was the provision of vertical differential displacement across the closure slab, assuming that the time-dependent deflection of the widening or stage II bridge was vertically downward without any significant rotation in the superstructure. The assumption was deemed reasonable as the flexural rigidity of the closure slab was typically small compared to the torsional rigidity of the superstructure. Figure 3.7 shows a schematic of the closure slab test setup. Differential displacement across the closure slab was imposed by a hydraulic actuator pulling up on the web identified as "existing" on the right in the figure. The pull force was transferred to the "existing" web via a set of steel rods threaded through PVC pipes cast in the web, and the steel rods were anchored at the bottom end with nuts and washers. The web identified as "widening" on the left was firmly bolted to a set of steel beams, which were in turn anchored to the laboratory strong floor. Four guide frames, two for each web, were used to ensure the verticality of the web during differential displacement. The steel frames guiding the moving web on the right were equipped with low-friction rollers with horizontal loadcells, while the steel frames on the non-moving web on the left were monitored with a set of horizontal loadcells. Loadcells together with the pull force measured in the actuator will enable the stress resultants on the closure slab to be determined. Inclinometer readings indicated that the rotation of the web was less than $1.2^\circ$ during testings of the four specimens. A photograph of the final test setup including the actuator, the loading frame, the test specimen, and guide frames is shown in Figure 3.8.

The pull force in the actuator was applied at a quasi-static rate with each test requiring over 5 or 6 hours to complete. The tests were also punctuated by frequent stops at predetermined levels for tracing and photographing of concrete surface cracks. During initial loading, stops were made at approximate strains from $250 \times 10^{-6}$ to $2250 \times 10^{-6}$ in $250 \times 10^{-6}$ increments by scanning the maximum reinforcement strain. Upon yielding of the reinforcement at critical sections, stops were made at approximately 0.2" increments in all specimens except in specimen CP24_12, where the closure slab failed soon after reinforcement yielding. Data was logged at 0.5 kips increment of the actuator force or at differential

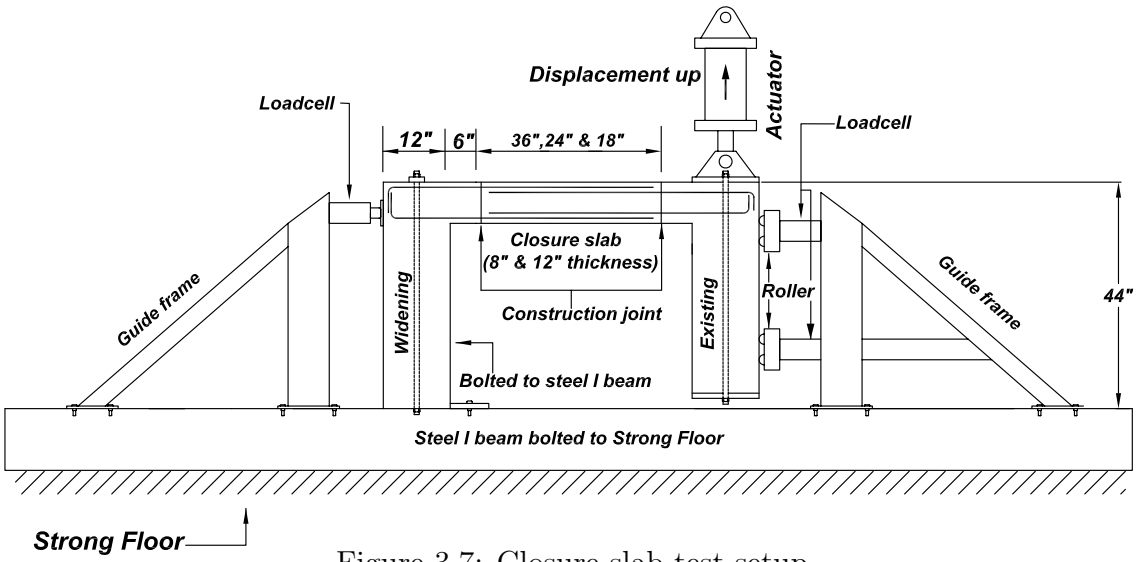


Figure 3.7: Closure slab test setup

displacement increment of 0.05", whichever was smaller.

## 3.5 Test Results

### 3.5.1 Load-Differential Displacement Response

Conceptually, the waiting time before closure pour may be determined on the basis of the remaining differential displacement that will occur in the future across the closure slab and the tolerable displacement limit given a certain closure slab width, thickness and reinforcement details. Thus a good estimate of the displacement capacity of the closure slab is of significance when determining the waiting period for closure pour.

Figure 3.9 shows the pull force versus the differential displacement of the specimen for the four tests. The y-axis in the figure corresponds to the pull force as applied to the "existing" web, while the x-axis corresponds to the vertical displacement measured at the location where the top concrete surface intersected the vertical inside plane of the "existing" web. Since the "widening" web had been assumed to be non-moving, the vertical displacement measured in the "existing" web was taken as the differential displacement imposed across the closure slab. It should also be noted that the differential displacement plotted in the figure corresponded to the average of two linear potentiometers in order to factor out any

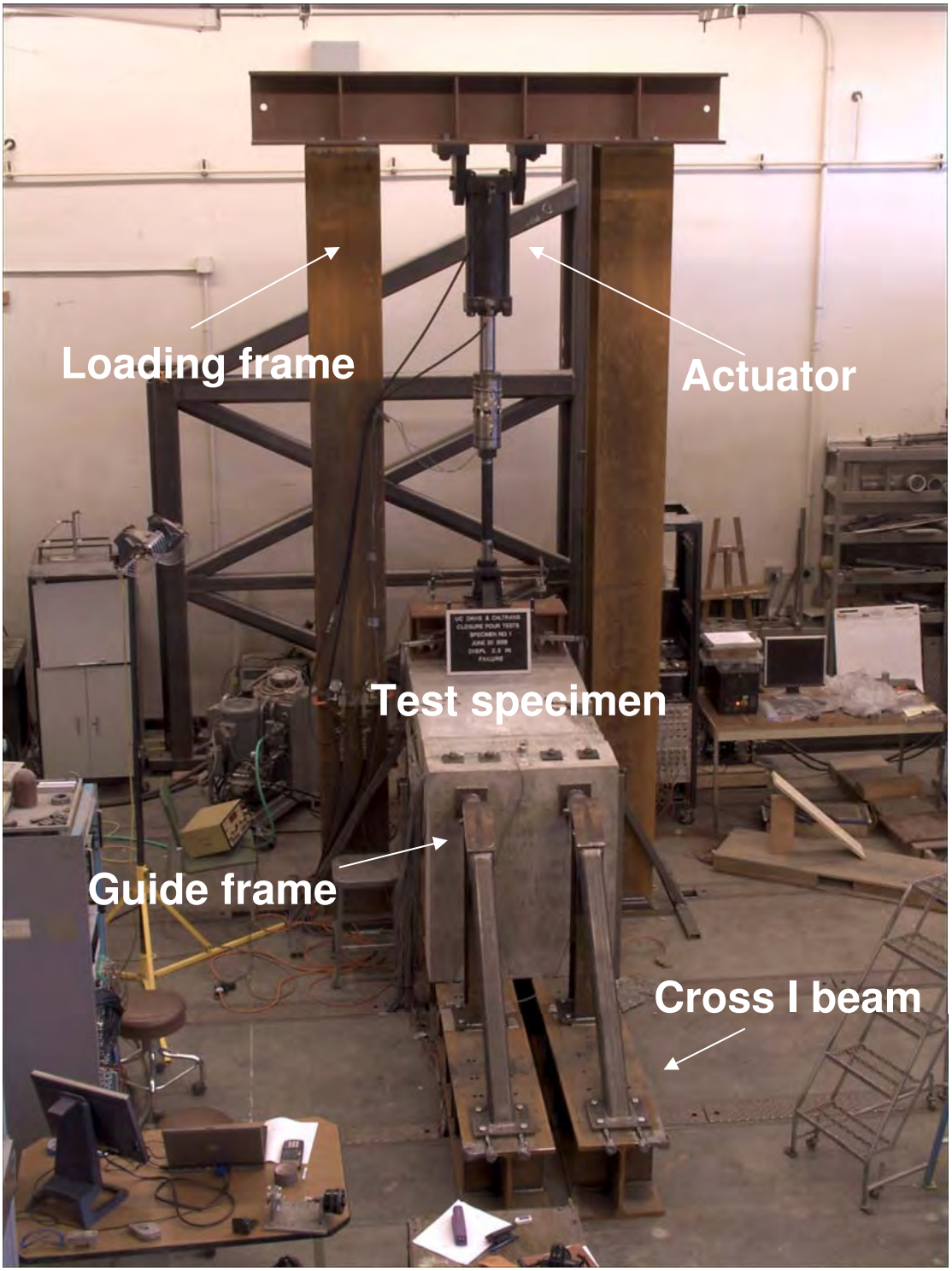


Figure 3.8: Final test setup

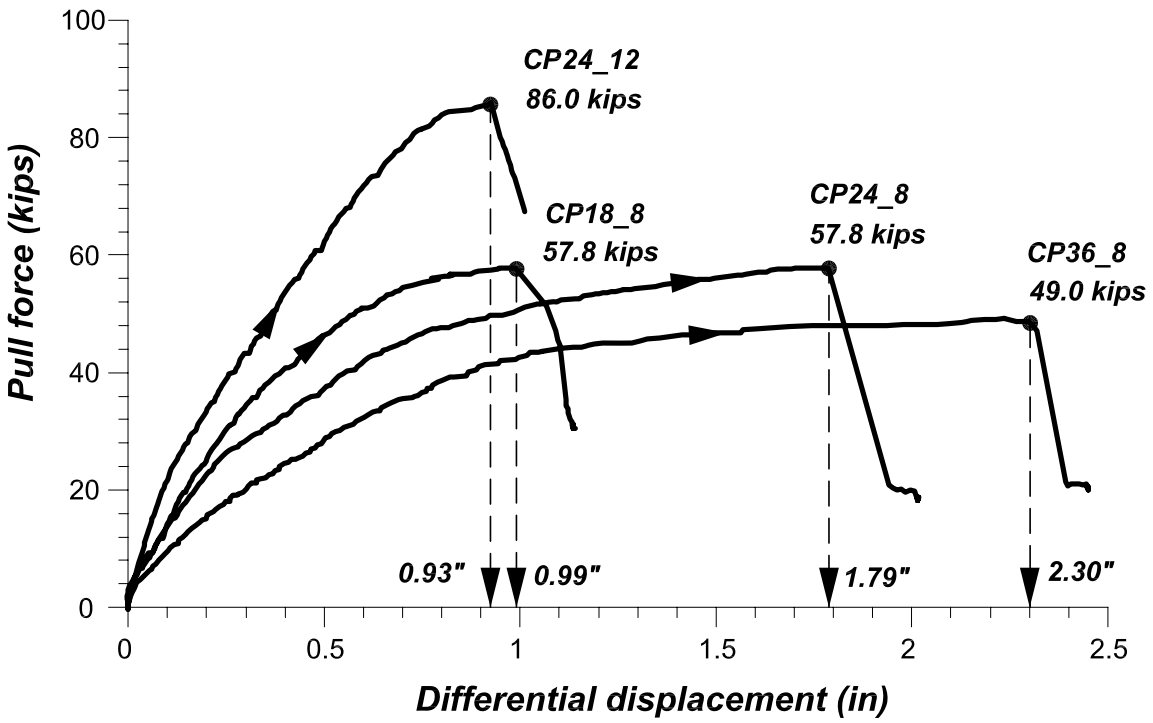


Figure 3.9: Force-differential displacement curves of closure slab specimens

twisting component in the closure slab, which was noted to be small during testing. It can be seen from Figure 3.9 that the four specimens were characterized by rather distinct load-displacement curves. Specimen CP36_8, having the widest width and a smaller thickness, exhibited the smallest stiffness among the four specimens, which was to be expected. At approximately 1" differential displacement, there was a noticeable flattening of the pull force primarily due to yielding of the reinforcement at critical sections. Specimen CP36_8 eventually registered a maximum pull force of 49.0 kips at a displacement very close to the ultimate displacement of 2.3". Final failure of the specimen was brittle and was precipitated by a major inclined flexural-shear crack initiated at the bottom corner of the slab where the deck overhang and the "existing" web intersected. The inclined flexural shear crack propagated at an angle of 20° relative to the horizon through the thickness of the slab. Photographs in Figure 3.10(a) show a side-view and a top-view after failure of specimen CP36_8.

The reduction of closure slab width to 24" in specimen CP24_8 resulted in an increase in the vertical stiffness and the maximum force, but a reduction in ultimate displacement, as

Side-view

Top-view

(a) Specimen CP36_8

Side-view

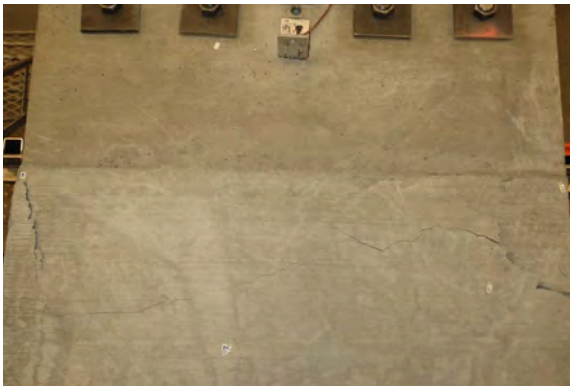

Top-view

(b) Specimen CP24_8

Figure 3.10: Final failure of test specimens

can be seen in Figure 3.9. Strain gage data indicated that the reinforcement in the specimen proceeded to yield at a differential displacement of 0.95", which corresponded to a pull force of 50 kips. Final failure of CP24_8 occurred at an ultimate displacement of 1.79" with a maximum pull force of 57.8 kips. The ultimate displacement was about 22% lower than that of the wider specimen CP36_8. The failure mode of CP24_8 was brittle, very similar to that of CP36_8, in that a major inclined flexural-shear crack, initiated at the bottom corner of the "existing" web, propagated rapidly through the slab. Photographs in Figure 3.10(b) show two views of the final failure of specimen CP24_8.

The third specimen, CP18_8, corresponded to the narrowest closure slab width currently used by Caltrans. As expected, the specimen showed the largest initial stiffness among the three slabs of the same thickness, as can be seen in Figure 3.9. Measured strain data indicated first-yielding of the main reinforcement occurred at a differential displacement of about 0.50" with a corresponding force of 45 kips. Brittle shear failure occurred at a differential displacement of 0.99", and was similarly precipitated by a major inclined flexural-shear crack as shown in the photographs in Figure 3.10(c). The ultimate displacement of 0.99" was only 43% that of specimen CP36_8 and 55% that of specimen CP24_8. It is of interest to note that the maximum pull force resisted by specimen CP18_8 was the same as that of specimen CP24_8, which was 57.8 kips.

With an increased thickness to 12", specimen CP24_12 showed a significant increase in the initial stiffness and maximum pull force, as can be seen in Figure 3.9. The brittleness of specimen CP24_12 was evidenced by the general lack of a yield plateau in the force-displacement curve, where the specimen failed suddenly soon after first-yielding of the main reinforcement. Specimen CP24_12 registered a maximum pull force of 86.0 kips at an ultimate displacement of 0.93". Compared to the specimen of a lesser thickness, i.e. CP24_8, the increase in thickness in specimen CP24_12 resulted in a 48% reduction in differential displacement capacity. Although quite limited in the number of tests, it is evident that a larger differential displacement capacity can be expected to result from a wider width and a thinner closure slab. It is thus recommended that, for closure slabs with width in the range of 18" to "36" (excluding deck overhang from the web), a thickness of 8" be adopted with

Side-view

Top-view

(c) Specimen CP18_8

Side-view

Top-view

(d) Specimen CP24_12

Figure 3.10: Final failure of test specimens (cont.)

reinforcement details following that of the slabs tested. Photographs in Figure 3.10(d) show a side-view and a top-view after failure of specimen CP24_12.

### 3.5.2 Bending Moment and Shear Force Distributions

For stress analysis in the closure slab, stress resultants in terms of bending moment and shear force at critical sections of the slab were calculated from loadcell readings. Since the test setup was identical for all four specimens, the bending moment and shear force imposed on the slab were similar. Figure 3.11 shows the expected bending moment distribution and shear force distribution acting on the test slab, ignoring the self-weight, when subjected to a differential displacement across the slab. The maximum positive moment $M_4$ and the

maximum negative moment $M_1$ corresponded to the moment acting at the intersection of the deck overhang with the web, while moments $M_2$ and $M_3$ corresponded to the bending moment at the construction joint between the closure slab and deck overhang. The shear force $V$, which was constant, corresponded to the slope of the bending moment distribution.

Tables 3.4-3.7 summarize the bending moments, $M_1$ to $M_4$, and the shear force $V$, at increasing magnitude of differential displacements across the closure slab for all four specimens. Although the theoretical bending moment distribution was expected to be anti-symmetric, with the magnitude of $M_1$ equaled to the magnitude of $M_4$, and the magnitude of $M_2$ equaled to the magnitude of $M_3$, actual bending moments, which were deduced from loadcell readings, deviated from the theoretical distribution, particularly at small differential displacements. For example, at the small differential displacement of 0.06" for specimen CP36_8 in Table 3.4, magnitudes of $M_1$ and $M_2$ were 15 kip.in and 21 kip.in, respectively, and these moments were correspondingly smaller than $M_4$ and $M_3$, which were 279 kip.in and 242 kip.in, respectively. The lack of symmetry in bending moments suggested that, despite a best attempt at ensuring verticality in the web displacement using low friction rollers as guides, rotation nonetheless occurred at the existing web end, causing a relaxation and hence a reduction in the magnitude of moment $M_1$ and $M_2$. At larger differential displacements, however, bending moments at the two ends showed better correlation. For instance, at the differential displacement of 2.30" for specimen CP36_8 in Table 3.4, the difference in bending moments was about 7% for $M_1$ and $M_4$ while the difference in bending moments was 9% for $M_2$ and $M_3$. It can also be seen from Tables 3.4 and 3.5 that the trend for bending moments was similar for specimens CP36_8 and CP24_8. On the other hand, the trend for bending moments in Tables 3.6 and 3.7 for specimens CP18_8 and CP24_12 was opposite in that of specimens CP36_8 and CP24_8 in that the bending moment was smaller at the widening web end than that at the existing web end, indicating that the widening web was likely to be experiencing a larger rotation than the existing web end. The shear force calculated from the slope of the bending moment diagrams matched reasonably well with the pull force when small differential displacement was applied to the closure slab. However, under a large differential displacement, the shear force was slightly larger than the pull force.

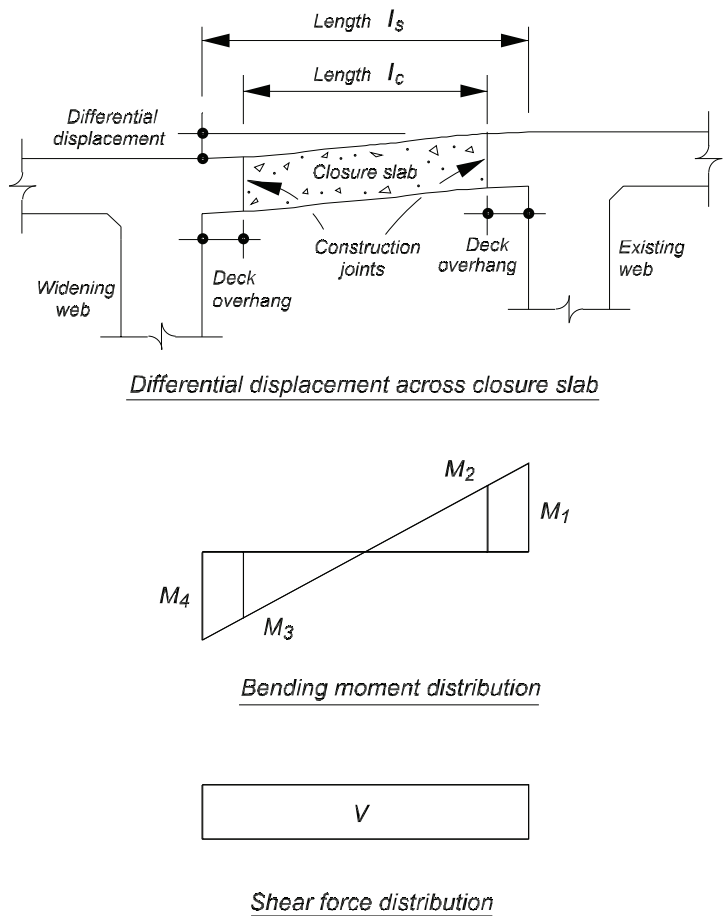


Figure 3.11: Bending moment and shear force distributions in the closure slab

The difference between the calculated shear force and the pull force mainly came from that the large differential displacement and the horizontal reaction forces from rollers resulted in an additional moment applied to the closure slab.

### 3.5.3 Reinforcement Strain Distributions

Since concrete cracking is directly related to the reinforcement strain, plots of reinforcement strain distributions provide an indication of the extent and severity of damage in the closure slab at different levels of differential displacements. Figures 3.12(a)-(f), 3.13(a)-(f), 3.14(a)-(f), and 3.15(a)-(f) show the strain distributions measured in three top and three bottom bars in specimens CP36_8, CP24_8, CP18_8, and CP24_12, respectively. For identification purposes, bars were labeled by the first letter T for top bars and B for bottom bars. The

| Differential displacement (in) | $M_1$ (kip-in) | $M_2$ (kip-in) | $M_3$ (kip-in) | $M_4$ (kip-in) | $V$ (kips) |
|---|---|---|---|---|---|
| 0.06 | -15 | 21 | 242 | 279 | 6.1 |
| 0.13 | -126 | -59 | 346 | 414 | 11.3 |
| 0.20 | -229 | -135 | 426 | 519 | 15.6 |
| 0.28 | -330 | -212 | 501 | 620 | 19.8 |
| 0.43 | -492 | -336 | 599 | 754 | 26.0 |
| 0.55 | -626 | -441 | 665 | 849 | 30.7 |
| 0.73 | -774 | -556 | 747 | 965 | 36.2 |
| 0.83 | -866 | -625 | 824 | 1066 | 40.3 |
| 1.07 | -983 | -723 | 840 | 1100 | 43.4 |
| 1.24 | -1030 | -752 | 918 | 1196 | 46.4 |
| 1.50 | -1094 | -810 | 895 | 1179 | 47.3 |
| 2.30 | -1180 | -874 | 963 | 1270 | 50.9 |

Table 3.4: Bending moments and shear force at critical sections of specimen CP36_8

| Differential displacement (in) | $M_1$ (kip-in) | $M_2$ (kip-in) | $M_3$ (kip-in) | $M_4(kip-in)$ | $V$ (kips) |
|---|---|---|---|---|---|
| 0.04 | -27 | 17 | 193 | 237 | 7.3 |
| 0.05 | -63 | -6 | 218 | 274 | 9.3 |
| 0.12 | -164 | -71 | 297 | 389 | 15.3 |
| 0.21 | -292 | -151 | 408 | 548 | 23.3 |
| 0.36 | -469 | -282 | 463 | 650 | 31.1 |
| 0.41 | -511 | -315 | 470 | 666 | 32.7 |
| 0.48 | -582 | -365 | 503 | 720 | 36.1 |
| 0.57 | -715 | -470 | 510 | 755 | 40.8 |
| 0.67 | -778 | -512 | 554 | 820 | 44.4 |
| 0.80 | -849 | -562 | 586 | 873 | 47.8 |
| 0.96 | -897 | -599 | 594 | 892 | 49.7 |
| 1.11 | -925 | -613 | 635 | 946 | 51.9 |
| 1.31 | -973 | -641 | 686 | 1018 | 55.3 |
| 1.79 | -1011 | -649 | 798 | 1160 | 60.2 |

Table 3.5: Bending moments and shear force at critical sections of specimen CP24_8

| Differential displacement (in) | $M_1$ (kip-in) | $M_2$ (kip-in) | $M_3$ (kip-in) | $M_4$ (kip-in) | $V$ (kips) |
|---|---|---|---|---|---|
| 0.04 | 30 | 68 | 183 | 223 | 6.4 |
| 0.05 | 39 | 88 | 233 | 282 | 8.1 |
| 0.08 | 10 | 81 | 293 | 364 | 11.8 |
| 0.11 | -72 | 17 | 287 | 376 | 14.9 |
| 0.15 | -101 | 15 | 363 | 479 | 19.4 |
| 0.19 | -200 | -57 | 365 | 506 | 23.5 |
| 0.26 | -320 | -136 | 407 | 589 | 30.3 |
| 0.33 | -381 | -166 | 461 | 672 | 35.1 |
| 0.41 | -515 | -265 | 457 | 700 | 40.5 |
| 0.50 | -643 | -359 | 458 | 734 | 45.9 |
| 0.59 | -753 | -430 | 488 | 798 | 51.7 |
| 0.70 | -859 | -509 | 470 | 803 | 55.4 |
| 0.99 | -903 | -523 | 519.9 | 876 | 59.2 |

Table 3.6: Bending moments and shear force at critical sections of specimen CP18_8

| Differential displacement (in) | $M_1$ (kip-in) | $M_2$ (kip-in) | $M_3$ (kip-in) | $M_4$ (kip-in) | $V$ (kips) |
|---|---|---|---|---|---|
| 0.06 | -128 | -36 | 332 | 424 | 15.3 |
| 0.09 | -261 | -136 | 361 | 487 | 20.8 |
| 0.15 | -429 | -266 | 385 | 551 | 27.2 |
| 0.26 | -683 | -445 | 504 | 750 | 39.8 |
| 0.34 | -803 | -527 | 568 | 853 | 46.0 |
| 0.37 | -867 | -561 | 653 | 971 | 51.0 |
| 0.43 | -995 | -658 | 674 | 1026 | 56.1 |
| 0.48 | -1098 | -732 | 715 | 1101 | 61.1 |
| 0.56 | -1242 | -830 | 796 | 1234 | 68.8 |
| 0.63 | -1346 | -902 | 849 | 1325 | 74.1 |
| 0.68 | -1428 | -961 | 878 | 1382 | 78.0 |
| 0.75 | -1530 | -1033 | 922 | 1461 | 83.1 |
| 0.93 | -1616 | -1090 | 972 | 1547 | 87.8 |

Table 3.7: Bending moments and shear force at critical sections of specimen CP24_12

bar location is identified in the slab cross-section in the figures. Strains were plotted for increasing differential displacement amplitude up to failure of the slab, with the strain plotted as positive for tension and negative for compression.

#### 3.5.3.1 Specimen CP36_8

Figures 3.12(a), (c) and (e) show the strain distributions in the three top bars - T1, T2 and T3 - of specimen CP36_8 for differential displacement from 0.06" to 2.30". It can be seen from these figures that the strain distributions were similar in all three bars as these bars were positioned at the same height in the slab. Large tensile strains were measured in the top region between the existing web to the construction joint, and these strains were due to the negative bending moment imposed in this region. The first top concrete surface cracking was noted at a differential displacement of 0.20". The largest corresponding tensile strain in the reinforcement was $527 \times 10^{-6}$, and was measured in bar T3. The reinforcement strain was significantly higher than the typical concrete cracking strain, expected to be in the range of $250 \times 10^{-6}$, indicating that visual identification of concrete cracking had likely missed the first true appearance of the concrete surface crack.

Upon differential displacement to 0.83", the tensile strain measured by gage T1_2 reached $2800 \times 10^{-6}$ which was larger than the yield strain of the reinforcement, estimated to be $2300 \times 10^{-6}$. Further differential displacement to 1.06" resulted in more gages, T1_1, T1_2, T2_1 and T3_1 registering strains greater than the yield strain of the reinforcement. Note that yielding of the reinforcement was consistent with the flattening of the load-deflection curve at differential displacement of 1". For differential displacement greater than 1", tensile strains measured by gages T1_1, T2_1 and T3_1 increased dramatically. For example, the strain measured by gage T3_1 increased from $2752 \times 10^{-6}$ to $11822 \times 10^{-6}$, i.e. about 430% increase, when the differential displacement was increased from 1.06" to 1.50". At the failure differential displacement of 2.30", strains measured by gages T1_1, T2_1 and T3_1 exceeded the operating range of the gage, estimated to be $\approx 20000 \times 10^{-6}$. Compressive strains were measured in the top reinforcement in the vicinity of the widening web, but these strains were small compared to measured tensile strains, as expected. For example, at a differential

displacement of 2.30" where failure occurred, measured compressive strains were all less than $-1000 \times 10^{-6}$, which was less than 1/2 of the yield strain of the reinforcement or less than 1/3 of the ultimate compressive strain of concrete used in flexural strength design.

Figures 3.12(b), (d) and (f) show the bottom reinforcement strains for specimen CP36_8 for differential displacement from 0.06" to 2.30". High tensile strains were similarly measured in the bottom bars in the region between the widening web and the construction joint. Although the pattern of tensile strains in the bottom bars was similar to that of the top bars, actual magnitudes were lower than that of the top bars at the same differential displacement. For example, at a differential displacement of 0.83", the tensile strain measured by the top gage T3_1 was $2237 \times 10^{-6}$ while the tensile strain measured by the bottom gage B3_6 was $2024 \times 10^{-6}$; less than 10% difference in the two strain readings. The lower tensile strain in the bottom bars was likely due to the higher percentage of reinforcement area, about 20% more as noted earlier, in the bottom steel compared to the top steel. Compressive strains were measured in the bottom reinforcement, similar to the top reinforcement, in the region near the existing web. Compressive strains in the bottom reinforcement were all less than $-1000 \times 10^{-6}$ even at the failure differential displacement of 2.30".

#### 3.5.3.2 Specimen CP24_8

Strain distributions for specimen CP24_8 are plotted in Figures 3.13(a)-(f) for different levels of differential displacement from 0.04" to 1.79". Note that three gages, namely T2_1, B3_1 and B3_2, were not plotted in Figures 3.13(c) and 3.13(f) as these gages were damaged during construction. It can be seen in these figures that the strain distributions in specimen CP24_8 were similar to specimen CP36_8 with large tensile strains measured in the top and bottom reinforcement in the region of overhang on both existing and widening webs. The large tensile strains corresponded to the large negative and positive moments in these two regions. More specifically, at a differential displacement of 0.67", tensile strains measured by gages T2_1 and B1_6 were $\approx 2000 \times 10^{-6}$, which was close to the yield strain of the reinforcement, estimated to be $2300 \times 10^{-6}$. Upon differential displacement increase to 0.8", strain readings in gages T3_1, B1_6 and B3_6 quickly jumped from $2000 \times 10^{-6}$ to almost

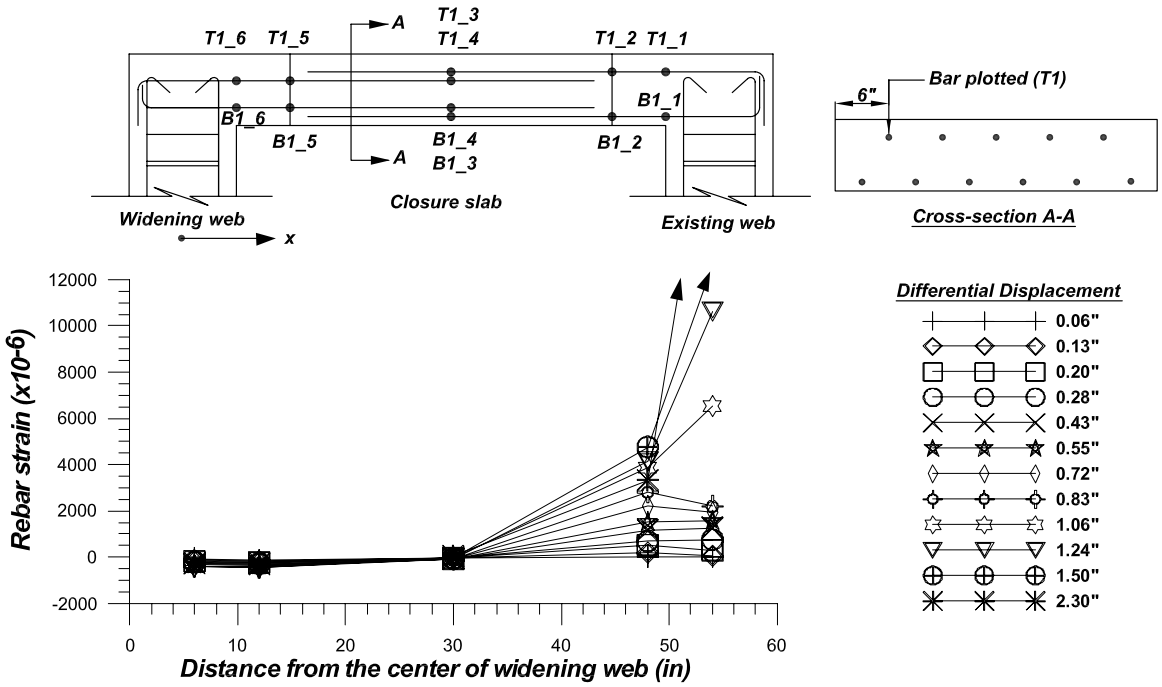


(a) Top bar T1

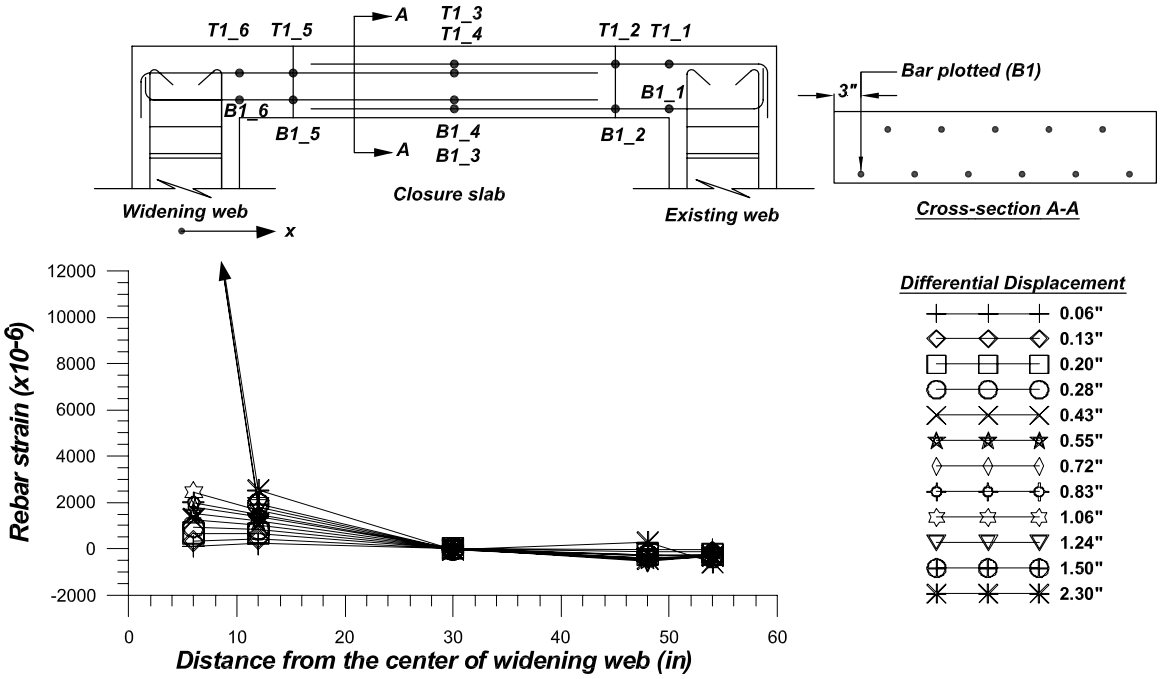


(b) Bottom bar B1

Figure 3.12: Specimen CP36_8 reinforcement strain

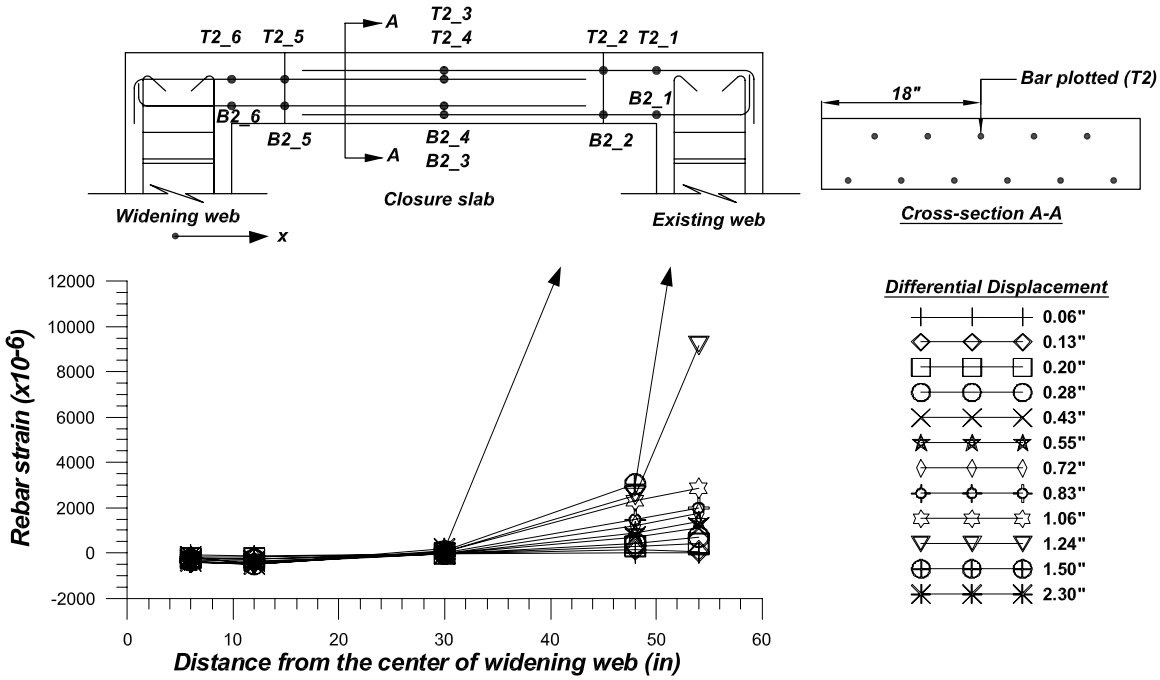


(c) Top bar T2

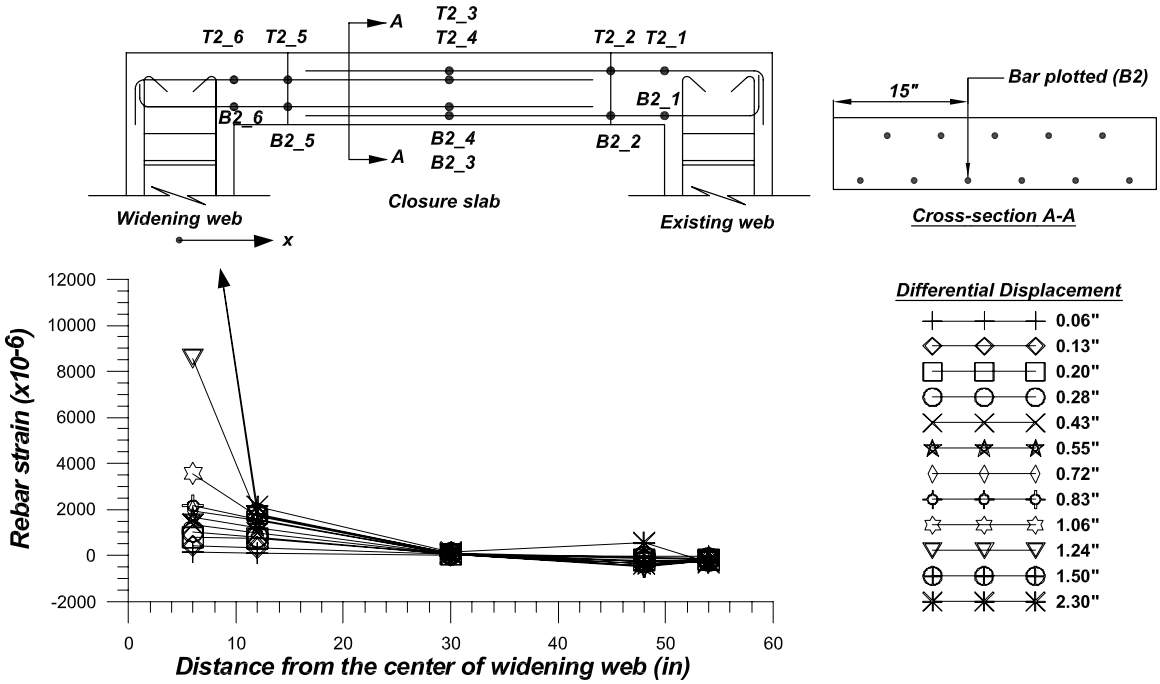


(d) Bottom bar B2

Figure 3.12: Specimen CP36_8 reinforcement strain (cont.)

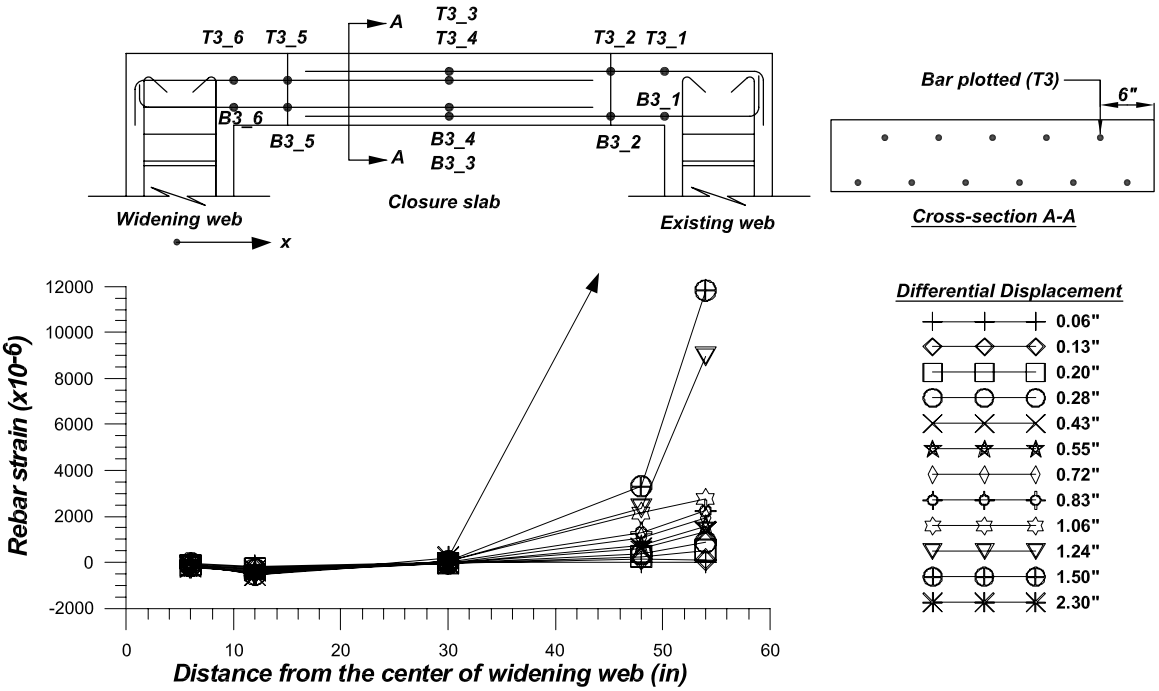


(e) Top bar T3

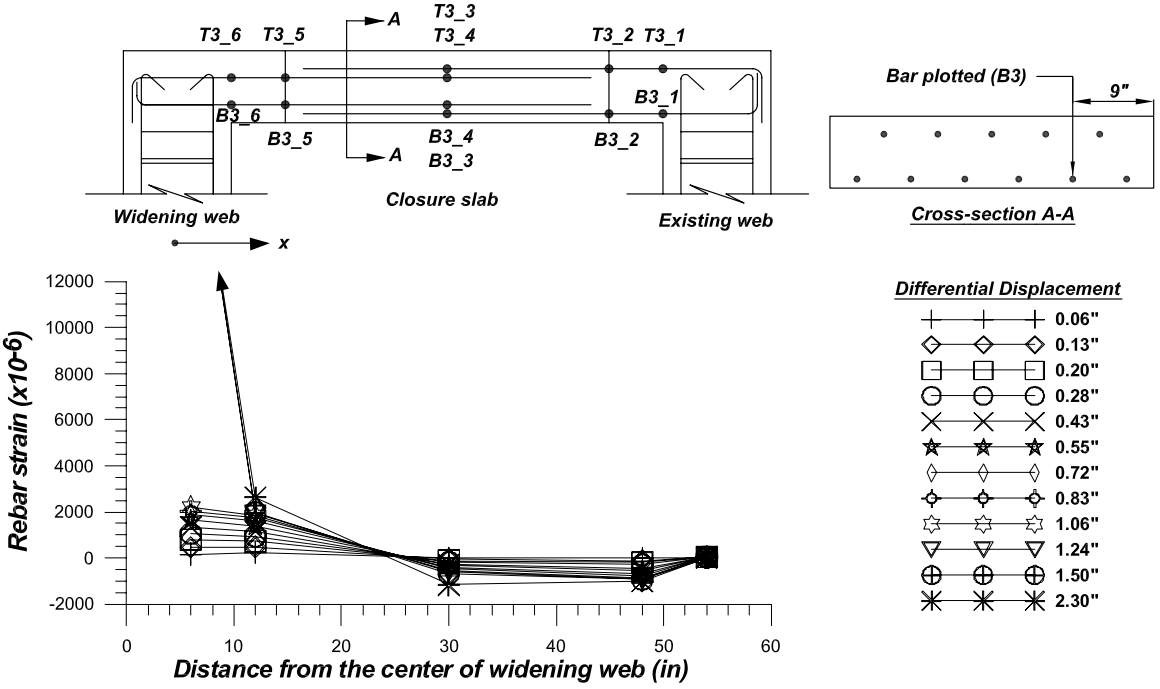


(f) Bottom bar B3

Figure 3.12: Specimen CP36_8 reinforcement strain (cont.)

$21000 \times 10^{-6}$, indicating that these gages might be damaged, thus rendering these readings unreliable. Readings from a functioning strain gage, T1_1 however, showed a strain increase from $3000 \times 10^{-6}$ to $9000 \times 10^{-6}$ upon differential displacement increase from 0.8" to 0.96". It is also evident from the strain plots that the bottom tensile strains near the widening web were less than the top tensile strains near the existing web, due to the 20% larger bottom reinforcement area, as noted previously for specimen CP36_8. Figures 3.13(a)-(f) also show that compressive strains were measured in the bottom reinforcement of the deck overhang at the existing web, and in the top reinforcement of the deck overhang at the widening web. Except for gage B2_6 which had a strain magnitude equaled to $-1636 \times 10^{-6}$, all measured compressive strains were smaller than $-1000 \times 10^{-6}$ at the ultimate differential displacement of 1.79".

#### 3.5.3.3 Specimen CP18_8

With the narrowest span, specimen CP18_8 showed the smallest ultimate differential displacement among the three slabs of the same 8" thickness. Reinforcement strain distributions for specimen CP18_8 are plotted in Figure 3.14(a)-(f) for differential displacements from 0.04" to 0.99". Since the test setup was identical to the previous two tests except for the change in closure slab width, regions of maximum tensile strains were the same as the previous two tests. An examination of the data indicated that first-yielding of the reinforcement occurred at a differential displacement of 0.50". At the ultimate differential displacement of 0.99", reinforcement strain in the deck overhang near the existing web increased significantly. However, the magnitude of the tensile strain in specimen CP18_8 at failure was distinctly smaller when compared to the previous two specimens. For specimens CP36_8 and CP24_8, strains at critical sections at failure were outside the operating range of the gage, estimated to be $20000 \times 10^{-6}$. On the other hand, tensile strains recorded at critical sections of specimen CP18_8 at failure were all functioning within the operating range of the gage, with some of the readings just slightly above the yield strain of the reinforcement. These strain readings agreed with the load-deflection curve where specimen CP18_8 developed very limited ductility before a brittle shear failure. Although the tensile strains were markedly different,

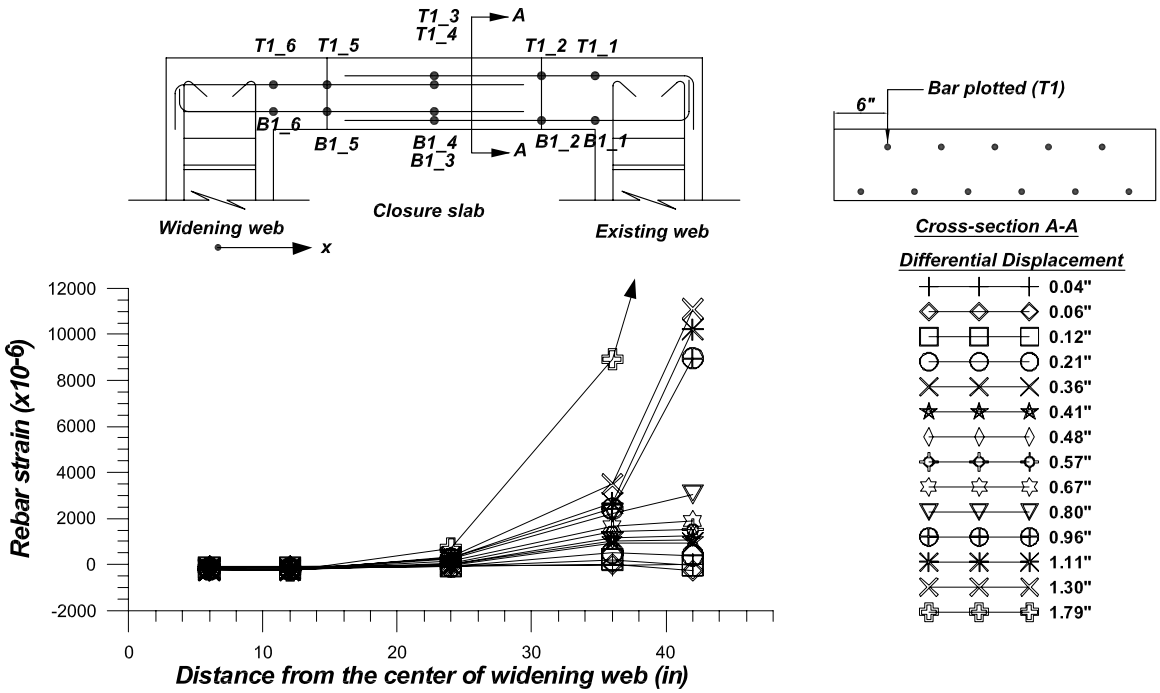


(a) Top bar T1

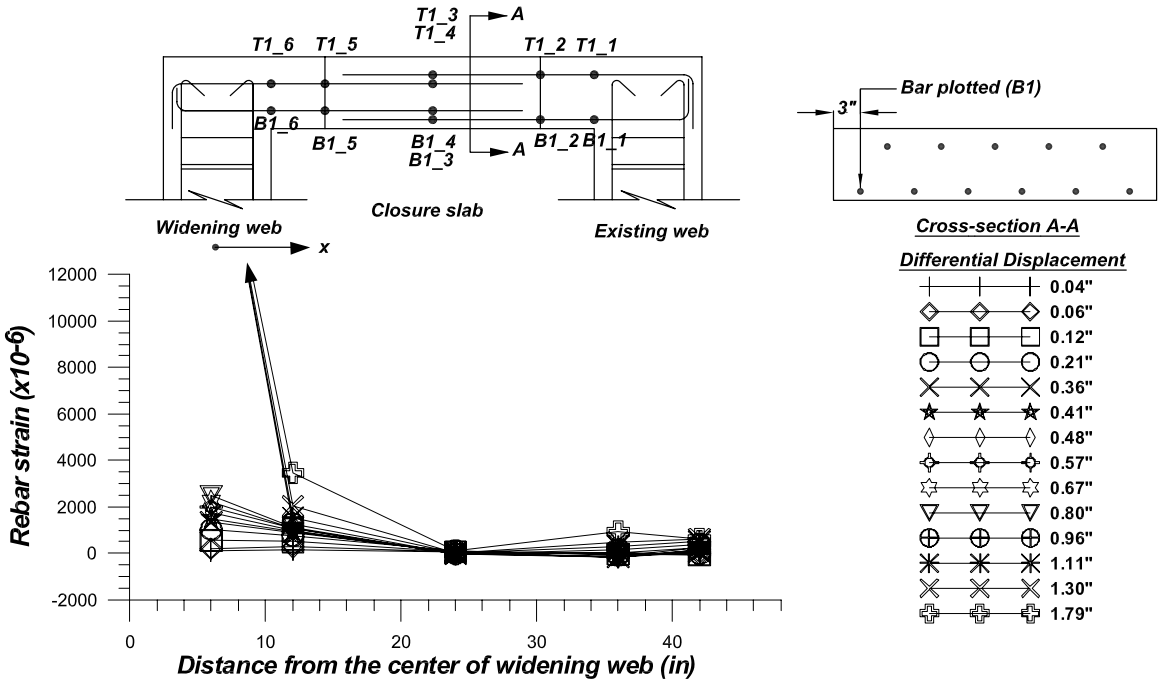


(b) Bottom bar B1

Figure 3.13: Specimen CP24_8 reinforcement strains

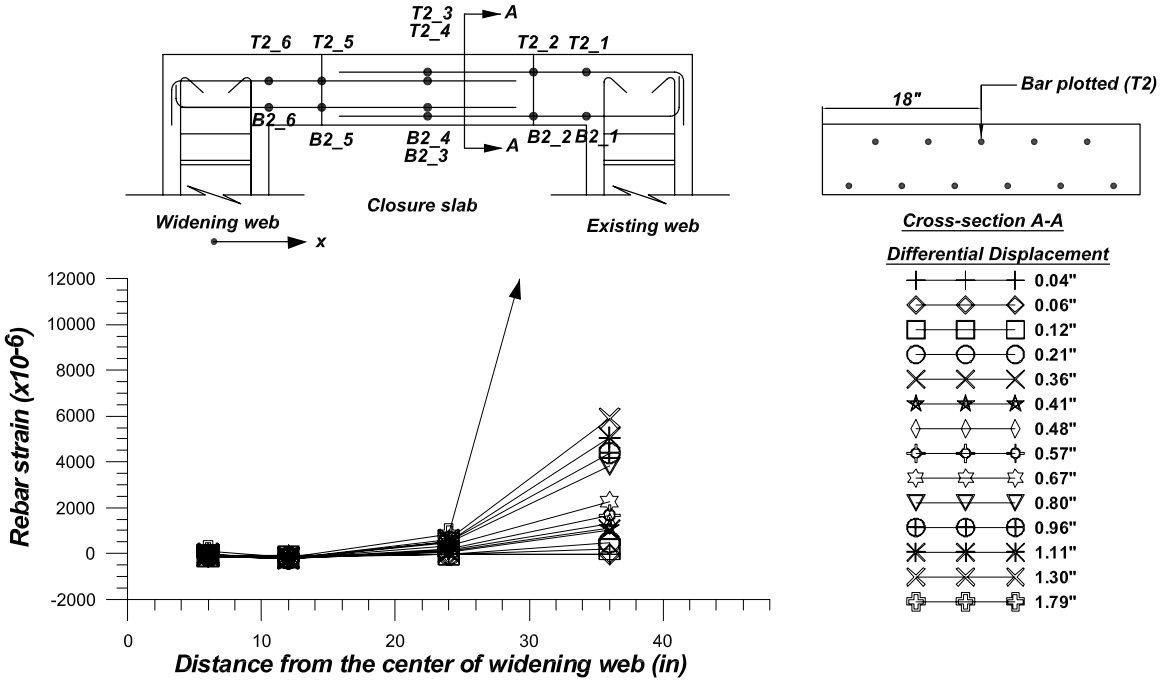


(c) Top bar T2

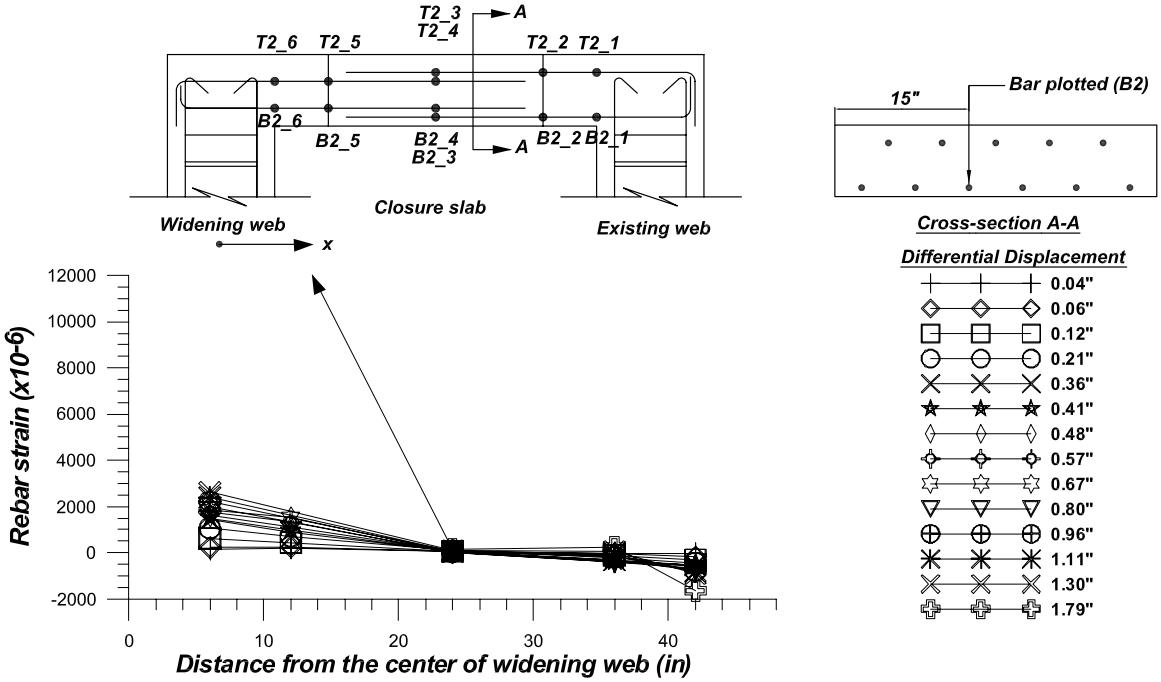


(d) Bottom bar B2

Figure 3.13: Specimen CP24_8 reinforcement strains (cont.)

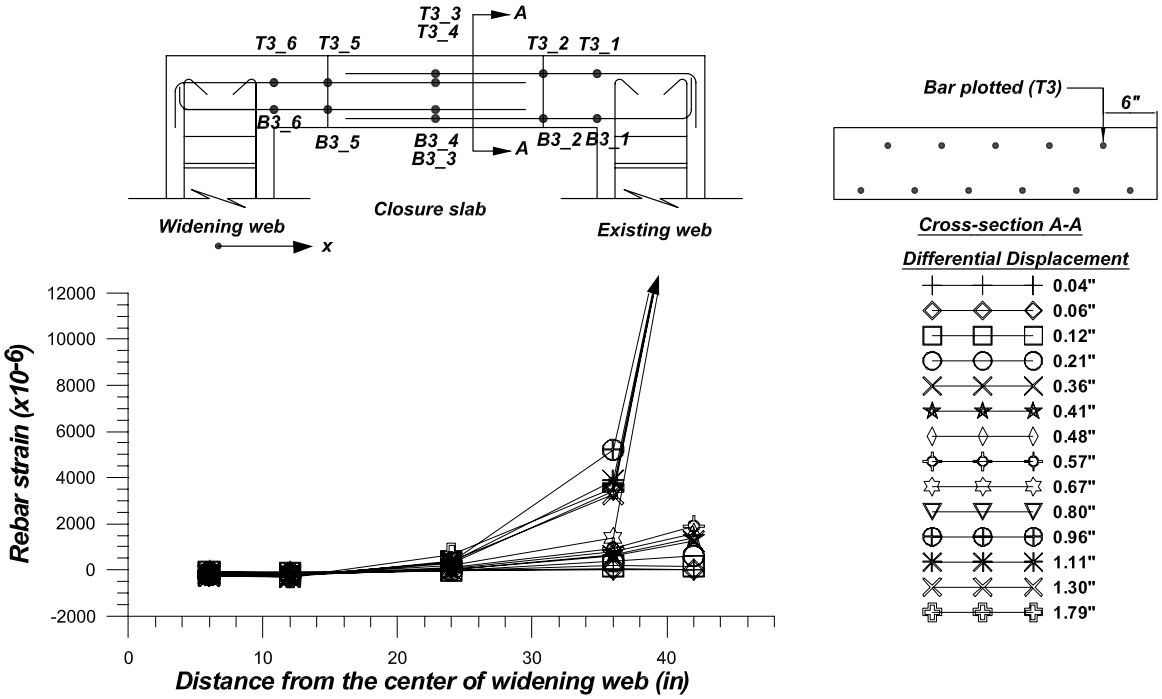


(e) Top bar T3

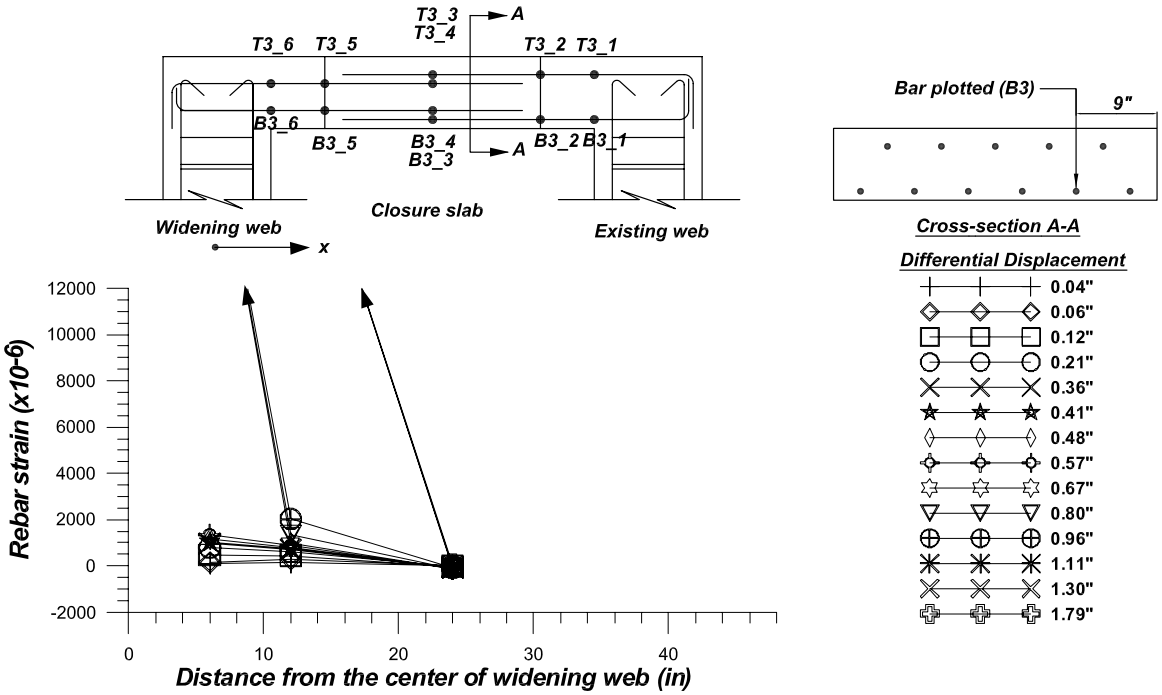


(f) Bottom bar B3

Figure 3.13: Specimen CP24_8 reinforcement strains (cont.)

compressive strains in the reinforcement of specimen CP18_8 were similar to the previous two specimens. Compressive strains at the ultimate differential displacement of 0.99" were generally below $-1000 \times 10^{-6}$ except for gage B1_1 and B2_1. The small compressive strains implied that flexural compression failure was unlikely to occur in the closure slabs of current design.

#### 3.5.3.4 Specimen CP24_12

For performance assessment of closure slabs of different thicknesses, a 24" wide and 12" thick closure slab, labeled as CP24_12, was included in the test matrix for comparison with specimen CP24_8. Figures 3.15 (a)-(f) show the strain distributions in the top and bottom reinforcement for differential displacements from 0.06" to 0.93". From cross-comparison of Figures 3.15(a)-(f) with Figures 3.13(a)-(f), it was evident that strains measured in specimen CP24_12 were much lower than in specimen CP24_8 at failure of the slab. While most of the gages at critical sections of specimen CP24_8 were showing strains over $20000 \times 10^{-6}$ at slab failure, the maximum tensile strain in specimen CP24_12, as measured by gage T3_1, was much smaller at $7761 \times 10^{-6}$. Moreover, top reinforcing bars T1 and T2 and bottom reinforcing bar B3 had not yielded at slab failure. The measured strains in specimen CP24_12 supported the observed lack of yield-plateau in the load-differential displacement curve of the specimen, as shown obviously in Figure 3.9. Furthermore, the comparison of measured strains in four test specimens showed specimens CP24_12 and CP18_8 had tensile strains smaller than the other two specimens before failure of the slab. The smaller ultimate displacement capacity of specimens CP24_12 and CP18_8 is expected to have an impact on the determination of the waiting time for closure pour.

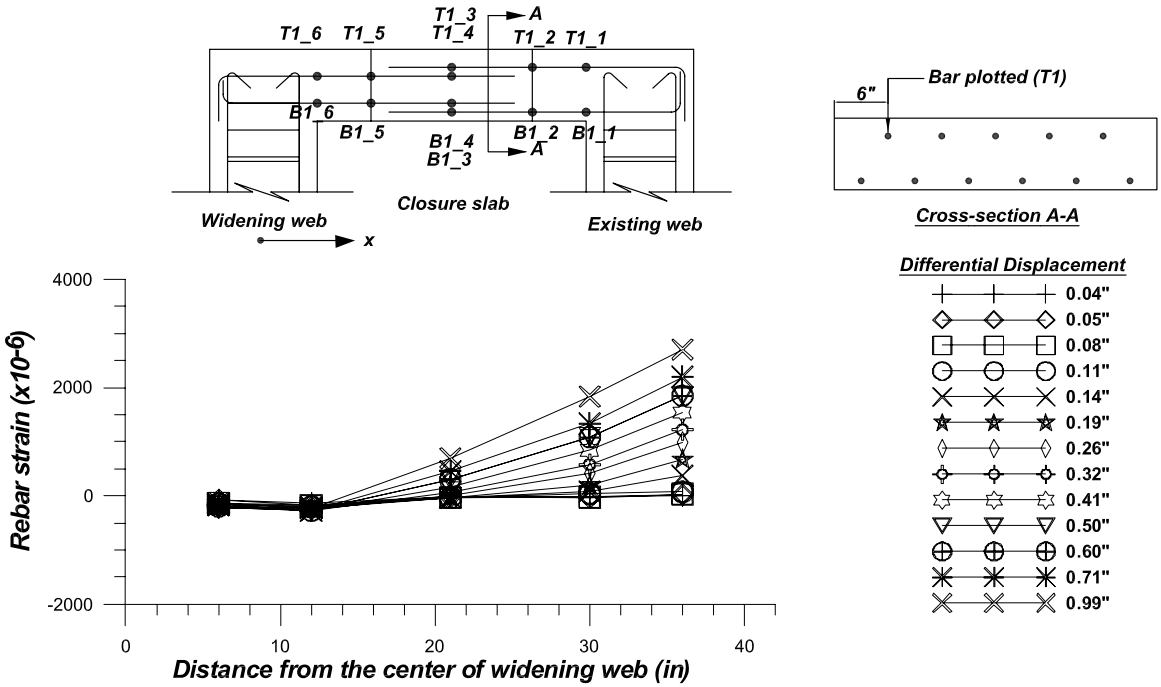


(a) Top bar T1

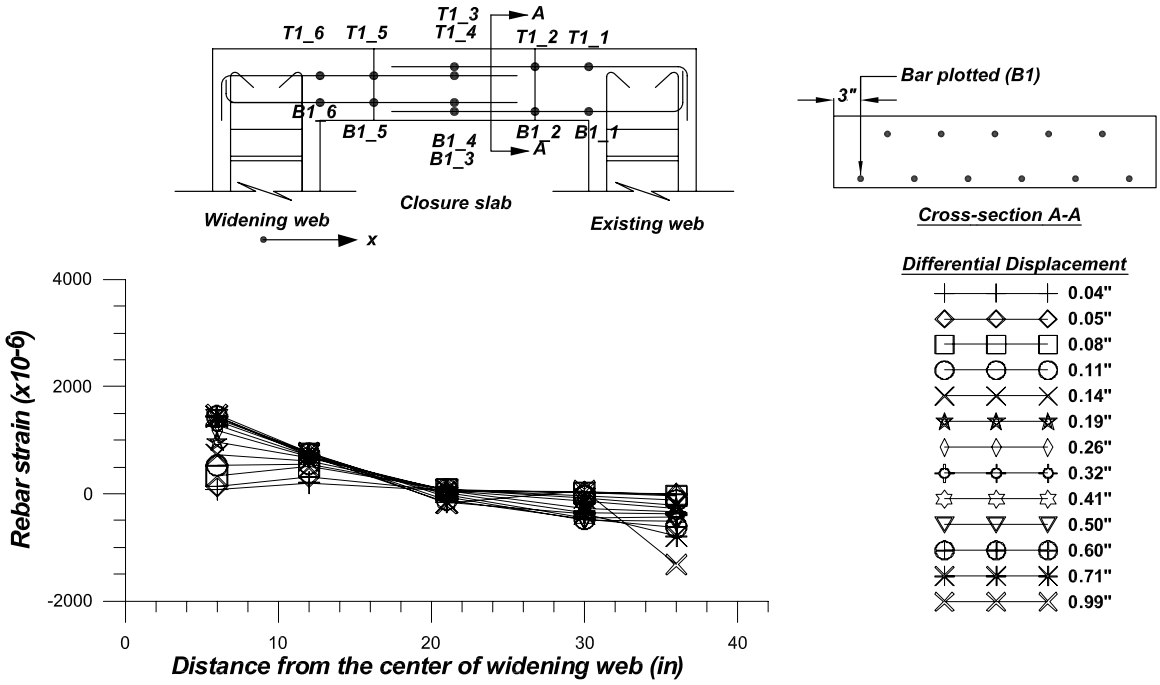


(b) Bottom bar B1

Figure 3.14: Specimen CP18_8 reinforcement strains

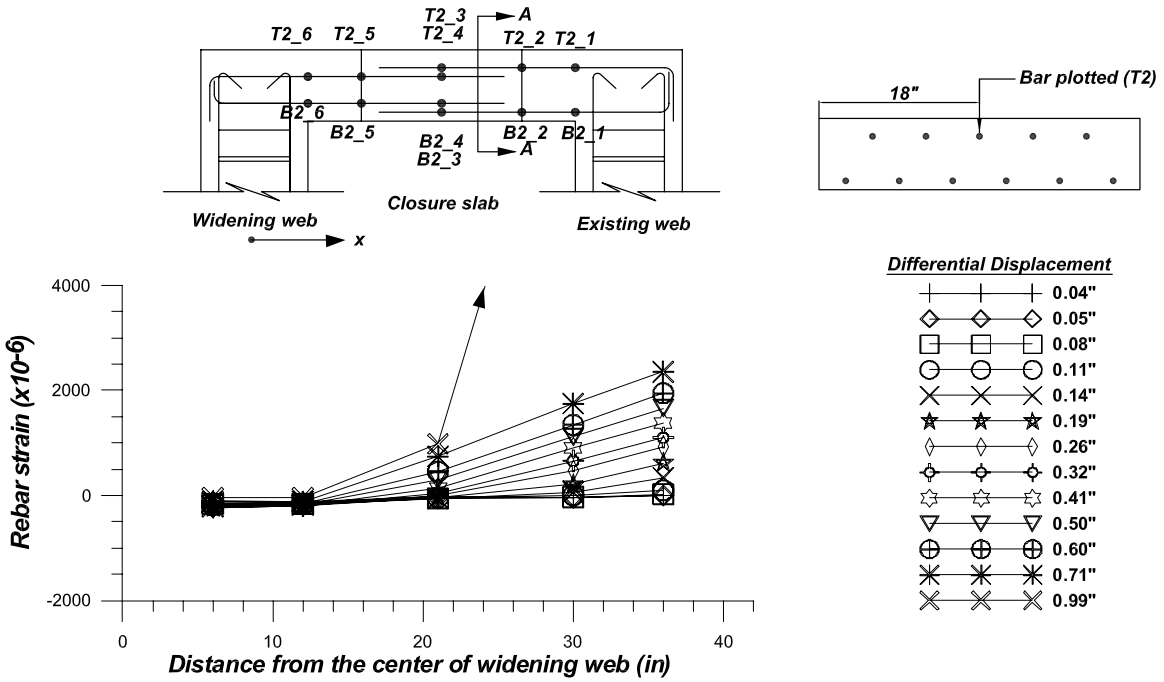


(c) Top bar T2

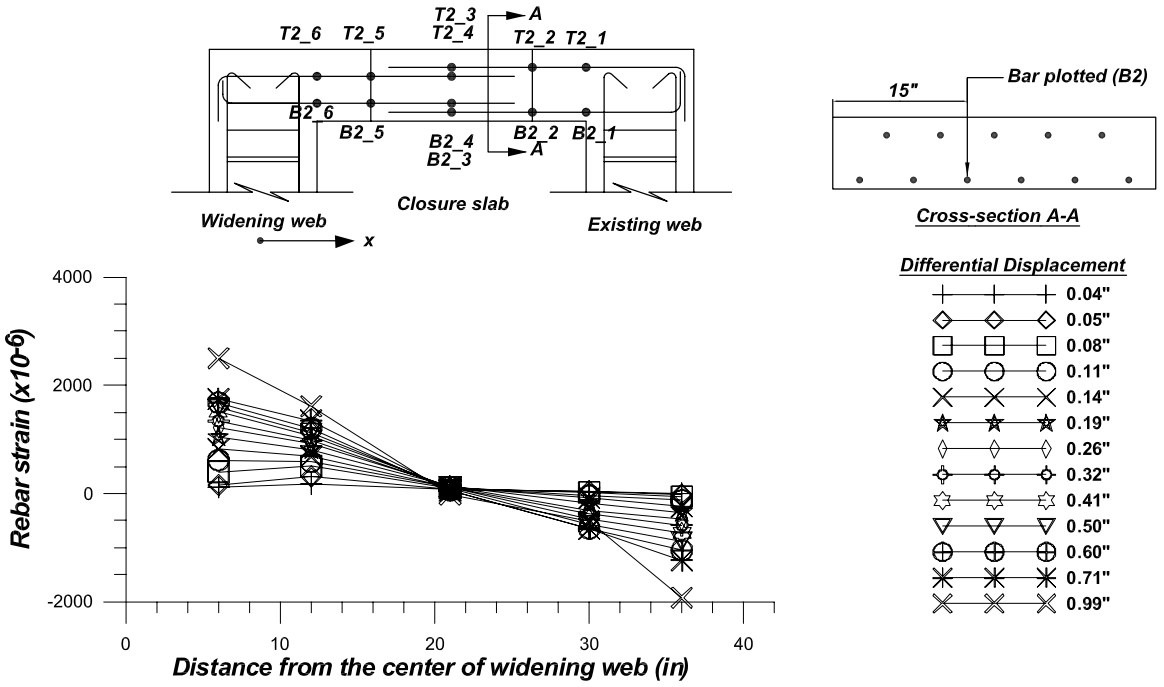


(d) Bottom bar B2

Figure 3.14: Specimen CP18_8 reinforcement strains (cont.)

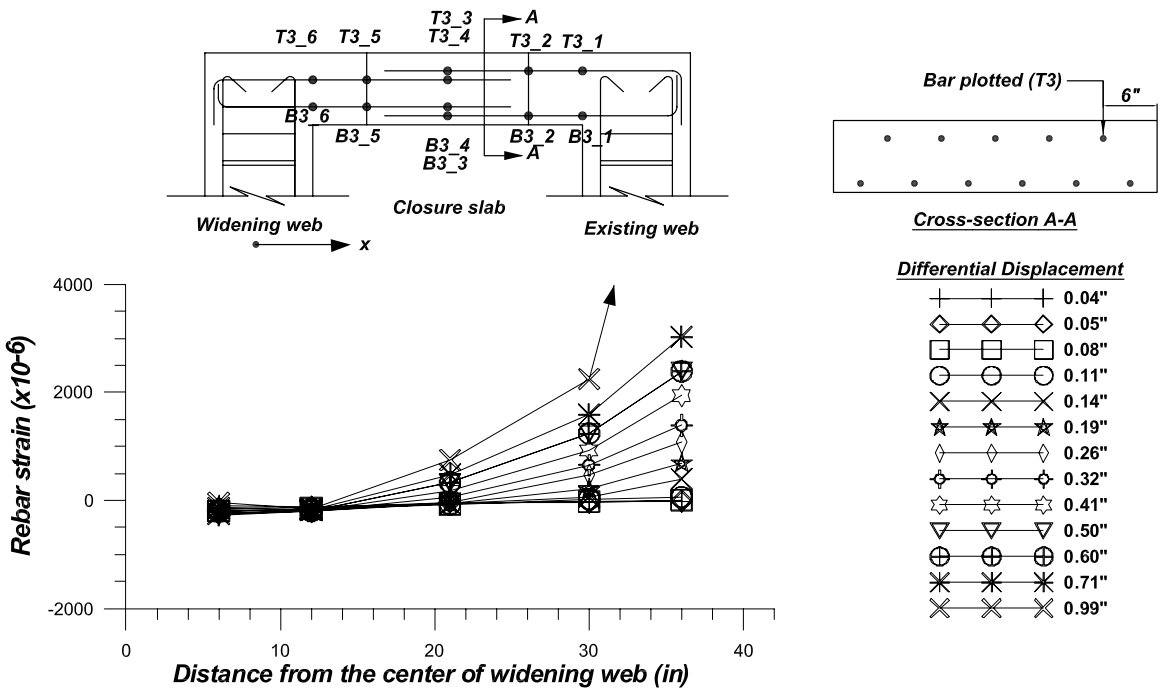


(e) Top bar T3

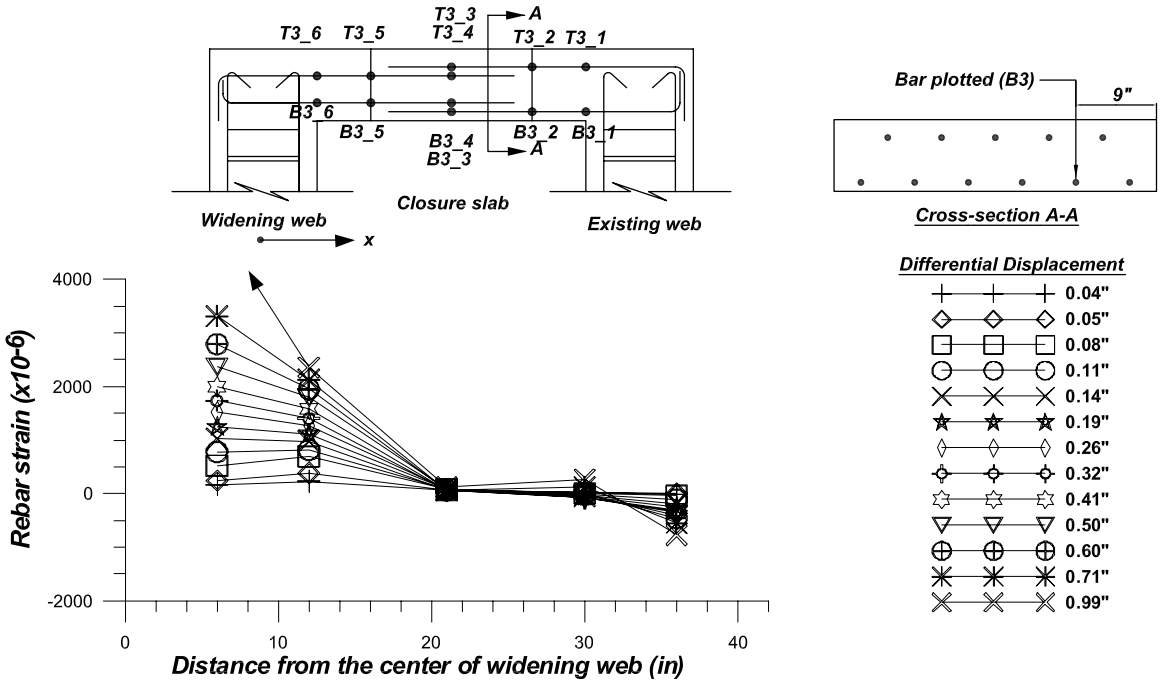


(f) Bottom bar B3

Figure 3.14: Specimen CP18_8 reinforcement strains (cont.)

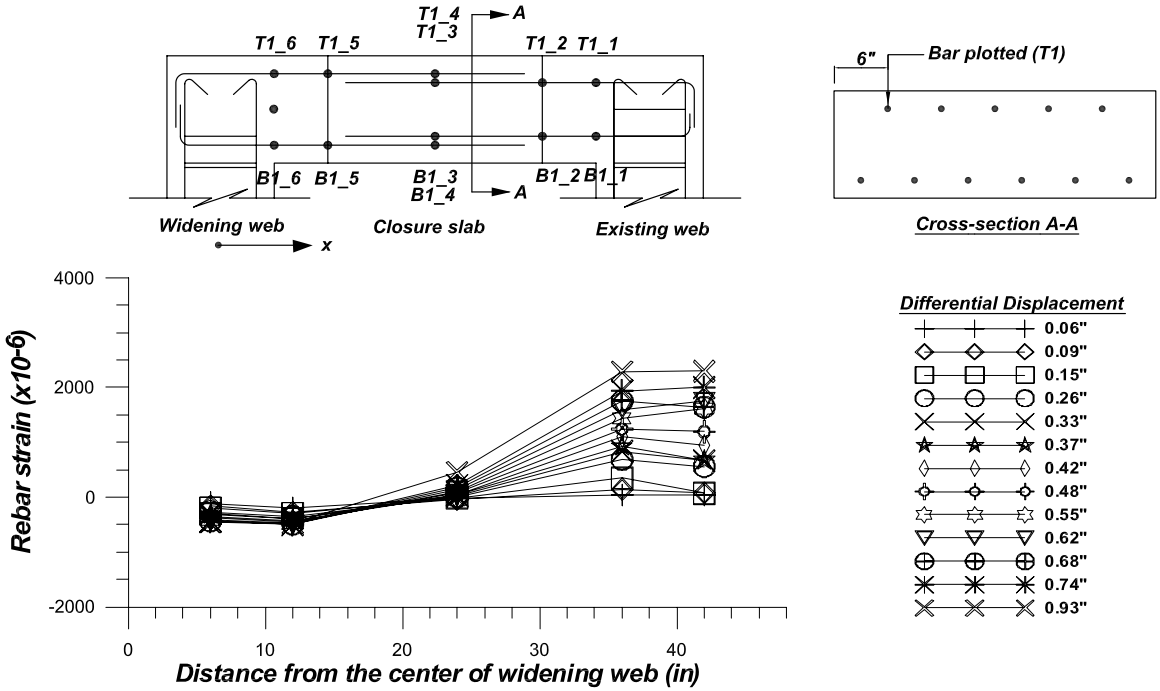


(a) Top bar T1

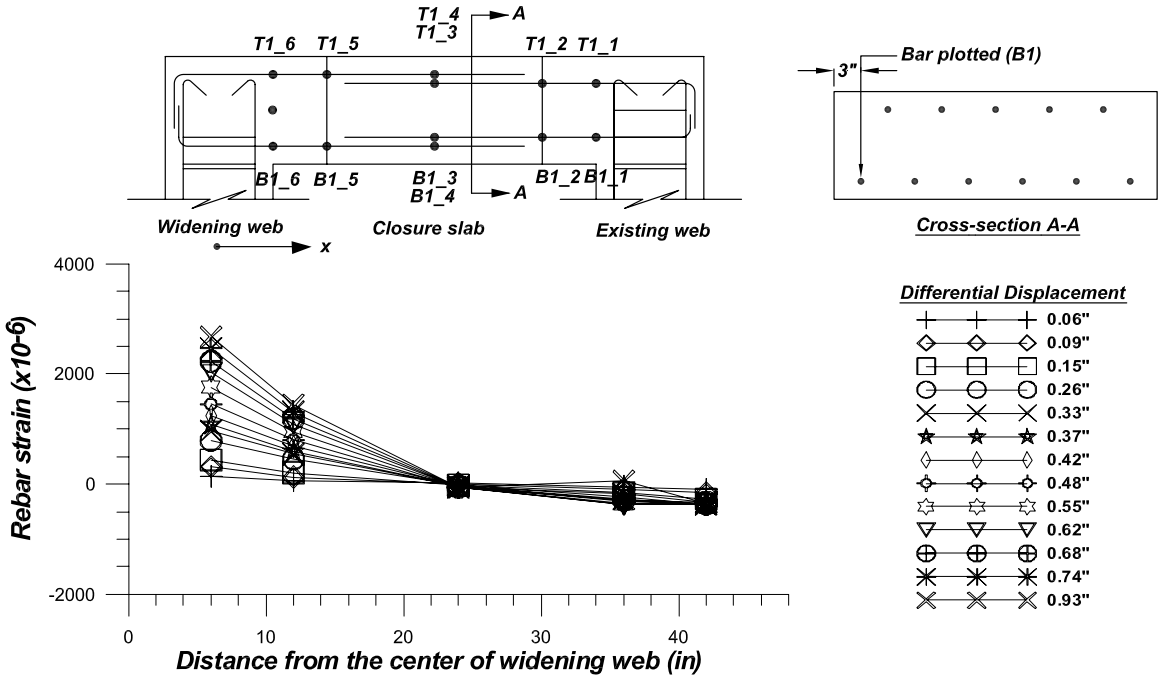


(b) Bottom bar B1

Figure 3.15: Specimen CP24_12 reinforcement strains

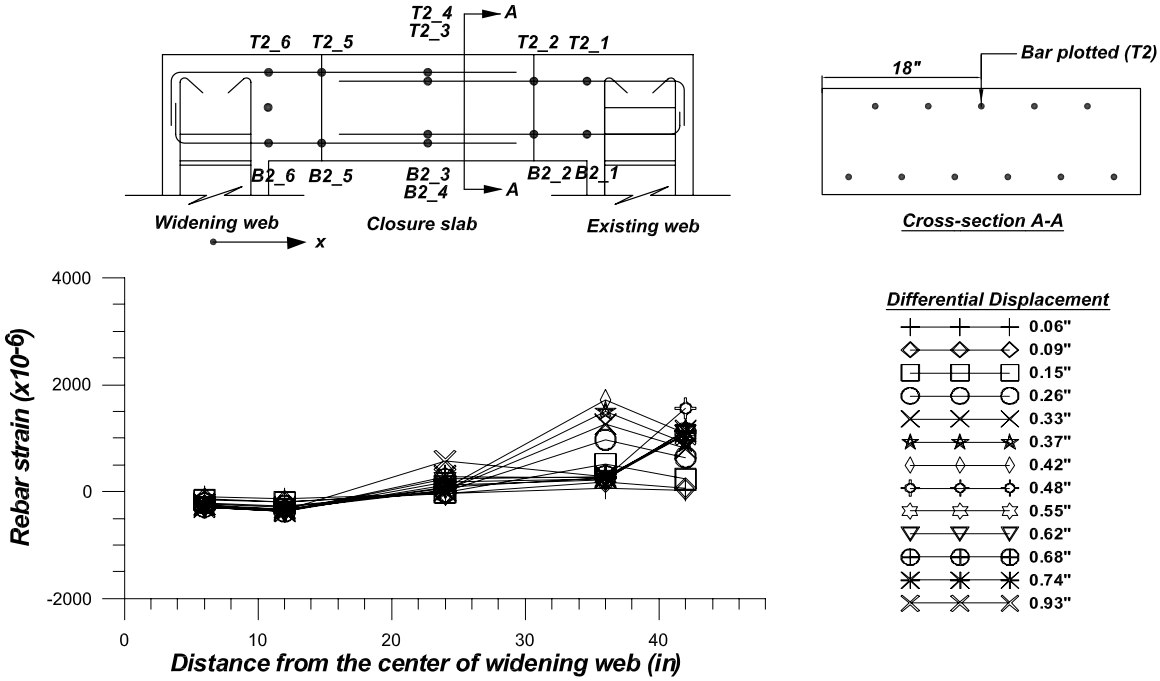


(c) Top bar T2

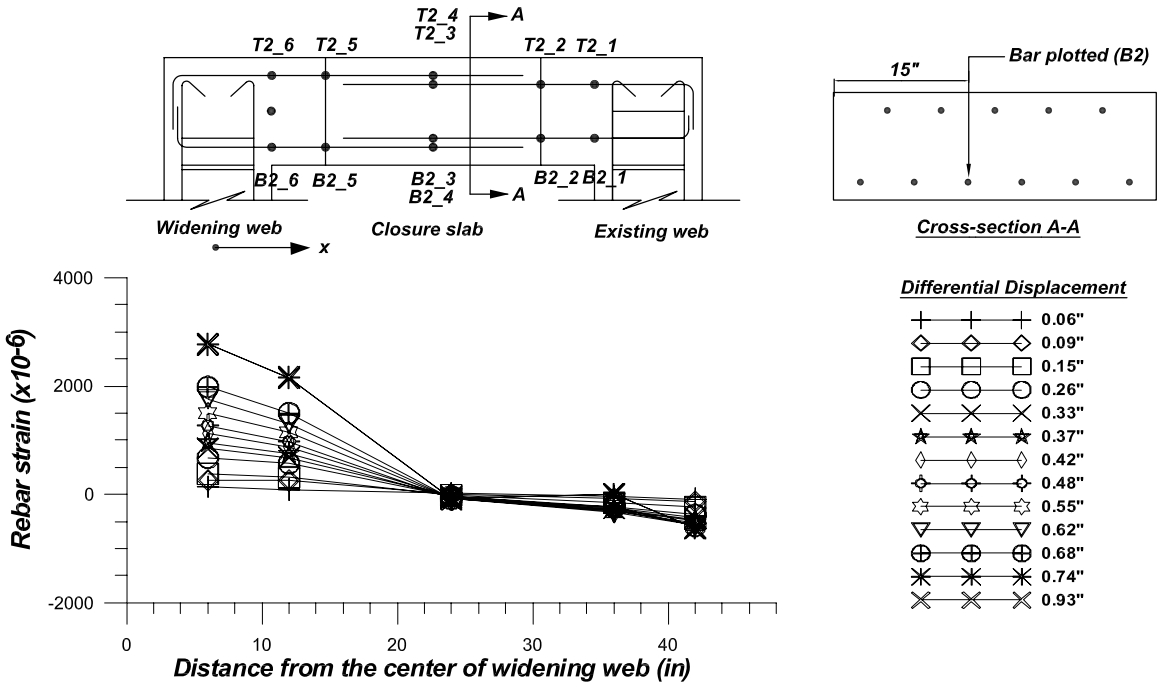


(d) Bottom bar B2

Figure 3.15: Specimen CP24_12 reinforcement strains (cont.)

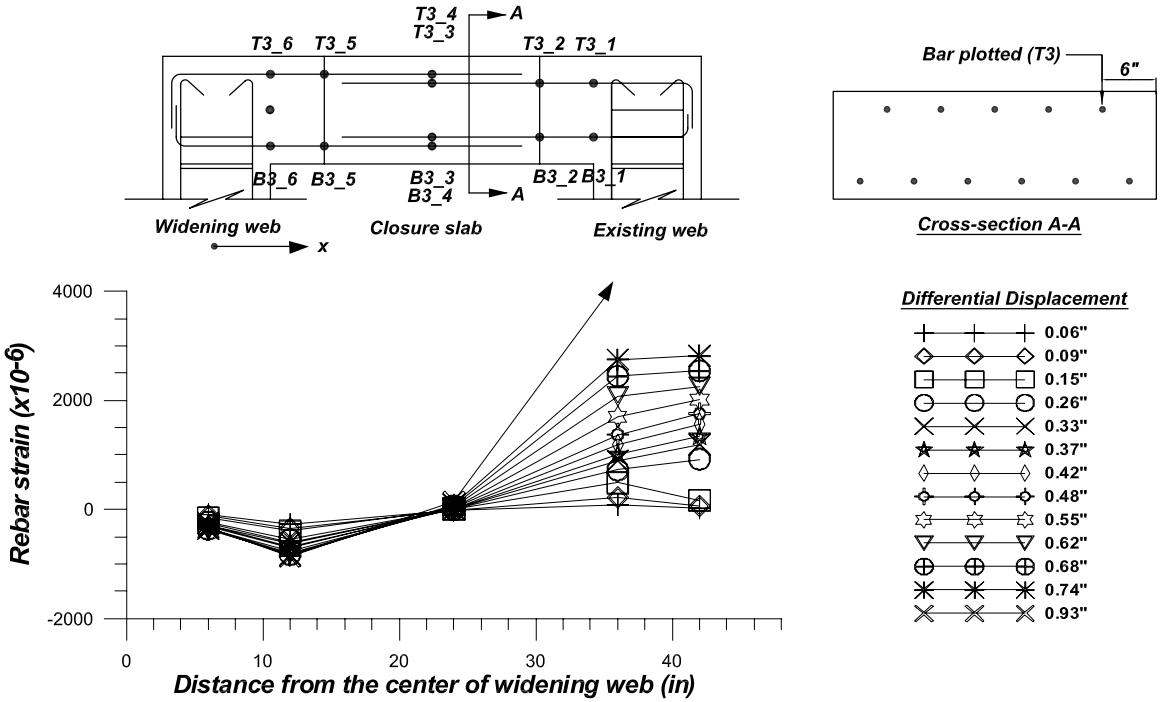


(e) Top bar T3

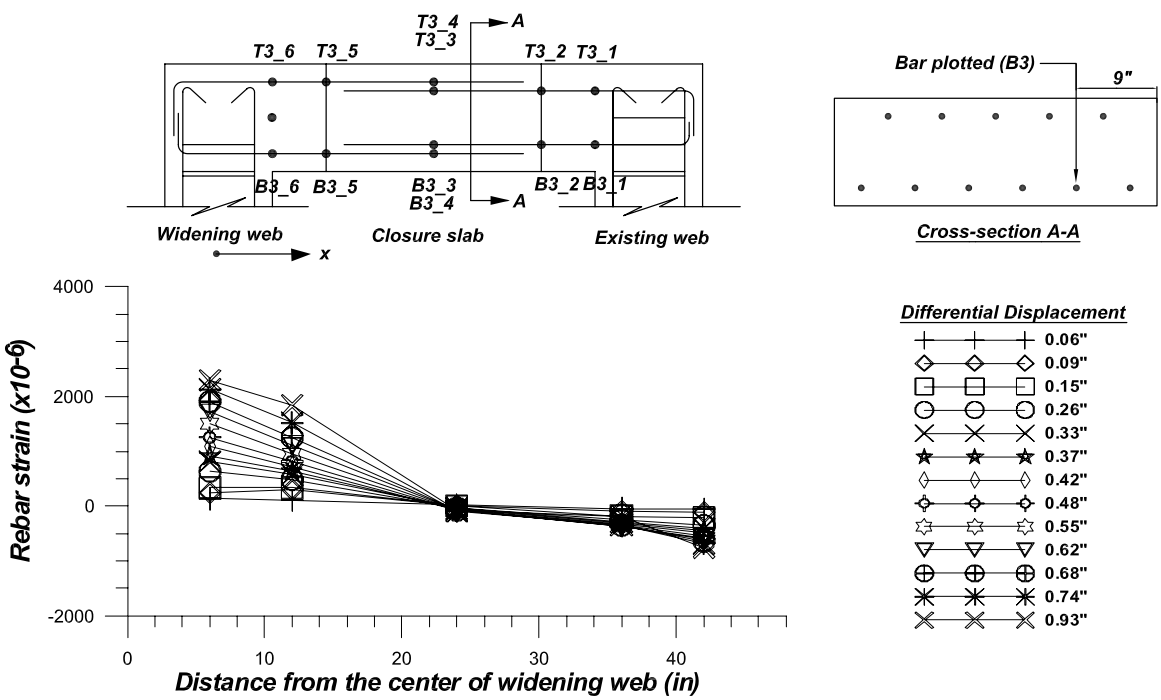


(f) Bottom bar B3

Figure 3.15: CP24_12 reinforcement strains (cont.)

# Chapter 4

# Procedure for Determining the Waiting Time for Closure Pour

## 4.1 Introduction

To determine the waiting time for closure pour, an ability to predict the time-dependent differential displacement between bridges constructed at different ages, as in widening or staged construction, is important. While accurate prediction of the time-dependent deformation of concrete members is invariably complex and involves a multitude of parameters, the process, particularly with reference to closure pour, may be facilitated by assuming a correspondence between structural level deformation and material level deformation, as commonly assumed in the theory of linear viscoelasticity [4, 5]. Although it is recognized that the correspondence between structural level deformation and material level deformation is strictly not applicable to aging materials, the assumption will nonetheless be made here for expediency. To that end, the differential displacement between existing and widening bridges, or between stage I and stage II bridges, upon falsework release of the new bridge, is determined using a suitable creep compliance function for the concrete.

## 4.2 Creep Compliance Function

### 4.2.1 Basic Definitions

Creep of concrete in compression is commonly characterized in terms of a creep coefficient, $\phi(t, t_1)$, defined as the ratio of the creep strain under a sustained constant stress to the

instantaneous elastic strain [6, 7]

$$\phi(t, t_1) = \frac{\epsilon_c(t, t_1)}{\epsilon_e(t_1)} \tag{4.1}$$

or alternatively

$$\epsilon_c(t, t_1) = \phi(t, t_1)\epsilon_e(t_1) \tag{4.2}$$

where $\epsilon_c(t, t_1)$ is the creep strain at time $t$, upon the application of the constant stress $\sigma(t_1)$ at $t_1$, and $\epsilon_e(t_1)$ is the instantaneous elastic strain at $t_1$. The time-dependent deformation of concrete under a constant compressive stress is shown schematically in Figure 4.1. As time $t \to \infty$, the creep strain approaches an ultimate creep strain, which is denoted by

$$\epsilon_c^\infty \equiv \epsilon_c(\infty, t_1) = \phi(\infty, t_1)\epsilon_e(t_1) \tag{4.3}$$

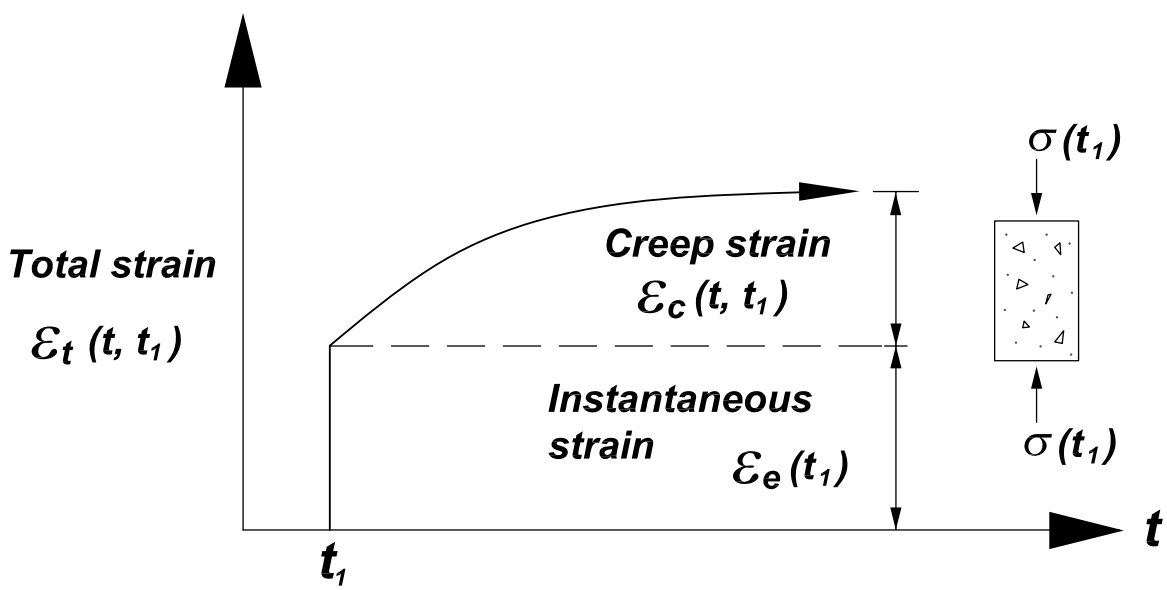


Figure 4.1: Creep of concrete under a sustained compressive stress

Concrete creep, however, is commonly characterized in terms of a specific creep, $C(t, t_1)$, which is defined as the creep strain at time $t$ due to a unit sustained stress at time $t_1$. Mathematically, the specific creep may be written as

$$C(t, t_1) \equiv \frac{\epsilon_c(t, t_1)}{\sigma(t_1)} \tag{4.4}$$

By assuming that the instantaneous elastic strain can be written as $\epsilon_e(t_1) = \sigma(t_1)/E_c(t_1)$, the specific creep can be related to the creep coefficient by

$$\phi(t, t_1) = C(t, t_1)E_c(t_1) \tag{4.5}$$

where $E_c(t_1)$ is the elastic modulus of the concrete at age $t_1$, the time of stress application. The total strain, i.e. sum of instantaneous strain and creep strain, due to a unit stress applied at $t_1$, is called the creep compliance, and can be expressed as

$$J(t, t_1) \quad \frac{\epsilon_t(t, t_1)}{\sigma(t_1)} = \frac{\epsilon_c(t, t_1) + \epsilon_e(t_1)}{\sigma(t_1)} = \frac{1}{E_c(t_1)}[1 + \phi(t, t_1)] \tag{4.6}$$

where $\epsilon_t(t, t_1)$ is the total strain due to the applied constant stress $\sigma(t_1)$ at time $t_1$.

Concrete creep deformation manifests itself as a complex time-dependent response depending on many factors including the age of concrete at loading, ambient and curing conditions, type of cement, water-to-cement ratio, size and shape of the member, load duration etc. Many models have been proposed in the literature for predicting the creep deformation of concrete, with perhaps ACI-209 [8], CEB-FIP Model Code 1990 [9], GL2000 model [10, 11] and B3 model [12, 13] among the most recognized. Most of these models however are empirically based, requiring a varying number of input parameters depending on the level of sophistication intended in the model. While the procedure proposed later in the chapter can be adapted, in principle, to any of these models, the 'short form' or abridged version of the so-called "B3" model by Bazant and Baweja [13, 14] is used to estimate differential displacement between new and existing bridges. The short form of the B3 model is selected for its noted accuracy on creep prediction, and yet sufficiently simple for general use in either design or field offices. It should be noted that the shrinkage component of the short form of the B3 model is not included in the proposed procedure.

### 4.2.2 Creep Compliance - Short Form of B3 Model

Despite its intended broad applications, the short form of the B3 model are nonetheless limited to Portland cement concrete, having a mean 28-day cylinder compressive strength in the range of 2500 to 10000 psi, a water-to-cement weight ratio 0.35 to 0.85, a cement

content in the range of 10 to 45 lb/ft$^3$, an aggregate-to-cement weight ratio 2.5 to 13.5, and a minimum curing of 1 day [13]. The range of parameters is however sufficiently large to encompass most of the concrete currently used for bridge construction in California.

The creep compliance of concrete, as proposed in the short form of the B3 model [13], is given by the sum of the instantaneous deformation, the basic creep deformation, and the additional deformation due to drying creep, and is expressed as

$$J(t, t_1) = \{q_1 + C_0(t, t_1) + C_d(t, t_1, t_o)\} \times 10^{-6} \qquad \text{where } t_1 > t_o \tag{4.7}$$

in which $t$ is the time at which the deformation is to be estimated in days, $t_1$ is the age of concrete at loading, $t_0$ is the age of concrete when drying starts (end of curing), $q_1$ is the instantaneous strain due to unit stress, scaled by a factor $1 \times 10^6$, to be calculated by

$$q_1 = \frac{0.6 \times 10^6}{E_{28}} \tag{4.8}$$

where $E_{28}$ is the elastic modulus of the concrete at 28 days in psi units, which can be calculated by $E_{28} = 57000\sqrt{\bar{f}_c}$, where $\bar{f}_c$ is the mean 28-day compressive strength of the concrete in psi units which may be related to the design strength $f'_c$ by $\bar{f}_c = f'_c + 1200$ psi [13]. The term $C_0(t, t_1)$ on the right hand side of Eq. 4.7 corresponds to the compliance function for basic creep, which is calculated from

$$C_0(t, t_1) = q_0 \ln\{1 + \Psi[(t_1)^{-m} + \alpha](t - t_1)^n\} \tag{4.9}$$

where $q_0 = 200(\bar{f}_c)^{-0.5}$, and material parameters $m = 0.5$, $n = 0.1$, $\alpha = 0.001$ and $\Psi = 0.3$. The term $C_d(t, t_1, t_o)$ on the right hand side of Eq. 4.7 corresponds to the compliance function for drying creep, which is calculated from

$$C_d(t, t_1, t_0) = q_5\{e^{-3H(t)} - e^{-3H(t_1)}\}^{1/2} \qquad \text{where } t_1 > t_o \tag{4.10}$$

where $q_5 = 6000(\bar{f}_c)^{-1}$ in units of 1/psi, and parameters $H(t)$ and $H(t_1)$ are related to the cross-section shape of the member as well as the ambient relative humidity, which are determined by

$$H(t) = 1 - (1 - h)S(t) \tag{4.11}$$

in which $h$ is the ambient relative humidity in decimal value (not percentage) with $0 \leq h \leq 1$, and $S(t)$ is a time-dependent function given by

$$S(t) = \tanh \sqrt{\frac{t - t_o}{\eta_{sh}}} \tag{4.12}$$

where $t_o$ is the age of concrete at the end of curing, as noted previously, and $\eta_{sh}$ is a size-dependent parameter which is given by

$$\eta_{sh} = 32D^2 \tag{4.13}$$

in which $D = 2v/s$ is an effective cross-section thickness in inches, where $v$ = volume of the member in in$^3$ and $s$ = surface area of the member in in$^2$. Hence $v/s$ represents the volume-to-surface ratio of the member.

Figure 4.2 shows schematically the influence of loading age on concrete creep compliance as it relates to the two options of falsework release currently specified by Caltrans. In the figure, falsework release for Alternative 1 is assumed to occur 10 days after last concrete pour, whereas falsework release for Alternative 2 is assumed to occur 28 days after last concrete pour. Alternative 2 is expected to give a lower creep compliance compared to Alternative 1, due to the longer waiting period resulting in longer time for aging of the young concrete before loading, which translates into a smaller differential displacement between existing and new bridges. Figure 4.3 shows a family of curves for the creep compliance function at different loading ages using the short form of the B3 model. The creep compliance is calculated based on a mean 28-day compressive strength of $\bar{f}_c = 5500$ psi, an ambient relative humidity of $h = 0.70$, a curing period of $t_o = 7$ days, and an effective cross-section thickness of $D = 12.4$". Numerical values indicate that, for falsework release at $t_1 = 10$, 28 and 60 days, the creep compliance at $t = 1000$ days is $0.772 \times 10^{-6}$, $0.586 \times 10^{-6}$ and $0.490 \times 10^{-6}$ psi$^{-1}$, respectively. The creep compliance for falsework release at $t_1 = 28$ days is about 24% smaller than the creep compliance for falsework release at $t_1 = 10$ days. At a later falsework release of $t_1 = 60$ days, the creep compliance is about 37% smaller than that of release at $t_1 = 10$ days. Since the overall bridge differential displacement is inherently related to the local deformation of the superstructure concrete, the decreasing creep compli-

ance at increasing loading ages implies that different falsework release time will significantly affect the differential displacement at closure.

Subsequent determination of the normalized bridge deflection, for purposes of determining the waiting time for closure pour, necessitates the calculation of the creep compliance function at the time of falsework release. The substitution of $t = t_1$ into the creep compliance function in Eq. 4.7 however gives rise to $J(t_1, t_1) = q_1 \times 10^{-6} = 0.6/E_{28}$, which is a constant independent of the time of falsework release. Since the value of the creep compliance function at the time of falsework release represents in essence the elastic deflection of the bridge at the structural level, a constant elastic deflection does not represent the elastic deflection expected of the bridge upon falsework release at different ages. To overcome the deficiency, the elastic modulus of the concrete is determined by a modification of the creep compliance function, as recommended by [13]

$$E_c(t_1) = 1/J(t_1 + \Delta t, t_1) \tag{4.14}$$

where $E_c(t_1)$ represents the elastic modulus of the concrete at time of falsework release, and $\Delta t$ corresponds to a time shift, or called a "stress duration", which may be taken as 0.01 day [13]. The creep compliance, $J(t_1, t_1)$, at the time of falsework release, can thus be approximated by

$$J(t_1, t_1) \approx 1/E_c(t_1) = J(t_1 + \Delta t, t_1) \tag{4.15}$$

By selecting a value of $\Delta t = 0.01$ day, Eq. 4.14 has been noted to give an elastic modulus that is in reasonable agreement with ACI's elastic modulus given by $57000\sqrt{\bar{f}_c(t_1)}$, where $\bar{f}_c(t_1)$ is the mean compressive strength of the concrete at the time of falsework release in psi units [13].

## 4.3 Bridge Deflection upon Falsework Release

Cast-in-place superstructure must be self-supporting upon a falsework release after gaining sufficient strength in the concrete. Although typical falsework release requires careful and coordinated removal of form support over a period ranging from a few hours to several

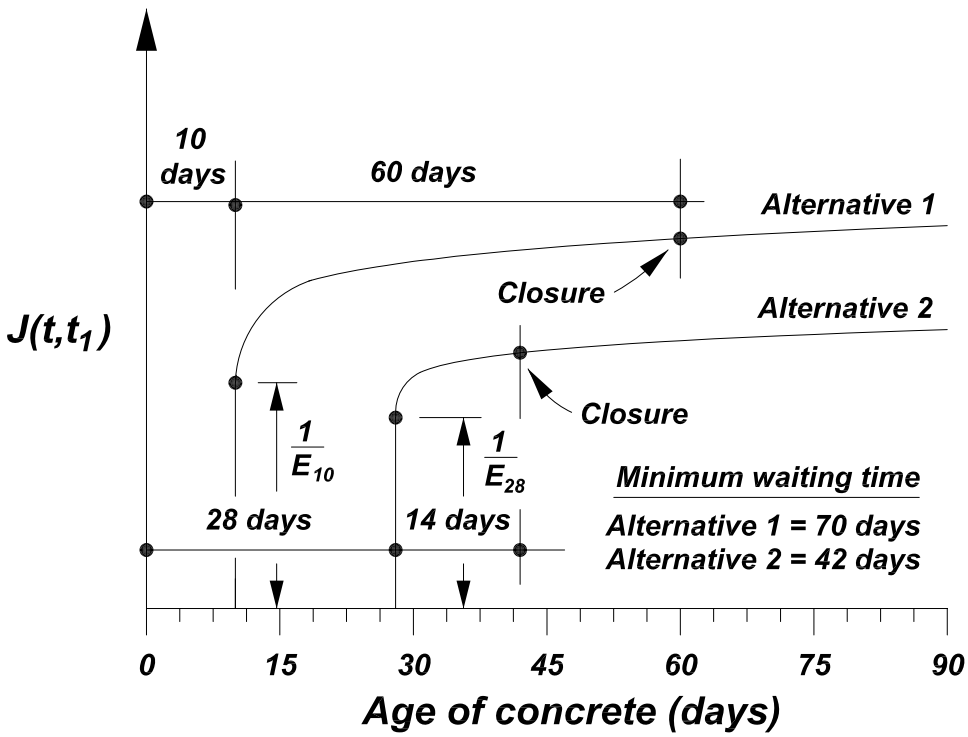


Figure 4.2: Influence of falsework release on creep compliance

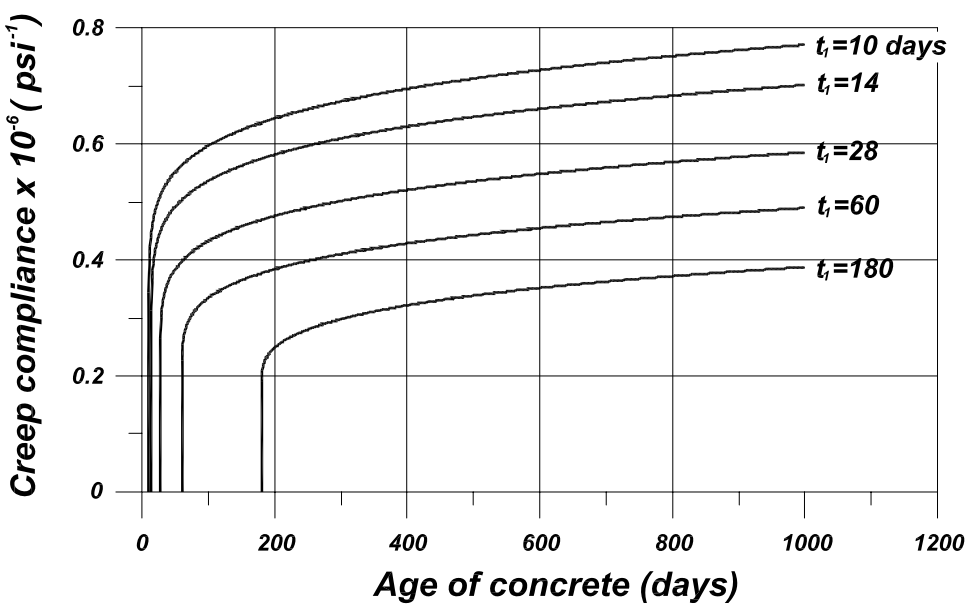


Figure 4.3: B3 creep compliance functions at different loading ages

days, the transfer of self-weight to the superstructure is more conveniently modeled as an instantaneous event with loading represented by a step function

$$w(t) = w_o \, U(t - t_1) \tag{4.16}$$

where $w_o$ is the self-weight of the superstructure, $t$ is the time referenced to the cast date, and $U(t - t_1)$ is a unit step function, which takes on a value of 0 for $t < t_1$ and a value of 1 for $t \geq t_1$.

Figure 4.4(a) shows an example of a simply-supported bridge where the mid-span deflection immediately after falsework release is denoted by $\delta_{instant}$. As time progresses, bridge deflection increases with mid-span deflection denoted by $\delta_{midspan}(t)$. The ratio of time-dependent mid-span deflection to instantaneous deflection, termed as the deflection factor in this report, can be defined as

$$\kappa_s(t) \quad \frac{\delta_{midspan}(t)}{\delta_{instant}} \tag{4.17}$$

Eq. 4.17 signifies the normalized time-dependent response of the bridge upon falsework release. By invoking the so-called "correspondence principle" commonly assumed in linear viscoelasticity [4, 5], the deflection factor $\kappa_s(t)$ in Eq. 4.17, which is established at the structural level, may be taken to correspond to the normalized creep compliance function, which is established at the material level. Although a direct correspondence between material level deformation and structural level deformation is strictly incorrect when estimating the time-dependent bridge deflection since concrete exhibits an aging behavior, the assumption will nonetheless be made here, but with a caveat that the correspondence is only approximately valid.

At the material level, time-dependent concrete deformation may be characterized using a creep compliance function, as discussed in Section 4.2. Figure 4.4(b) shows the time-dependent response of concrete under a unit compressive stress of $\sigma_o = 1$ at time $t_1$. The instantaneous elastic strain under the unit compressive stress is given by the creep compliance value at time $t = t_1$, i.e. $\epsilon_e(t_1) = J(t_1, t_1)$. For time $t > t_1$, the time-dependent strain is characterized by the creep compliance function, i.e. $\epsilon_t(t, t_1) = J(t, t_1)$. Thus a normalized

creep compliance function may similarly be defined as the ratio of time-dependent strain to the instantaneous strain

$$\kappa_m(t) \qquad \frac{\epsilon_t(t,t_1)}{\epsilon_e(t_1)} = \frac{J(t,t_1)}{J(t_1,t_1)} \tag{4.18}$$

For estimating the waiting time for closure pour, it is hereby assumed that the equality between the normalized deflection, as given by Eq. 4.17, and the normalized creep compliance function, as given by Eq. 4.18, holds by virtue of the "correspondence principle" [4, 5] i.e.

$$\kappa_s(t) = \kappa_m(t) \Rightarrow \frac{\delta_{midspan}(t)}{\delta_{instant}} = \frac{J(t,t_1)}{J(t_1,t_1)} \tag{4.19}$$

or equivalently

$$\delta_{midspan}(t) = \delta_{instant}\frac{J(t,t_1)}{J(t_1,t_1)} \tag{4.20}$$

Eq. 4.20 permits an estimation of the time-dependent deflection of the bridge if the instantaneous elastic mid-span deflection immediately after the falsework release is measured via field survey. The normalized creep compliance function can be substituted from the ratio of Eq. 4.7 to Eq. 4.15 on the basis of the short form of the B3 model.

The time-dependent deflection in Eq. 4.20 assumes an instantaneous release of the falsework, but in reality, the actual falsework release in the field may take several hours or days to complete. The duration of the falsework release can be taken into account approximately by modifying Eq. 4.20. To that end, let $t_1$ be time at initial or start of falsework release, $t_2$ be time at the end or final release, and $\delta_{measured}$ be the deflection measured <u>at the end of the falsework release</u>. In this case, the time-dependent mid-span deflection may be approximated by

$$\delta_{midspan}(t) = \delta_{measured}\frac{J(t,t_1)}{J(t_2,t_1)} \tag{4.21}$$

where $J(t_2,t_1)$ is the creep compliance calculated from Eq. 4.7 by substituting $t = t_2$. It is important to note that Eq. 4.21 assumes that a 100% transfer of self-weight to the superstructure immediately after the start of the falsework release and survey measurements of mid-span deflection are made at a later time at the end of the complete falsework release. The transfer of self-weight to the superstructure during a gradual falsework release is admittedly difficult to quantify in the field, and in those cases, it is recommended that Eq. 4.20

be used with $\delta_{instant}$ taken as the measured deflection at the end of the falsework release i.e. at $t_2$, and with $t_1$ be replaced by $t_2$, where $t_2$ is the time at the end of falsework release. The resulting creep compliance $J(t_2, t_2)$ is to be similarly calculated in Eq. 4.15 with $t_1$ replaced by $t_2$ and the stress duration taken as $\Delta t = 0.01$ days.

The prediction of bridge deflection based on creep compliance function will now be compared with the field instrumented bridges, where the data have been presented in Chapter 2. Figure 4.5 (a) shows the normalized mid-span deflection as measured in the Santa Rosa Creek Bridge and the prediction by using Eq. 4.21. It should be noted that both experimental and theoretical curves are normalized by the 'instantaneous' deflection at the end of the falsework release, which took two days to complete. In the prediction using the short form of the B3 model, the following values are assumed: start of release $t_1 = 12$ days, end of release $t_2 = 14$ days, duration of concrete curing $t_o = 7$ days, mean 28-day compressive strength $\bar{f}_c = 6200$ psi, ambient relative humidity $h = 0.7$, volume-to-surface area ratio $v/s = 4.9$" for the cross-section and an effective cross-section thickness of $D = 9.8$". It can be seen from Figure 4.5 (a) that the short form of the B3 model predicted the normalized mid-span deflection quite well for the Santa Rosa Creek Bridge for up to about 180 days, after which the measured deflection became affected by the traffic load upon closure.

Figure 4.5 (b) shows the comparison of the normalized mid-span deflection of the San Joaquin River Bridge and the prediction by the short form of the B3 model. Since the falsework release for span 5 of the San Joaquin River Bridge took less than one day to complete, the prediction of time-dependent mid-span deflection shall be made using Eq. 4.20. The following values are assumed for the B3 model: time of falsework release $t_1 = 33$ days, duration of concrete curing $t_o = 7$ days, mean 28-day compressive strength $\bar{f}_c = 6200$ psi, ambient relative humidity $h = 0.6$, volume-to-surface area ratio $v/s = 3.6$" for the cross-section and an effective cross-section thickness of $D = 7.2$". Unlike the Santa Rosa Creek Bridge, the San Joaquin River Bridge exhibited somewhat unusual response in that the time-dependent mid-span deflection remained rather constant immediately after falsework release, but showed a rapid increase at time $t = 56$ days and 102 days. These step-like increases make

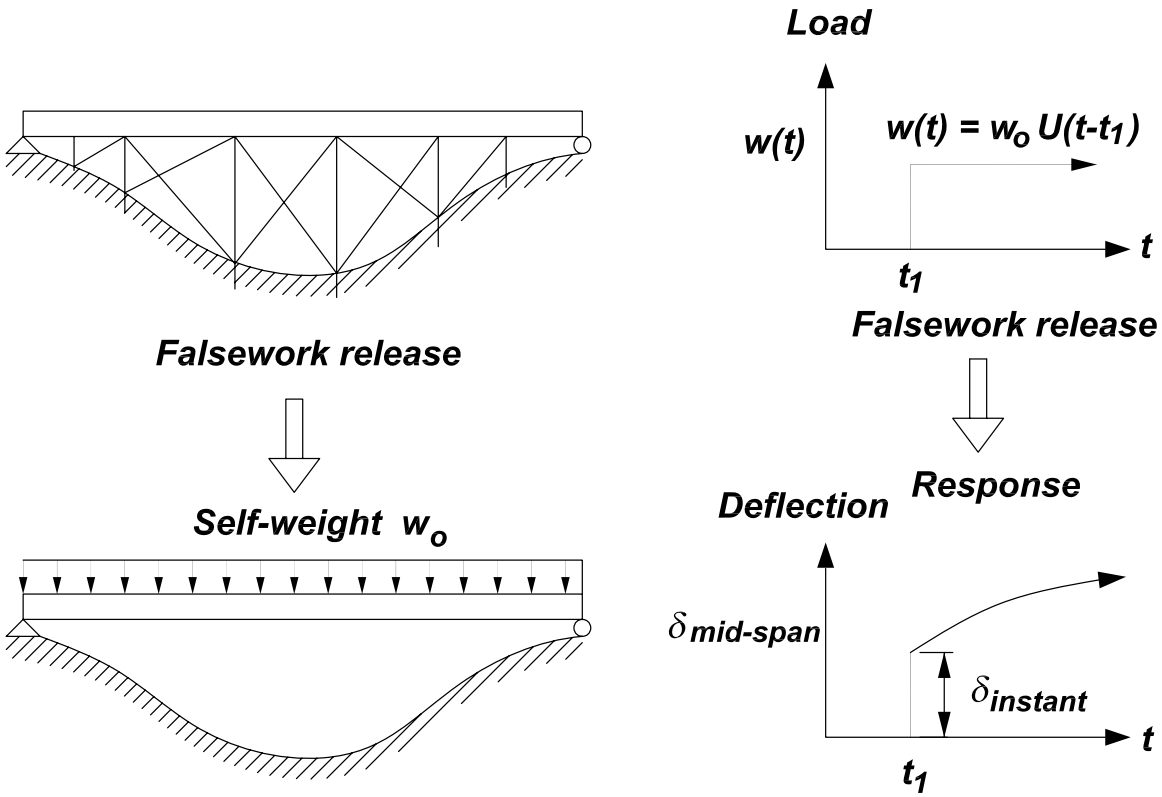


(a) structural level

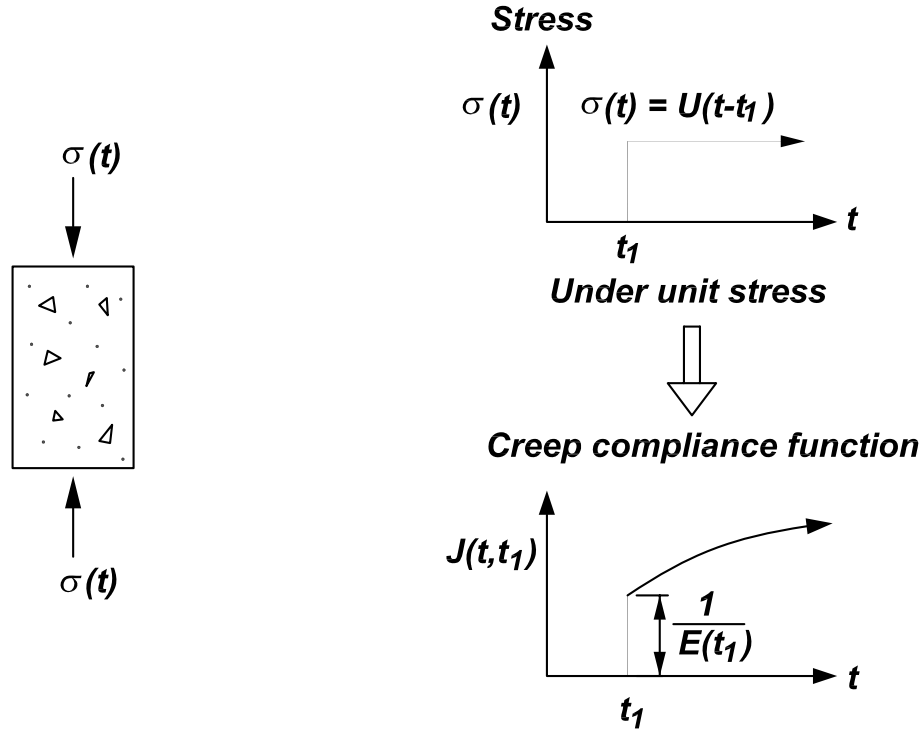


(b) material level

Figure 4.4: Correspondence between span deflection and creep compliance function

deflection prediction difficult as analytical models tend to give smooth increase in deflection with time. Consequently, the short form of the B3 model over-estimated the mid-span deflection of the San Joaquin River Bridge between the time of falsework release and about 110 days, after which the measured deflection catches up with the model with reasonable prediction for $t > 110$ days. While reasons for the near constant deflection immediately after falsework release remain unclear, it is recognized that bridge deflections are often affected by unscheduled construction maneuvers, including the placing and removal of heavy equipment or construction materials on the adjacent spans.

Although the normalized deflection based on creep compliance function does not provide a perfect match of the measured deflections, the proposed adoption of the short form of the B3 model nonetheless offers a simple and improved means of deflection prediction over that currently used by Caltrans, as presented previously in Figure 2.15. The uncertainty in deflection prediction can be further mitigated by a factor of safety for the differential displacement capacity of the closure slab when dealing with the closure pour waiting time.

## 4.4 Design Procedure for Closure Pour Waiting Time

A methodology for determining the closure pour waiting time may be formulated on the basis that the differential displacement between existing and new bridges must be less than or equal to by the design displacement capacity of the closure slab. Figure 4.6 shows a plot of the experimental displacement capacity of the 8" closure slab, versus the closure slab width, for three tests presented in Chapter 3. Since the number of closure slab specimens tested in the project was small, it is prudent to adopt a conservative design displacement capacity, denoted by $\delta_c$, that is a fraction of the experimental ultimate displacement capacity $\delta_u$. It will be assumed that a design displacement capacity at 60% of the measured ultimate displacement capacity is appropriate for the determining the closure pour waiting time i.e. $\delta_c = 0.6\delta_u$.

The following steps are proposed for determining the closure pour waiting time:

(i) Determine the instantaneous deflection, $\delta_{instant}$ for use in Eq. 4.20, or $\delta_{measured}$ in

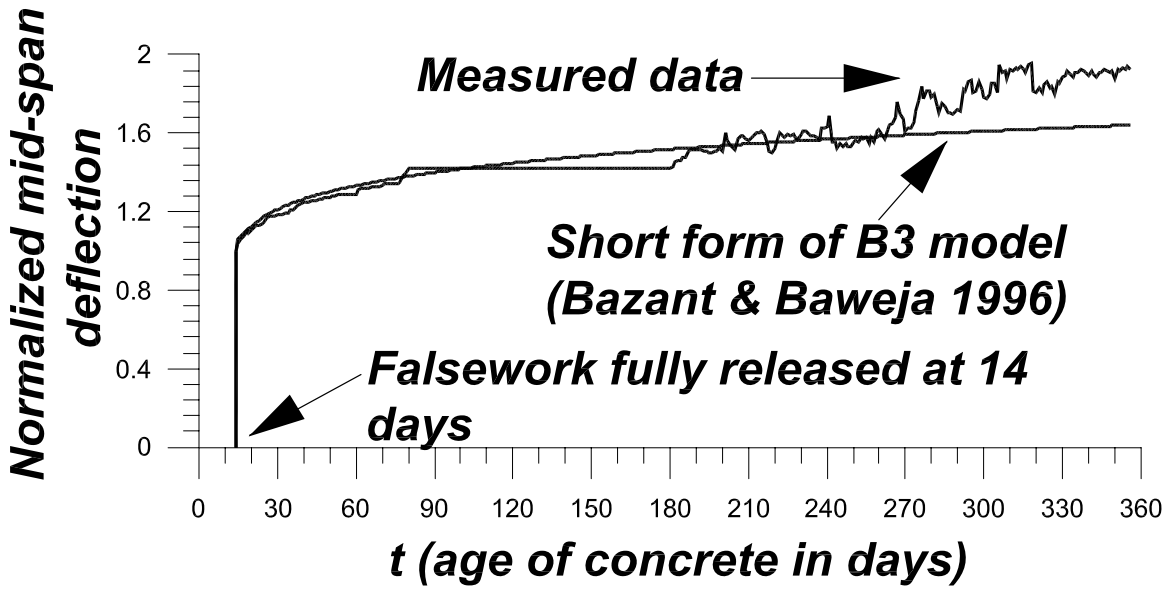


(a)

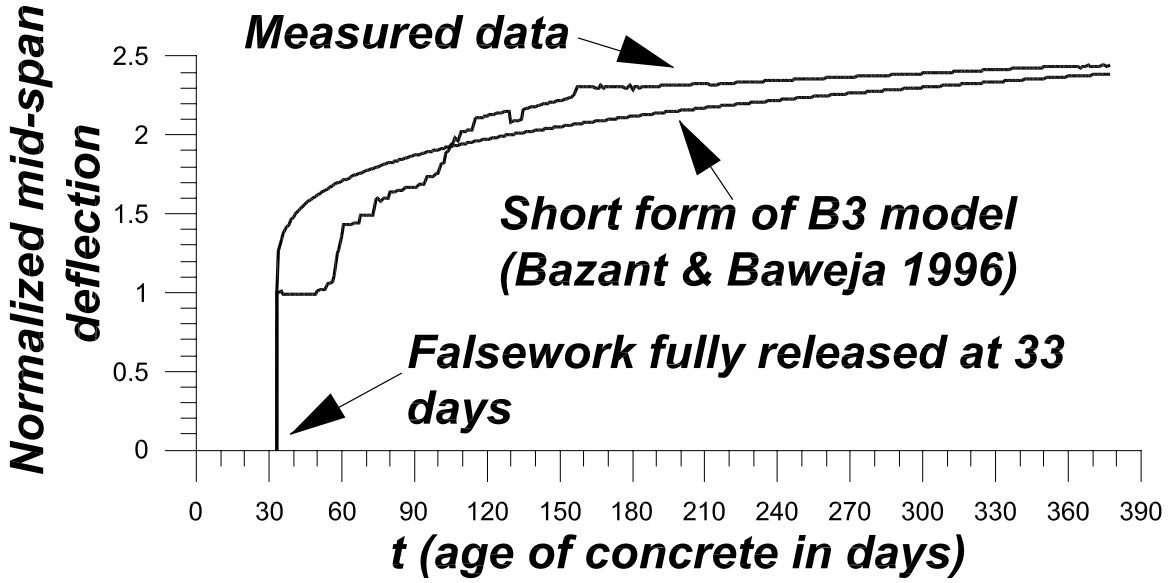


(b)

Figure 4.5: Comparison of measured mid-span deflections with the short form of the B3 model

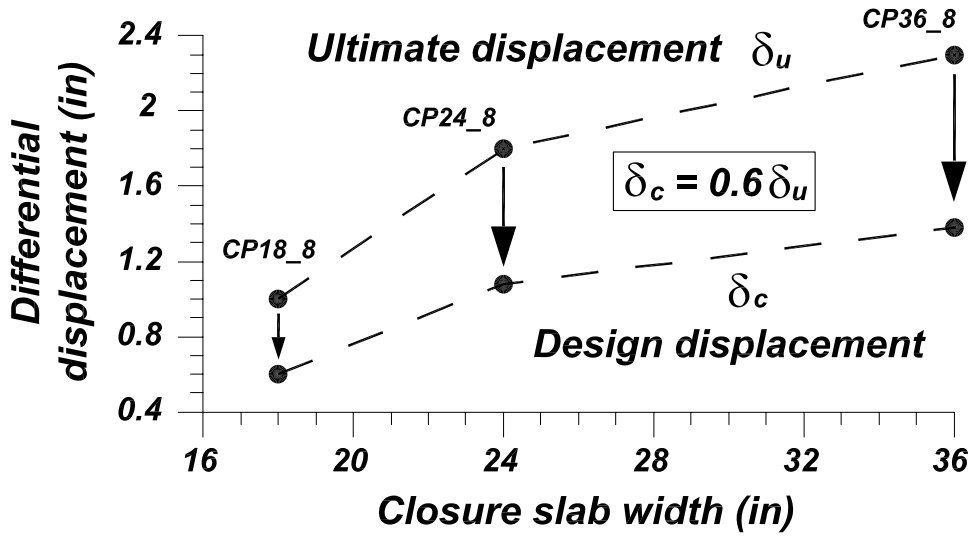


Figure 4.6: Differential deflection with different closure slab width

Eq. 4.21. The instantaneous deflection is best provided by field measurements of the bridge upon falsework release, even though an estimation of the instantaneous deflection is theoretically possible via elastic beam theory. For a simply-supported span, the instantaneous deflection corresponds to the mid-span displacement, whereas for continuous spans, the instantaneous deflection should correspond to the largest downward displacement in any of the spans.

(ii) The task at hand is to determine that whether a closure slab of a given width and reinforcement details has adequate design displacement capacity to cope with the differential displacement for a selected closure time. To that end, let $t_c$ denotes the time at closure pour relative to the last concrete pour of the new bridge in widening or stage II bridge, which allows the waiting period for closure pour can be written as $\Delta t_w = t_c - t_1$, where $t_1$ is the time at falsework release. Figure 4.7 shows the definition of these time parameters. In addition, mid-span deflection as $t \to \infty$ is needed, which is represented by $t_\infty \approx 10000$ days or about 30 years. Calculate the time-dependent mid-span deflection at closure, $\delta_{midspan}(t_c)$, using $t_1$ in Eq. 4.20 for short duration falsework release, and using $t_1$ and $t_2$ for long duration falsework release in Eq. 4.21. Similarly, calculate the mid-span deflection as $t \to \infty$, i.e. $\delta_{midspan}(t_\infty)$, using the same equation, Eq. 4.20 or Eq. 4.21. The displacement demand on the closure slab is then

given by

$$\delta_d = \delta_{midspan}(t_\infty) - \delta_{midspan}(t_c) \qquad \text{for bridge widening} \tag{4.22}$$

The same approach for displacement demand can be extended to staged construction. In this case, mid-span deflections need to be computed for both stage I and stage II bridges, taking into account of the age difference in the concrete of the two bridges at closure. More specifically, mid-span deflections for stage I and II bridges can be calculated as $\delta^I_{midspan}(t_c + \Delta t_{age})$ and $\delta^{II}_{midspan}(t_c)$, using their respective $t_1$ and $t_2$ in Eq. 4.20 or Eq. 4.21, where $\Delta t_{age}$ represents the age difference of the concrete in the two bridges. Similarly, mid-span deflections as $t \to \infty$ can be calculated as $\delta^I_{midspan}(t_\infty)$ and $\delta^{II}_{midspan}(t_\infty)$ for stage I and stage II bridges, respectively. Thus the displacement demand on the closure slab can be written as

$$\delta_d = [\delta^{II}_{midspan}(t_\infty) - \delta^{II}_{midspan}(t_c)] - [\delta^I_{midspan}(t_\infty) - \delta^I_{midspan}(t_c + \Delta t_{age})] \qquad \text{for staged construction} \tag{4.23}$$

(iii) By comparing the displacement demand, $\delta_d$, on the closure slab with the displacement capacity, $\delta_c$, of the closure slab, a decision can be made on whether a selected or proposed closure time $t_c$ is acceptable. Thus,

(a) If $\delta_d \leq \delta_c$, the proposed closure pour time $t_c$, or equivalently waiting period $\Delta t_w$, is acceptable,

(b) If however $\delta_d > \delta_c$, the proposed waiting period is unacceptable, and the process can be repeated with a longer period until the displacement demand is smaller or equal to the displacement capacity of the slab

Two examples are used to demonstrate the methodology for assessing the acceptability of proposed closure pour waiting time. The first example assumes a staged construction involving a simply-supported bridge, while the second example assumes widening of an existing multiple-span continuous bridge.

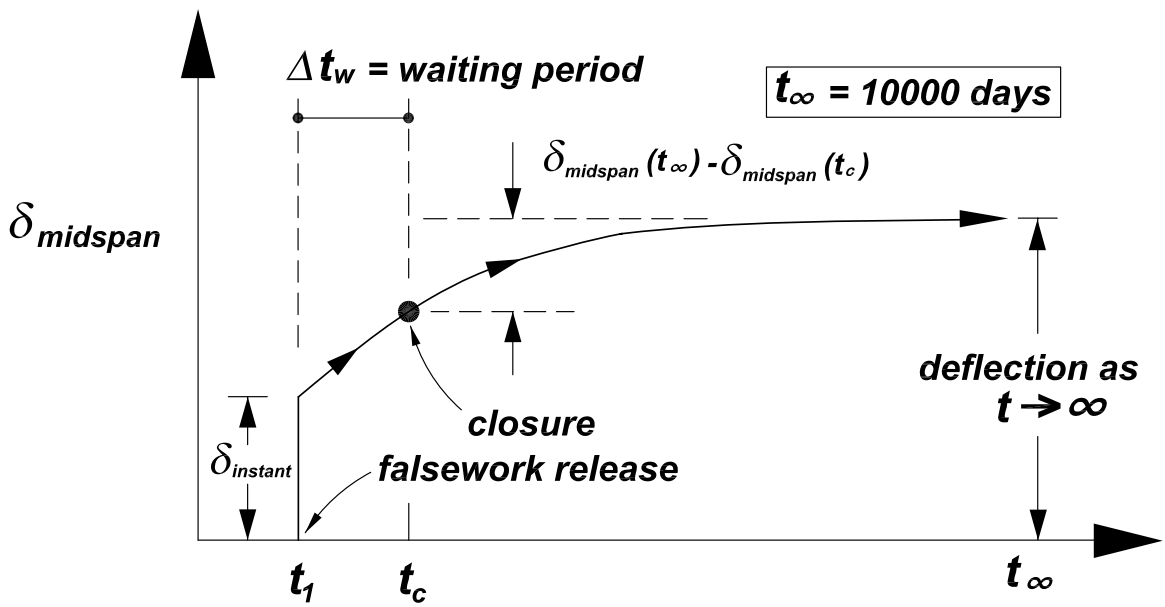


Figure 4.7: Definition of time parameters - $t_c$ and $t_\infty$

### 4.4.1 Example 1 - Simply-Supported Bridge

Assume two simply-supported bridges with the same span of 170 ft are built by staged construction, with falsework release for both stage I and II bridges started at 10 days after the last concrete deck pour, and taking three days to achieve full falsework release for both bridges. The falsework release, and subsequent schedule for closure pour, essentially follows Alternative 1 of current Caltrans practice [1]. Thus the time parameters for this example are $t_1 = 10$ days and $t_2 = 13$ days for both bridges. It is assumed that the mid-span deflection for stage I bridge at $t_2 = 13$ days is $\delta^I_{measured} = 1.30$", and for stage II bridge is $\delta^{II}_{measured} = 1.25$", and these deflections are reasonable for prestressed concrete bridges of that span in California. It is further assumed that the age of the concrete for stage I bridge is 360 days older than that of stage II bridge i.e. $\Delta t_{age} = 360$ days. Duration of curing is assumed to be 7 days, i.e. $t_o = 7$ days, and the ambient relative humidity is assumed to be $h = 0.7$, for both bridges. The same mean 28-day compressive strength of $\bar{f}_c = 6200$ psi, and the same effective cross-section thickness of $D = 10$", are used for both bridges. It is assumed that the closure is made by a slab of 24" width and 8" thickness with #6@6" c/c for both top and bottom. The differential displacement capacity, taken from Figure 4.6, is

$\delta_c = 1.1$" for the closure slab. It is proposed that the waiting period for closure pour be shortened to 1/2 of that in current specification, i.e. $\Delta t_w = 30$ days, compared to the 60-day waiting period currently specified in Alternative 1. The objective here is to determine if the proposed waiting time is acceptable with respect to the design displacement capacity of the closure slab. Using the procedure outlined above, we have

(i) The measured mid-span deflections at the end of falsework release $t_2$ are

$$\delta^{I}_{measured} = 1.30" \qquad \text{for stage I bridge}$$

and

$$\delta^{II}_{measured} = 1.25" \qquad \text{for stage I bridge}$$

(ii) Using the following time parameters

$$t_c = t_1 + \Delta t_w = 10 + 30 = 40 \text{ days (for stage II bridge)}$$

$$t_c + \Delta t_{age} = 40 + 360 = 400 \text{ days (for stage I bridge)}$$

$$t_\infty = 10000 \text{ days (for both bridges)}$$

the following values can be calculated

$$q_1 = \frac{0.6 \times 10^6}{57000\sqrt{\bar{f}_c}} = \frac{0.6 \times 10^6}{57000\sqrt{6200}} = 0.134$$

$$q_0 = \frac{200}{\sqrt{\bar{f}_c}} = \frac{200}{\sqrt{6200}} = 2.54$$

$$q_5 = \frac{6000}{\bar{f}_c} = \frac{6000}{6200} = 0.968$$

$$\begin{aligned} H(t_1) &= 1 - (1-h)\tanh\sqrt{\frac{t_1 - t_o}{32D^2}} \\ &= 1 - (1-0.7)\tanh\sqrt{\frac{10-7}{32 \times 10^2}} \\ &= 0.991 \end{aligned}$$

$$
\begin{aligned}
H(t_2) &= 1 - (1-h)\tanh\sqrt{\frac{t_2 - t_o}{32D^2}} \\
&= 1 - (1-0.7)\tanh\sqrt{\frac{13-7}{32\times 10^2}} \\
&= 0.987
\end{aligned}
$$

$$
\begin{aligned}
H(t_\infty) &= 1 - (1-h)\tanh\sqrt{\frac{t_\infty - t_o}{32D^2}} \\
&= 1 - (1-0.7)\tanh\sqrt{\frac{10000-7}{32\times 10^2}} \\
&= 0.717
\end{aligned}
$$

These values of $q_1$, $q_0$, $q_5$, $H(t_1)$, $H(t_2)$ and $H(t_\infty)$ are applicable to both stage I and II bridges. The parameter for drying creep, given in Eq. 4.11, is

$$
\begin{aligned}
H(t_c + \Delta t_{age}) &= 1 - (1-h)\tanh\sqrt{\frac{t_c + \Delta t_{age} - t_o}{32D^2}} \\
&= 1 - (1-0.7)\tanh\sqrt{\frac{400-7}{32\times 10^2}} \\
&= 0.899 \qquad \text{for stage I bridge}
\end{aligned}
$$

and

$$
\begin{aligned}
H(t_c) &= 1 - (1-h)\tanh\sqrt{\frac{t_c - t_o}{32D^2}} \\
&= 1 - (1-0.7)\tanh\sqrt{\frac{40-7}{32\times 10^2}} \\
&= 0.970 \qquad \text{for stage II bridge}
\end{aligned}
$$

The creep compliance values are

$$
\begin{aligned}
J(t_c + \Delta t_{age}, t_1) &= (q_1 + q_0\, ln\{1 + \Psi[(t_1)^{-m} + \alpha](t_c + \Delta t_{age} - t_1)^n\} \\
&+ q_5[e^{-3H(t_c+\Delta_{age})} - e^{-3H(t_1)}]^{0.5}) \times 10^{-6} \\
&= (0.134 + 2.54 ln\{1 + 0.3[(10)^{-0.5} + 0.001](400-10)^{0.1}\} \\
&+ 0.968[e^{-3\times 0.899} - e^{-3\times 0.991}]^{0.5}) \times 10^{-6} \\
&= 0.662 \times 10^{-6} \ \ \text{psi}^{-1} \quad \text{for stage I bridge}
\end{aligned}
$$

and

$$
\begin{aligned}
J(t_c, t_1) &= (q_1 + q_0 ln\{1 + \Psi[(t_1)^{-m} + \alpha](t_c - t_1)^n\} \\
&+ q_5[e^{-3H(t_c)} - e^{-3H(t_1)}]^{0.5}) \times 10^{-6} \\
&= (0.134 + 2.54 ln\{1 + 0.3[(10)^{-0.5} + 0.001](40 - 10)^{0.1}\} \\
&+ 0.968[e^{-3\times 0.970} - e^{-3\times 0.991}]^{0.5}) \times 10^{-6} \\
&= 0.509 \times 10^{-6} \text{ psi}^{-1} \quad \text{for stage II bridge}
\end{aligned}
$$

and

$$
\begin{aligned}
J(t_\infty, t_1) &= (q_1 + q_0 ln\{1 + \Psi[(t_1)^{-m} + \alpha](t_\infty - t_1)^n\} \\
&+ q_5[e^{-3H(t_\infty)} - e^{-3H(t_1)}]^{0.5}) \times 10^{-6} \\
&= (0.134 + 2.54 ln\{1 + 0.3[(10)^{-0.5} + 0.001](10000 - 10)^{0.1}\} \\
&+ 0.968[e^{-3\times 0.717} - e^{-3\times 0.991}]^{0.5}) \times 10^{-6} \\
&= 0.925 \times 10^{-6} \ \text{ psi}^{-1} \quad \text{for both bridges}
\end{aligned}
$$

Since the 'instantaneous compliance' is assumed to correspond to the deflection measured at the end of falsework release i.e. at $t_2$, Eq. 4.21 should be used. In this case, $J(t_2, t_1)$ can be calculated as

$$
\begin{aligned}
J(t_2, t_1) &= (q_1 + q_0 ln\{1 + \Psi[(t_1)^{-m} + \alpha](t_2 - t_1)^n\} \\
&+ q_5[e^{-3H(t_2)} - e^{-3H(t_1)}]^{0.5}) \times 10^{-6} \\
&= (0.134 + 2.54 ln\{1 + 0.3[(10)^{-0.5} + 0.001](13 - 10)^{0.1}\} \\
&+ 0.968[e^{-3\times 0.987} - e^{-3\times 0.991}]^{0.5}) \times 10^{-6} \\
&= 0.414 \times 10^{-6} \text{ psi}^{-1} \ \text{ which is applicable for both bridges}
\end{aligned}
$$

Thus the mid-span deflections for stage I bridge are

$$
\begin{aligned}
\delta^I_{midspan}(t_c + \Delta t_{age}) &= \delta^I_{measured}[J(t_c + \Delta t_{age}, t_1)/J(t_2, t_1)] \\
&= 1.30[0.662/0.414] = 2.08" \\
\delta^I_{midspan}(t_\infty) &= \delta^I_{measured}[J(t_\infty, t_1)/J(t_2, t_1)] \\
&= 1.30[0.925/0.414] = 2.90"
\end{aligned}
$$

and the mid-span deflections for stage II bridge are

$$\begin{aligned}
\delta^{II}_{midspan}(t_c) &= \delta^{II}_{measured}[J(t_c, t_1)/J(t_2, t_1)] \\
&= 1.25[0.509/0.414] = 1.54" \\
\delta^{II}_{midspan}(t_\infty) &= \delta^{II}_{measured}[J(t_\infty, t_1)/J(t_2, t_1)] \\
&= 1.25[0.925/0.414] = 2.79"
\end{aligned}$$

Finally, the differential displacement demand on the closure slab, determined according to Eq. 4.23, is

$$\begin{aligned}
\delta_d &= [\delta^{II}_{midspan}(t_\infty) - \delta^{II}_{midspan}(t_c)] - [\delta^{I}_{midspan}(t_\infty) - \delta^{I}_{midspan}(t_c + \Delta t_{age})] \\
&= [2.79 - 1.54] - [2.90 - 2.08] \\
&= 0.43"
\end{aligned}$$

(iii) The comparison of the displacement demand with the estimate displacement capacity of the closure slab indicates

$$\delta_d = 0.43" \leq \delta_c = 1.1"$$

implying that the closure slab of 24" width and 8" thickness has sufficient displacement capacity to tolerate the differential displacement across the closure slab. Thus the proposed 30 days waiting period for closure pour is deemed acceptable in the context of the assumptions made in the proposed methodology.

### 4.4.2 Example 2 - Three-Span Continuous Bridge

Consider a widening situation for a three-span continuous, prismatic bridge, as shown in Figure 4.8. It is assumed that all three spans are cast at the same time. Falsework is released for span 1 first at 28 days, followed by span 3 at 29 days, and then span 2 at 30 days. It is further assumed that the falsework release took less than one day to achieve. The schedule for falsework release and closure pour in essence follows Alternative 2 of current

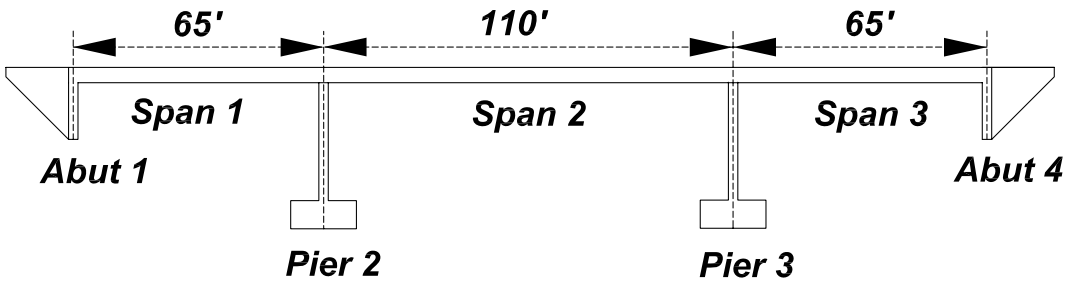


Figure 4.8: Example 2 - three-span continuous bridge

Table 4.1: Assumed instantaneous deflections of the three-span continuous bridge

| Span | $\delta^1_{max}$ | $\delta^2_{max}$ | $\delta^3_{max}$ | falsework release |
|---|---|---|---|---|
| 1 | 0.15" | 0" | 0" | 28 days |
| 3 | 0.17" | 0" | 0.15" | 29 days |
| 2 | 0.18" | 0.55" | 0.16" | 30 days |

Caltrans practice[1]. Time parameters for this example are $t_1 = 28$ days for span 1, $t_1 = 29$ days for span 3 and $t_1 = 30$ days for span 2. The maximum downward deflection of each span is assumed to be measured immediately after falsework release, and are listed in Table 4.1, with the largest deflection occurring in span 2, which is the longest of the three spans. It is assumed that the concrete is cured for a period of $t_o = 7$ days for all three spans, and the ambient relative humidity is $h = 0.6$. The mean 28-day compressive strength is taken as $\bar{f}_c = 6200$ psi, and an effective cross-section thickness of $D = 10$" is used for all three spans. It is also assumed that the closure is made by a slab of 36" width and 8" thickness with #6@6" c/c for both top and bottom reinforcement. The differential displacement capacity of the closure slab is $\delta_c = 1.4$", which is reduced from the experimental results and taken from Figure 4.6. Consideration is made to whether the waiting period for closure pour can be shortened to 1/2 of that specified for Alternative 2, i.e. $\Delta t_w = 7$ days, compared to 14-day waiting period currently specified. Using the design procedure as proposed

(i) Since the duration of falsework release is assumed to less than one day, Eq. 4.20 will be used. The determination of the waiting period for closure is made using the largest instantaneous deflection among the three spans, i.e.

$$\delta_{instant} = \delta^2_{max} = 0.55"$$

(ii) Using the time for closure

$$t_c = t_1 + \Delta t_w = 30 + 7 = 37 \text{ days}$$

and

$$t_\infty = 10000 \text{ days}$$

the following values are calculated

$$q_1 = \frac{0.6 \times 10^6}{57000\sqrt{\bar{f}_c}} = \frac{0.6 \times 10^6}{57000\sqrt{6200}} = 0.134$$

$$q_0 = \frac{200}{\sqrt{\bar{f}_c}} = \frac{200}{\sqrt{6200}} = 2.54$$

$$q_5 = \frac{6000}{\bar{f}_c} = \frac{6000}{6200} = 0.968$$

$$\begin{aligned} H(t_1) &= 1 - (1-h)\tanh\sqrt{\frac{t_1 - t_0}{32D^2}} \\ &= 1 - (1-0.6)\tanh\sqrt{\frac{30-7}{32 \times 10^2}} \\ &= 0.966 \end{aligned}$$

$$\begin{aligned} H(t_1 + \Delta t) &= 1 - (1-h)\tanh\sqrt{\frac{t_1 + \Delta t - t_0}{32D^2}} \\ &= 1 - (1-0.6)\tanh\sqrt{\frac{30.01-7}{32 \times 10^2}} \\ &= 0.966 \quad \text{essentially the same as } H(t_1) \end{aligned}$$

$$\begin{aligned} H(t_c) &= 1 - (1-h)\tanh\sqrt{\frac{t_c - t_0}{32D^2}} \\ &= 1 - (1-0.6)\tanh\sqrt{\frac{37-7}{32 \times 10^2}} \\ &= 0.961 \end{aligned}$$

$$\begin{aligned} H(t_\infty) &= 1 - (1-h)\tanh\sqrt{\frac{t_\infty - t_0}{32D^2}} \\ &= 1 - (1-0.6)\tanh\sqrt{\frac{10000-7}{32 \times 10^2}} \\ &= 0.623 \end{aligned}$$

The creep compliance values for the widening bridge are

$$
\begin{aligned}
J(t_c, t_1) &= (q_1 + q_0\, ln\{1 + \Psi[(t_1)^{-m} + \alpha](t_c - t_1)^n\} \\
&\quad + q_5[e^{-3H(t_c)} - e^{-3H(t_1)}]^{0.5}) \times 10^{-6} \\
&= (0.134 + 2.540\, ln\{1 + 0.3[(30)^{-0.5} + 0.001](37 - 30)^{0.1}\} \\
&\quad + 0.968[e^{-3\times 0.961} - e^{-3\times 0.966}]^{0.5}) \times 10^{-6} \\
&= 0.325 \times 10^{-6} \quad \text{psi}^{-1}
\end{aligned}
$$

and

$$
\begin{aligned}
J(t_\infty, t_1) &= (q_1 + q_0\, ln\{1 + \Psi[(t_1)^{-m} + \alpha](t_\infty - t_1)^n\} \\
&\quad + q_5[e^{-3H(t_\infty)} - e^{-3H(t_1)}]^{0.5}) \times 10^{-6} \\
&= (0.134 + 2.540\, ln\{1 + 0.3[(30)^{-0.5} + 0.001](10000 - 30)^{0.1}\} \\
&\quad + 0.968(e^{-3\times 0.623} - e^{-3\times 0.966})^{0.5}) \times 10^{-6} \\
&= 0.768 \times 10^{-6} \quad \text{psi}^{-1}
\end{aligned}
$$

Since the falsework release is assumed to take less than 1 day to complete, Eq. 4.20 should be used. In this case, $J(t_1, t_1)$ can be calculated as

$$
\begin{aligned}
J(t_1, t_1) \approx 1/E_c(t_1) &= J(t_1 + \Delta t, t_1) \\
&= J(30.01, 30) \\
&= (q_1 + q_0\, ln\{1 + \Psi[(t_1)^{-m} + \alpha](t_1 + \Delta t - t_1)^n\} \\
&\quad + q_5[e^{-3H(t_1+\Delta t)} - e^{-3H(t_1)}]^{0.5}) \times 10^{-6} \\
&= (0.134 + 2.540\, ln\{1 + 0.3[(30)^{-0.5} + 0.001](30.01 - 30)^{0.1}\} \\
&\quad + 0.968(e^{-3\times 0.966} - e^{-3\times 0.966})^{0.5}) \times 10^{-6} \\
&= 0.222 \times 10^{-6} \quad \text{psi}^{-1}
\end{aligned}
$$

Thus the deflections for the widening bridge at closure and at $t_\infty$ are

$$\begin{aligned}
\delta_{midspan}(t_c) &= \delta_{instant}[J(t_c, t_1)/J(t_1, t_1)] \\
&= 0.55[0.325/0.222] = 0.81" \\
\delta_{midspan}(t_\infty) &= \delta_{instant}[J(t_\infty, t_1)/J(t_1, t_1)] \\
&= 0.55[0.768/0.222] = 1.90"
\end{aligned}$$

which gives the differential displacement demand across the closure slab, according to Eq 4.22, as

$$\begin{aligned}
\delta_d &= [\delta_{midspan}(t_\infty) - \delta_{midspan}(t_c)] \\
&= [1.90 - 0.81] \\
&= 1.09"
\end{aligned}$$

(iii) The differential displacement demand is smaller than the estimated displacement capacity of the closure slab as

$$\delta_d = 1.09" \leq \delta_c = 1.4"$$

Thus a closure slab of 36" width and 8" thickness is expected to have sufficient displacement capacity to the differential displacement across the closure slab. The shortening of the waiting period to 7 days for closure pour is deemed acceptable.

# Chapter 5

# Conclusions

Bridge closure slab and its waiting time during construction serve two purposes. First, the waiting time before closure defers the final connection of the widening bridge to the existing bridge till after a certain portion of long term dead load deflection has occurred on the widening bridge. The extra waiting time reduces the stress build-up on the closure slab caused by the differential displacement after the connection. Second, the bridge closure slab provides a smooth transition in the final grade of the two bridges. Waiting time for closure pour depends on the time-dependent deflection, arising primarily from the dead load after the closure slab is placed. Current bridge design and construction practices in the state of California require the closure pour to have up to 60 days waiting period after falsework release. The 60 days waiting period does not take into account the type of bridges and different displacement capacities of the closure slab leading to unnecessary long waiting period in some cases.

In this project, evaluation of closure pour waiting period is made in three steps. In step 1, time-dependent displacements of a simply supported span and a multiple-span concrete bridges were monitored in the field over a period up to 12 months. A model for time-dependent displacement, based on the creep compliance function, is proposed for the prediction of the bridge time-dependent deflection. Compared with measured displacements, the model is shown to provide a reasonable prediction of bridge deflection in the range of practical closure time period. In step 2, four full-size closure slabs of common California dimensions and details were tested in the laboratory to determine their load-deformation

response and differential displacement capacity. The response of the closure slab is evaluated in terms of the following parameters: (i) load-differential displacement response, (ii) bending moment and shear force distributions, and (iii) reinforcement strain distributions. In step 3, a procedure is proposed to determine the waiting time for closure pour using the predictive model from step 1 and the displacement capacity of the closure slab from step 2. Based on this study, the following conclusions are made:

- The closure pour waiting period should be determined according to the instantaneous displacement of the widening bridge. Irrespective of the type of bridge support, whether simply supported or continuous multiple-span, a small instantaneous displacement implies that a small differential displacement will be imposed on the closure slab upon connection. Consequently, a shorter waiting time is appropriate for a bridge with a smaller instantaneous displacement than a bridge with a larger instantaneous displacement. Thus the use of one waiting period, for example 60 days for all bridges, causes an unnecessarily long waiting time for closure pour in short bridges, which are expected to exhibit small instantaneous displacements.

- The closure pour waiting period should be determined based on the displacement capacity of the closure slab, as reported in Chapter 3. Observation from laboratory tests shows that a wider and thinner closure slab has a larger displacement capacity than a narrower and thicker closure slab. This implies that a larger differential displacement can be imposed on a wider and thinner closure slab compared to a narrower and thicker closure slab. Thus a shorter waiting time should be permitted for a wide and thin closure slab.

- The closure pour waiting time should take into account the type of construction. Widening of an existing bridge and stage-constructed bridges should not use the same waiting period for closure pour. For widening of an existing bridge, the existing bridge is usually much older than the widening bridge, and in that context, the time-dependent deflection of the existing bridge affecting the differential displacement of the closure slab is expected to be small and may be assumed to be equal to zero. In contrast, how-

ever, both stage I and stage II bridges in staged construction are expected to deflect after closure pour albeit differently. If the instantaneous displacements are measured for both stage I and stage II bridges, the differential displacement between the two bridges in staged construction will be smaller than the differential displacement in the widening of an existing bridge. This observation suggests that a shorter waiting time is appropriate for closure pour in a staged construction than in the widening of an existing bridge.

- Time-dependent displacement of a newly constructed bridge is highly dependent on the age of the concrete at the time of first loading. In that regard, the time of falsework release should be taken into account when determining the appropriate closure pour waiting time. For instance, a falsework release at 10 days should not use the same waiting time as the falsework release at 20 days since the falsework release at a later age would result in a smaller time-dependent displacement. The longer the falsework is left in place, the shorter waiting period is needed for closure pour.

- Waiting period for closure pour should be determined considering the demand of the time-dependent displacement as well as the displacement capacity of the closure slab. The methodology proposed on Section 4.4, which is capable of accounting for the time-dependent displacement demand and the displacement capacity of closure slab, is recommended for use in the determination of the closure pour waiting period.

- Special attention needs to be paid to stiff closure slabs, i.e. narrow and thick closure slabs, as brittle failure may occur at small differential displacement without much warning. Laboratory test of a closure slab of 24" width and 12" thickness resulted in failure of the slab at differential displacement of less than 1" almost instantaneously upon reaching first-yielding of the reinforcement. Tests also found that a wider closure slab not only has a larger displacement capacity but is also more ductile. Under a large differential displacement, reinforcement bars of a wider closure slab tend to yield before reaching a flexural-shear failure.

# Bibliography


[1] California Department of Transportation, Sacramento, California. *Widening Existing Bridges, Memos to Designers 9-3*, April 1991.

[2] California Department of Transportation, Sacramento, California. *Standard Specifications*, July 1999.

[3] California Department of Transportation, Sacramento, California. *Hinge Curl, Memos to Designers 11-34*, November 1996.

[4] Z. P. Bazant and Z. Cedolin. *Stability of Structures*. Oxford University Press, New York, NY 10016, 1991.

[5] W. Flugge. *Viscoelasticity*. Springer-Verlag, New York, 1975.

[6] R. I. Gilbert. *Time Effects in Concrete Structures*. Elsevier Science Publishers, New York NY 10017, 1988 pp. 1-22.

[7] A. Ghali, R. Favre, and M. Elbadry. *Concrete Structures*. Spon Press, New York NY 10001, third edition, 2002 pp. 1-14.

[8] American Concrete Institute. *Prediction of Creep, Shrinkage, and Temperature Effects in Concrete Structures (209R-92)*, 1992. Farmington Hills, Michigan.

[9] Euro-Inernational Du Beton. *CEB-FIP Model Code 1990: Design Code*, 1993. London.

[10] N. J. Gardner and J. W. Zhao. Creep and shrinkage revisited. *ACI Material Journal*, 90(3):236–246, 1993.

[11] N. J. Gardner and M. J. Lockman. Design provisions for drying shrinkage and creep of normal-strength concrete. *ACI Material Journal*, 98(2):159–167, 2001.

[12] Z. P. Bazant and S. Baweja. Creep and shrinkage prediction model for analysis and design of concrete structures - model B3. *Materials and Structures*, 28:357–495, 1995.

[13] Z. P. Bazant and S. Baweja. Short form of creep and shrinkage prediction model B3 for structures of medium sensitivity. *Materials and Structures*, 29:587–593, 1996.

[14] Z. P. Bazant and J. C. Chern. Log double power law for concrete creep. *ACI Journal*, 82(5):665–675, 1985.